

A Multi-Fidelity Workflow to Derive Physics-Based Conceptual Design Methods

Vom Promotionsausschuss der
Technischen Universität Hamburg-Harburg
zur Erlangung des akademischen Grades
Doktor-Ingenieur (Dr.-Ing.)
genehmigte Dissertation

von
Daniel Böhnke

aus
Trier

2015

Übersicht der Gutachter

1. Gutachter

Prof. Dr.-Ing. Volker Gollnick

2. Gutachter

Prof. Dr.-Ing. Arthur Rizzi

Vorsitzender des Prüfungsausschusses

Prof. Dr.-Ing. Frank Thielecke

Tag der mündlichen Prüfung: 16. Januar 2015

Danksagung

Dieses Dokument ist im Verlauf der letzten 5 Jahre während meiner Zeit am Institut für Lufttransportsysteme am Deutschen Zentrum für Luft- und Raumfahrt entstanden. Fokus der Abteilung für integrierten Luftfahrzeugentwurf ist es Zusammenarbeit im Entwurf zu ermöglichen und zu fördern und in diesem Sinne freue ich mich umso mehr an dieser Stelle all denen Dank sagen zu können, mit denen ich zusammen arbeiten konnte.

Einen herzlichen Dank meinem Doktorvater Prof. Dr.-Ing. Volker Gollnick für die fachliche Betreuung der Arbeit. Herrn Prof. Dr.-Ing. Arthur Rizzi und Herrn Prof. Dr.-Ing. Frank Thielecke danke ich für die Prüfung meiner Promotion und die Übernahme des Vorsitzes des Promotionsausschusses.

Viele Kollegen haben mich in den letzten Jahren unterstützt und ich danke Björn für die Rückendeckung, Alexander und Pier für die Freundschaft im gemeinsamen Büro, Felix und Till fürs Debuggen und die Geduld, Jonas für die Geometrie, Erwin für die vielen Diskussionen am Freitagmorgen und allen, die ich an dieser Stelle vergessen habe.

Die bedingungslose Unterstützung meiner Eltern und Ihr geduldiges, offenes Ohr sind der Grund dafür, dass ich an dieser Stelle angekommen bin, und Ihnen gilt mein besonderer Dank. Gunda, ohne Dich wäre die Sache nie so entspannt gelaufen, wie Du immer behauptet hast. Ich danke Dir.

Hamburg, April 2015

Daniel Böhnke

Abstract

An advanced model-based aircraft design system needs to predict the properties of several aircraft configurations as early as possible in the design process. Given the fact that the first steps of the design process apply mostly historical-based design methods, the domain of definition of conceptual design is limited, and sophisticated predictions are possible only with the aid of physics-based analysis models that are usually employed at the later, preliminary design stage. However, neither sufficient information is available at the very early design stages to trigger physics-based analysis nor does the large number of necessary evaluations permit the high computational cost of these methods. The present study focused on the question of whether it is possible to include physics-based rather than historical-based methods during conceptual design with a comparable level of complexity and computational cost. Therefore, the study developed an extensible multi-fidelity loop that bridged the information gap between conceptual design and preliminary design. In a subsequent step, the multi-fidelity loop was coupled in a workflow that encompasses a surrogate modeling method based on symbolic regression. The workflow created a global surrogate of the multi-fidelity loop that had low complexity and high accuracy. The proposed body of methods was applied to two design studies resulting in new, physics-based equations for the Oswald factor, and the mass of a conventional wing that are suitable for very early design stages. Furthermore, a strut-braced wing was examined with the aid of the multi-fidelity workflow to enable the conceptual design of such a configuration. Hence, the study significantly extended the domain of definition of conceptual design and outlined topics for related future research.

Contents

1	Introduction	1
1.1	Situation	1
1.2	Problem Definition	6
1.3	Solution	8
1.4	Outline	15
2	State of the Art	17
2.1	Conceptual Design	19
2.2	Design Environments	25
2.3	Multi-Fidelity	33
2.4	Surrogate Models	39
3	Multi-Fidelity Workflow	51
3.1	Conceptual Design	55
3.2	Multi-Fidelity	63
3.3	Design of Experiments	68
3.4	Symbolic Regression	75
4	Design Studies	89
4.1	Oswald Factor	89
4.2	Wing Mass	107
4.3	Strut-Braced Wing Mass	121
5	Discussion	131
6	Conclusion	137

Contents

Bibliography	144
A Complexity	159
B Validation Data	161
C Design of Experiments	167
D Oswald Factor	171
E Wing Mass	175
F Strut Braced Wing Mass	179

Figures

1.1	Simplified design process	2
1.2	Interaction among properties and characteristics	5
1.3	Closed multi-fidelity loop	9
1.4	Uni-directional and central model approach	10
1.5	Components of the proposed multi-fidelity workflow	12
1.6	Schematic symbolic regression approach	14
2.1	Dimensions of aircraft design	18
2.2	Design environment	25
2.3	Levels of fidelity in aerodynamic analysis of a BWB	34
2.4	Collaborative aircraft design system, [141]	37
2.5	Motivations for multi-fidelity	38
2.6	Artificial neuron	48
2.7	Artificial neural network	48
3.1	Multi-fidelity workflow	51
3.2	Object oriented structure of VAMPzero	57
3.3	Calculation approaches in conceptual design	58
3.4	Qualitative dependencies of the reference area	60
3.5	Sensitivities of the reference area	62
3.6	Double trapezoid wing planform	64
3.7	Three-dimensional geometry initialized by VAMPzero	65
3.8	Comparison of level of detail of the SFC	67
3.9	Latin square with three elements	69
3.10	Design space coverage as three dimensional plot	71
3.11	Design space coverage as scatter-matrix plot	72
3.12	Histogram of x_1 distribution	73
3.13	Evolutionary algorithm principle	75
3.14	Surrogate models for Shevell	81
3.15	Surrogate models for Raymer	83
3.16	Surrogate models for Raymer	85

Figures

4.1	Finite wing as lifting line	91
4.2	C_1 as a function of λ and AR , [54]	95
4.3	δ depending on the taper ratio, [49]	97
4.4	Design of experiments: Oswald factor	99
4.5	Multi-fidelity loop: Oswald factor	100
4.6	Vortex lattices on double trapezoid wing	101
4.7	Verification: Oswald factor	103
4.8	Surrogate model: Oswald factor	104
4.9	Validation: Oswald factor	106
4.10	Multi-fidelity loop: Wing mass	114
4.11	Design concept: Wing mass	116
4.12	Verification: Wing mass	118
4.13	Surrogate model: Wing mass	119
4.14	Validation: Wing mass	121
4.15	Existing approaches: Strut-braced wing	122
4.16	Design concept: Strut-braced wing	125
4.17	Surrogate model: Strut-braced wing	128
4.18	Verification: Strut-braced wing	129
5.1	Historic vs. physics-based domain of definition	132
6.1	Iterative multi-fidelity workflow	143

Tables

2.1	Conceptual aircraft design performance criteria	22
2.2	Qualitative comparison of conceptual design models	24
2.3	Level of fidelity classification	27
2.4	Design environment performance criteria	29
2.5	Qualitative comparison of design environments	33
2.6	Performance criteria for surrogate models	41
2.7	Experimental error classification	42
3.1	Dimensionless constants	65
3.2	Space fillingness of DOE algorithms	74
3.3	Qualitative comparison of surrogate models	87
4.1	Existing approaches: Oswald factor	97
4.2	Domain of definition: Oswald factor	98
4.3	Verification: Oswald factor	103
4.4	Existing approaches: Wing mass	111
4.5	Domain of definition: Wing mass	112
4.6	Verification: Wing mass	118
4.7	Domain of definition: Strut-braced wing	126
4.8	Verification: Strut-braced wing	129
A.1	Complexity cost for various building blocks	159
B.1	Validation data: A300, A310, A318, A319, A320	162
B.2	Validation data: A321, A332, A333, A342, A345	163
B.3	Validation data: A346, A380, B707, B717, A732	164
B.4	Validation data: B734, B735, B737, B738, B744	165
B.5	Validation data: B752, B753, B762, B763, B772	166
C.1	Full factorial sample plan	167
C.2	Monte Carlo sample plan	168
C.3	Latin hypercube sample plan	169

Tables

D.1	Oswald factor: sample points	173
D.2	Oswald factor: verification points	174
E.1	Wing mass: sample points	177
E.2	Wing mass: verification points	178
F.1	SBW mass: sample points	186
F.2	SBW mass: verification points	187

Glossary

Acronyms

3DOPT	3-Dimensional Design Optimization Code
AAA	Advanced Aircraft Analysis
ANN	Artificial Neural Networks
BPR	Bypass Ratio
BWB	Blended Wing Body
CAD	Computer Aided Design
CDA	Complex-step Derivative Approximation
CEASIOM	Computerised Environment for Aircraft Synthesis and Integrated Optimisation Methods
CFD	Computational Fluid Dynamics
CFRP	Carbon fiber reinforced plastic
CPACS	Common Parametric Aircraft Configuration Schema
DACE	Design and Analysis of Computer Experiments
DLR	German Aerospace Center
DOE	Design of experiments
EIS	Entry into service
FLOPS	Flight Optimization System
HEB	High-dimensional, Expensive (computationally), Blackbox
HSCT	High Speed Civil Transport
KBE	Knowledge Based Engineering
MDAO	Multi-disciplinary Design Analysis and Optimization
MDOPT	Multi-Disciplinary Design Optimization Framework
MICADO	Multidisciplinary Integrated Conceptual Aircraft Design and Optimization
MRO	Maintenance, Repair and Overhaul
NASA	National Aeronautics and Space Administration
ONERA	Office national d'Études et de recherches aérospatiales
PASS	Program for Aircraft Synthesis Studies
PrADO	Preliminary Aircraft Design and Optimisation Program

Glossary

RANS	Reynolds averaged Navier Stokes
RCE	Remote Component Environment
RDS	Raymer Design Software
SAM	Structural and Aeroelastic Analysis Module
SFC	Thrust Specific Fuel Consumption
SimSAC	Simulating Aircraft Stability And Control Characteristics for Use in Conceptual Design
SQL	Structured Query Language
SUGAR	Subsonic ultra green aircraft concept
TLAR	Top level aircraft requirements
TLU	Threshold Logic Unit
VAMP	Virtual Aircraft Multidisciplinary Analysis and Design Processes

Indices

$1, \dots, k$	Number of design variables
$1, \dots, m$	Model order
$1, \dots, n$	Number of samples

Mathematical Symbols

β	Regression coefficients
ϵ	Model error
\hat{y}	Surrogate response
μ	Mean value
π	Dimensionless quantities
σ	Variance
$c(x)$	Correlation model
$h(x)$	High-Fidelity model
$l(x)$	Low-Fidelity model
r	Rank of dimensional matrix
$r(x)$	Regression model
$s(x)$	Surrogate model
y	Model response

Physical Symbols

α	[]	Angle of attack
δ	[]	Spanwise vortex lines
η_k	[]	Kink ratio
η_{strut}	[]	Spanwise strut position

Glossary

γ	[]	Chordwise vortex lines
λ	[]	Taper ratio
ψ	[]	Dihedral angle
ρ_∞	[kgm^{-3}]	Free stream density
τ	[]	Twist angle
Γ	[]	Circulation
φ	[]	Sweep angle
AR	[]	Aspect ratio
b	[m]	Span
BPR	[]	Bypass ratio
C_D	[]	Drag coefficient
C_L	[]	Lift coefficient
c_{strut}	[]	Chord depth of the strut
D	[N]	Drag
e	[]	Oswald factor
L	[N]	Lift
L'	[Nm^{-1}]	Lift per unit span
M_N	[]	Mach number
m_{TOM}	[kg]	Maximum takeoff mass
m_{wing}	[kg]	Wing mass
m_{ZFM}	[kg]	Maximum zero fuel mass
n_{ult}	[]	Ultimate load factor
S	[m^2]	Reference area
SFC	[$kg h^{-1} N$]	Thrust specific fuel consumption
t/c	[]	Thickness to chord ratio
V_∞	[ms^{-1}]	Free stream velocity
w	[ms^{-1}]	Downwash velocity

1 Introduction

We are searching for some kind of harmony between two intangibles: a form which we have not yet designed and a context which we cannot properly describe.

(Christopher Alexander)

Within his book “Notes on the synthesis of form,” the architect Alexander [1] outlines some of the difficulties faced by designers during the creative process of developing a new product. Development in such a case can be substituted by synthesis, i.e., the process of determining a product’s form from the context it is supposed to fit.

Alexander’s work was a major driving force of the introduction of design patterns and has hence had great influence on software development. Design patterns describe an abstract process for solving design tasks. One might argue that Alexander therefore implies that the automation of design tasks is possible because the solution to each design task can be reduced to a predefined pattern; however, this is a contentious statement among engineers.

Influenced by the work of Alexander, the following section of this chapter outlines the current situation in aircraft design and the subsequent section derives the problem statement that led to this research. Thereafter, the scientific approach is explained in more detail. Finally, the last section of this chapter provides an overview of the structure of this dissertation.

1.1 Situation

Aircraft design is an example of development of a highly complex product, and the gap between *form* and *context* spreads widely. In engineering, *form* and *context* are better known as “configuration” and “requirements,” respectively. A configuration describes the specific, technical arrangement of components to fulfill a set of requirements, and hence, the term “configuration” encompasses the overall geometric layout as well as all internal aspects of the aircraft such as the system layout. The development of an

aircraft configuration involves several process steps. When a new configuration finally takes off for the first time, several years, or even decades, may have passed since the time of definition of the first requirements.

As shown in figure 1.1, in the context of the present study, the design process is grouped into different stages: definition of the top level aircraft requirements (TLAR), conceptual design, preliminary design, and finally, detailed design and entry into service (EIS). Apart from the requirements, which should be independent of the design process, bi-directional interactions occur at all levels of the design process more often than not in an iterative fashion. The focus of this study is limited to the interaction among requirements, conceptual design, and preliminary design.



Figure 1.1: Simplified design process

Requirements

From a manufacturer's perspective, a good design results in an aircraft configuration that generates high incomes at a low production cost. Consequentially, requirements are derived mostly from customer demands. Airlines, as the operators (and often owners) of the aircraft, decide to invest into a new aircraft configuration in accordance with their economic and ecological goals. The operator's decision is constrained by other stakeholders of the air transportation system, such as the airport, air traffic management agencies and regulatory agencies, as outlined by Weiss et al. [138]. However, the designer seldom has a major impact on the requirements, as these stem from a context he/she can hardly influence. At the most, the designer assists with the adaption of the requirements so that a proposed aircraft configuration may exploit its potential to the best possible extent. This is, more often than not, an iterative process.

The most important requirements relate to the number of passengers and

the design range and belong to the performance properties of the aircraft. These requirements are key factors for satisfying the requirements of the airline's market. Other properties such as the cruise speed, expected maintenance cost, cabin flexibility, and fuel consumption differentiate the quality of a configuration.

In some cases, strategic decisions produce requirements that are merely connected to performance characteristics. For example, some products are designed for commonality rather than for optimum performance, e.g., a mid-range aircraft family. Furthermore, strategic decisions may be related to technology development and emerge as additional requirement, e.g., the introduction of CFRP materials. It is therefore possible that requirements are not preferentially driven by primary product properties, e.g., operating cost.

Conceptual Design

As the name suggests, the goal of conceptual design is to derive a concept, i.e., to select and size an aircraft configuration that promises to be the most valuable candidate for the given requirements. Therefore, La Rocca [68] defines it as a diverging process. At this design stage, a multitude of concepts are derived that are subsequently compared, developed, and selected. The results of conceptual design include an overall geometric description, performance properties such as fuel consumption, and a first estimate of the mass breakdown. Subsequently, the design process continues with models of increasing fidelity that are applied to fewer concepts.

Given the fact that only a small amount of information, i.e., the requirements, is available, conceptual design may include only simple methods. For example, conceptual design applies empirical methods that rely on historical data, e.g., a wing mass estimation based on the wing planform. In addition, simplified physics-based methods such as the general range equation facilitate the quantification of the aircraft characteristics.

As the baseline concept(s) originates from the conceptual design stage, important strategic decisions are made at this point. For example, the fuselage diameter and shape are crucial design variables that need to be fixed early in the design process and have a large impact on the overall design.

As pointed out by Stark et al. [130, 11] large sums allotted to the overall development cost are fixed along with these decisions.

Preliminary Design

Since conceptual design provides more detailed information to the subsequent preliminary design stage, it enables the use of higher fidelity analysis models. Preliminary design aims to derive the properties of the aircraft, e.g., lift over drag, from its characteristics, e.g., wing planform, that are a result of the previous design step. As the number of concepts that need to be evaluated is already reduced at the conceptual design stage, the computational cost per analysis in preliminary design may increase.

Hence, preliminary design employs mostly physics-based models. For example, wing mass estimations are based on beam- or shell-theory finite element models and rely on detailed characteristics, i.e., a sufficient geometric description and loads estimation. Three or six degree of freedom models are applied for mission analysis as well as stability and control. The level of fidelity in all other disciplines scales accordingly. In addition, disciplines and physical effects that are not part of conceptual design, e.g., aeroelastics, start to influence the aircraft configuration during preliminary design.

The design stage subsequent to preliminary design, detailed design, is already out of the scope of the present study. However, it is important to establish a differentiator between the two design stages. In preliminary design, the so-called primary structures of the aircraft are described by physics-based analysis models, e.g., a skin panel on a wing that is represented in a finite element model. Secondary¹ structures are usually expressed by empirics, e.g., hydraulic pipes and mounts, and hence, secondary structures are only included implicitly in the analyses methods. In detailed design, most of the components of the aircraft are modeled explicitly. The level of detail of the aircraft representation rises, and so does

¹ In accordance with the proposed aircraft configuration, different technical aspects may be examined at a higher level of detail at an earlier design stage. For example, the design of a *more electric aircraft* depends on a detailed system analysis prior to other aspects of that configuration. Hence, the distinction between primary and secondary structures of an aircraft needs to be adapted with respect to the configuration.

the level of confidence of the analysis, e.g., the accuracy of the mass breakdown.

Multi-Fidelity

With the interaction of the different design phases, the term multi-fidelity needs to be defined. Two different definitions of this term exist and need to be distinguished to thoroughly derive the problem statement.

A well-known definition and field of application for multi-fidelity is mono-disciplinary, i.e., limited to one domain of physical modeling. As an example of mono-disciplinary, multi-fidelity aerodynamic analysis uses models based on different levels of fidelity, such as vortex-lattice, Euler and RANS methods. An Euler method may be used to determine approximate properties of the configuration. Subsequently, at selected design points the more expensive RANS methods are applied to correct the initial results.

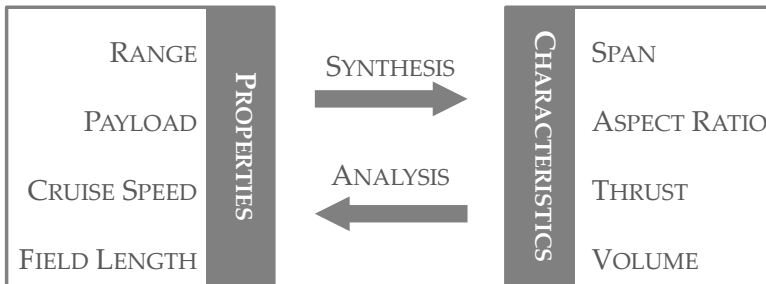


Figure 1.2: Interaction among properties and characteristics

This study applies an inter-disciplinary definition of multi-fidelity, which is based on the interaction of conceptual design (synthesis) with preliminary design (analysis), as shown in figure 1.2. Weber et al. [136, 137] specify the terms “analysis” and “synthesis” in an engineering context. Here, analysis deduces the properties of a product from its characteristics, and

synthesis executes vice versa². With the requirements taken as an initial set of properties, conceptual design derives the first characteristics of the aircraft, e.g., the wing reference area from the required takeoff field length. Preliminary design applies these characteristics to derive properties again, albeit at a higher level of detail, e.g., lift induced drag from the given wing planform. Several configurations with different characteristics may share similar properties.

1.2 Problem Definition

The existing design process assesses new technologies unreliably. In the initial phase, conceptual design often derives aircraft characteristics on the basis of assumptions that have origins in pre-existing designs, i.e., are historical-based³ and hence unreliable for evolving technologies. For example, Raymer and Roskam [105, 114] outline handbook methods for the thrust specific fuel consumption that relate to engines with small to medium bypass-ratios. State of the art technologies such as engines with high bypass-ratios can be described only by (often illegitimate) extrapolations of these methods.

For example, several handbook methods exist for the mass estimation of an aircraft's wing and chapter 4 discusses some of these in more detail. All of the available handbook methods take into account the sweep angle of the wing. However, the sweep angle is usually included in the form of one over the cosine of the sweep angle, and hence, the formulation is symmetric with respect to the unswept wing. While the handbook methods predict the wing mass of backward-swept configurations in a reasonable manner

- 2 The interpretation of "analysis" and "synthesis" is controversial. The word analysis originates from the Greek word *analusis*, i.e., to unloose or break something up. The Oxford Dictionary [131] defines "analysis" as a *detailed examination of the elements or structure of sth.* The contrasting term "synthesis" is defined as *the combination of components or elements to form a connected whole.* Weber et al. extend these abstract definitions to fit into the context of a design process.
- 3 The terms "empirical" and "historical" need to be distinguished clearly. The Oxford Dictionary [131] defines empirical as *based on, concerned with, or verifiable by observation or experience rather than theory or pure logic.* Hence, a decision driven by empirics during the design of an unconventional aircraft configuration may still result in a suitable solution; for example, an aerodynamics specialist may determine a well-designed solution for a wing-strut intersection based on his/her experience in belly fairings. On the contrary, a decision driven by analysis methods based on historical data and pure statistical observations cannot provide valid information for a design space outside of its initial data set.

and are proven by substantial data, whether the handbook methods are applicable for forward-swept wings remains questionable. Given the fact that a forward swept wing made from isotropic materials suffers from an angle of attack increase at the wing tip under positive loads (wash-in) rather than a decrease (wash-out) and that this effect must be countered by additional structures and hence weight, the symmetric formulation seems unreliable and prohibits extrapolation.

Technology factors are often applied to enable the assessment of new technologies. An increase in the bypass-ratio is a result of evolving technologies, and first assumptions of the engine performance based on technology factors may be possible. However, the application of simple technology factors alters existing design methods, but comes short of modeling physical dependencies. Whether or not radical changes in aircraft concepts, such as forward-swept or strut-braced wings, can be handled by technology factors remains questionable.

Since technology factors and extrapolation are no appropriate approaches for the assessment of new technologies and unconventional configurations, detailed physics-based analysis is necessary. These analyses are usually conducted at the preliminary design stage, posteriori to conceptual design. However, as preliminary design determines the properties of the aircraft based on the inputs derived at the conceptual design stage, the design process remains prone to errors.

A standalone application of physics-based analysis models fails on account of insufficient information⁴ being available in the very early design phases. Further, physics-based analysis is often time intensive and may be unsuitable for the number of design loops that are necessary to quantify the properties of an aircraft configuration. In this context, physics-based analysis models seldom cover the aspects of overall aircraft design. For example, a physics-based estimation of wing masses coupled with aerodynamic analysis provides detailed estimates of certain performance properties of the aircraft. However, this analysis step does not include any iterative design

⁴ In this context “complexity” may be a synonym for “information”. Torenbeek [135] states that *conceptual design is characterized by cyclic design improvements and complexity increasing in time*. As the increment may not only be in granularity, i.e., expressing a piece of information at a higher level of detail but also additive, i.e., taking into account pieces of information not available at the previous design step, the term “information” is chosen for this study.

loop, and hence, it is unknown whether the design is still valid and whether it fulfills the top level aircraft requirements or not.

In summary, physics-based analysis is necessary to reliably quantify the impact of new technologies and concepts in aircraft design, and it should be included as early as possible in the design process. However, two major obstacles to the implementation of physics-based analysis can be identified:

Information: The existing information gap between requirements and preliminary design needs to be bridged to enable physics-based analysis.

Time: Even if the information gap can be bridged, physics-based analysis remains extremely time consuming owing to the large number of evaluations necessary in conceptual aircraft design.

The goal of this work is to develop, test, and validate techniques to improve the quality of conceptual design methods to such an extent that these methods reflect the behavior of physics-based analysis. Furthermore, the low computational cost and preferentially, the high transparency of conceptual design methods will be maintained.

1.3 Solution

This study proposes the development of an extensible multi-fidelity loop that bridges the information gap between the conceptual design and preliminary design stages. In a subsequent step, the multi-fidelity loop is coupled to a surrogate modeling method based on symbolic regression. The workflow creates a global surrogate of the physics-based analysis part of the multi-fidelity loop at low complexity and high accuracy. The following sections outline the selected methods in brief.

Multi-Fidelity Loop

A seamless multi-fidelity loop, as depicted in figure 1.3, is proposed with the aim of bridging the information gap between requirements and physics-based analysis. It is composed of requirements, a central data model, a conceptual design model, and several higher fidelity physics-based analysis models.

The multi-fidelity loop starts from a set of requirements. These are a mix

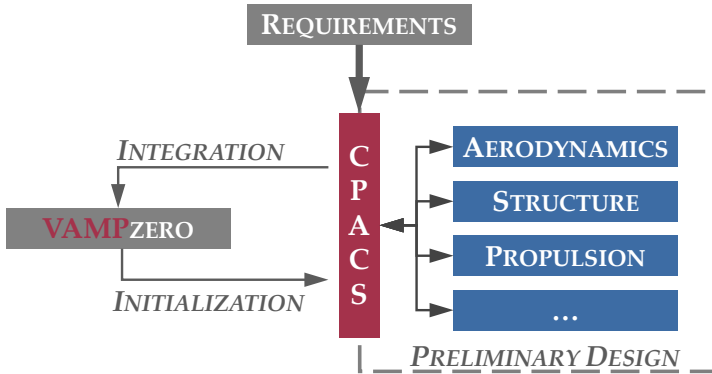


Figure 1.3: Closed multi-fidelity loop

of both properties, e.g., range and payload, and a few characteristics, e.g., wing sweep. The additional characteristics serve as constraints to define the location within the design space at which the design is performed. For example, the wing sweep can be included to examine the effects of forward swept wings, a technology on which research is ongoing but very few conceptual design models have delivered satisfying results. Without further definition of these constraints, the subsequent conceptual design would always drift toward a conventional aircraft configuration that fulfills the top level aircraft requirements, since no other solutions are available within its database. The constraints are often related to the aircraft geometry, but may include any technical parameter, e.g., the aspects of a hybrid laminar flow system.

The requirements are stored in a central data model that transfers information during all design steps. The model is known as the Common Parametric Aircraft Configuration Schema (CPACS), and its development was an ongoing task during the present study, as described in [15, 93]. A central model significantly reduces the number of necessary interfaces within the multi-fidelity loop. Figure 1.4 shows these benefits in comparison to an $n(n - 1)$ approach. CPACS stores not only product information, e.g., geometry, mass, and performance, but also process information, e.g., tool-specific settings such as convergence criteria. It is therefore possible for

analysis models to exchange information amongst themselves to control the development process, e.g., a thrust scaling for the engine performance map.

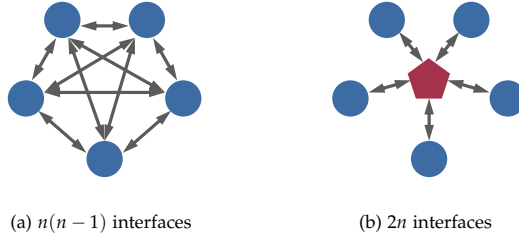


Figure 1.4: Uni-directional and central model approach

In the next step of the design process, a conceptual design is performed. In this phase, historical-based and simplified physics-based methods, also known as handbook methods, are applied. This complies with state of the art conceptual design codes such as FLOPS by McCullers [86] and PASS of Stanford University [6, 66]. At this stage, the properties and characteristics lead to the sizing of a new configuration. It can be assumed, that conceptual design methods return only disputable results for unconventional configurations as the design space explored is often outside of the underlying database of the historical methods. Hence, one of the key requirements of the conceptual design model is stability, i.e., return not necessarily accurate but sufficient information to trigger further analysis, as its results will in any case be overwritten by physics-based methods in later design steps. Therefore, it is more important to transfer the necessary information to bridge the gap toward the preliminary design stage than to obtain reliable results at this stage.

In addition to stability, flexibility is a key requirement of a conceptual design code in the context of this study. Conversely, flexibility is important due to the rapidly changing requirements of the aircraft design process, e.g., a design for a specified range or a redesign with a given fuel volume. Alternatively, at a later point of the study, the integration of results that have their origin in higher-fidelity analysis models requires dynamic changes in the behavior of the conceptual design model, e.g., the inclu-

sion of an aerodynamic performance map. Prior to this study none of the available conceptual design codes could satisfy these requirements.

The results of conceptual design describe a configuration, i.e., the overall geometric layout, mass and system breakdown, but they usually deliver insufficient information to trigger physics-based analysis. This is most noticeable for two-dimensional geometries (on a conceptual design level) and three-dimensional geometries (a necessity for most physics-based analyses). Therefore, the available information is transformed and extended to *initialize* the physics-based analysis by knowledge based engineering techniques. Along with the product information, process information is also exported for further analysis. In the course of this study, a new conceptual design model named VAMPzero has been developed that performs these tasks.

Several preliminary analysis models are connected to CPACS, most of which obtain sufficient input from VAMPzero. Zill et al. [141] demonstrated that these models can be triggered as either standalone (decoupled) models or in a complete design process. It is therefore possible to trigger analysis models individually without the overhead of an overall aircraft design process. Owing to the nature of preliminary design, the results obtained from the models are more detailed, e.g., engine performance maps or aerodynamic characteristics, and are a function of various other parameters.

Subsequently, results from the preliminary design level are *integrated* at the conceptual design level to reflect their impact on the overall aircraft design. In some cases this can be achieved by simple value replacements, e.g., overwriting the wing mass estimated by handbook methods with the result of preliminary design. In other cases, calculation methods need to be replaced, for example, to take into account additional information contained in an engine performance map. This leads to the replacement of the original conceptual design methods; for example the method that determines the thrust specific fuel consumption from the bypass ratio of the engine is replaced with a method that interpolates in the engine performance map. In this way, the detailed information of the physics-based analysis becomes interpretable on the conceptual design level.

With the aid of a multi-fidelity loop, the information gap between requirements and physics-based analysis may be bridged. Hence, at an early design stage, new technologies and concepts may be quantified reliably.

However, the computational cost of the process remains driven mostly by the physics-based analysis and may be very high for the large number of evaluations necessary in conceptual aircraft design. Hence, a subsequent step must address the obstacle of computational cost.

Surrogate Modeling

In the course of this study, surrogate modeling is applied to overcome the remaining issue of high computational cost of physics-based analysis. The idea is to construct surrogate models of the multi-fidelity loop and include them in the conceptual design model.

The proposed solution, termed multi-fidelity workflow, follows a sequential process of three steps: a) a design of experiments (DOE), b) the multi-fidelity loop and c) a surrogate model. The result is a surrogate model that reflects the behavior of physics-based analysis at very low computational cost and that is transparent and can be included in the conceptual design model. Figure 1.5 shows the structure of the workflow.

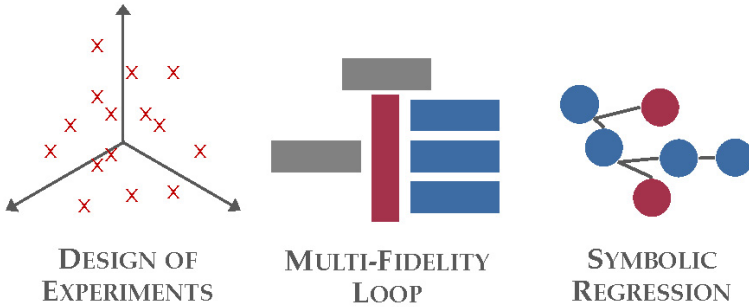


Figure 1.5: Components of the proposed multi-fidelity workflow

This workflow is explained on the basis of an example of a design study that quantifies the Oswald or span efficiency factor. Within a given design space, several wing geometries are explored by a DOE. The initial configuration is created by a conceptual design model and transferred to

a physics-based analysis model to determine the aerodynamic properties. The results are fed back to the conceptual design model to reduce their complexity and derive the Oswald factor. Finally, a surrogate is created that consists of a single equation that is included in the conceptual design model to quantify the Oswald factor of future designs. Once this process is completed, designers are able to assess configurations by physics-based methods at the conceptual design stage. Given the fact that the methods are physics- and not historical-based, estimations are also valid outside of the pre-existing design space. At the best, no additional inputs are needed and the change in runtime is negligible.

Design of Experiments

In the first step, a design space is explored by a design of experiments. The key requirement for a DOE is that the design space needs to be covered by a *space-filling* distribution of experiments to examine the underlying model behavior while maintaining the number of samples as small as possible to limit the computational cost. In other words the goal is to distribute as few measurements as possible in a multi-dimensional space while observing all effects within that space.

The designer defines the outer boundaries of the multi-dimensional design space; however, these boundaries may often arise from the underlying design concept. The DOE can be obtained from several algorithms or may be fed back from the surrogate modeling algorithm in an iterative fashion. Noticeably, many of the points within the covered design space may result in designs that are far from being a sensible aircraft configuration. However, these points are necessary to capture the behavior of the physics-based analysis method and hence foster the argument for a high stability of the applied analysis model.

Albeit beyond the scope of this study, several DOE algorithms are outlined in the subsequent chapters and will be evaluated in terms of their performance criteria in the context of the described problem definition.

Symbolic Regression

Several approaches for surrogate modeling are known and will be further investigated in the course of this study. As an outstanding candidate, symbolic regression is a recent type of surrogate modeling technique and promises to be a valuable solution to address the challenge of creating a surrogate model with high accuracy while maintaining the high level of transparency that is required in conceptual design.

In 2009, Schmidt and Lipson [121] distilled the equations for the laws of momentum conservation by applying symbolic regression to the measurements of angles and angular velocities of a double pendulum. No prior knowledge of geometry, physics, or kinematics was provided to the algorithm. Through the monitoring of a physical system, a formulation could be derived that not only described the behavior of the system but also granted insight into the physical coherence.

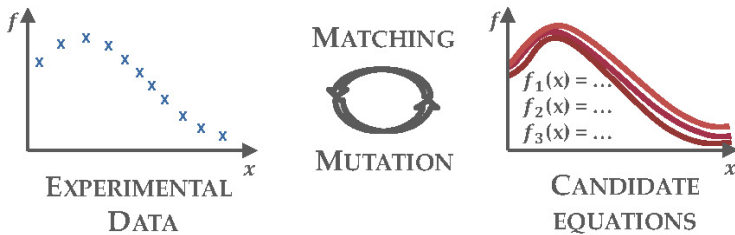


Figure 1.6: Schematic symbolic regression approach

Figure 1.6 shows a schematic of a symbolic regression approach. The goal is to find an equation $f(x)$ that fits to a set of experimental data that may originate either from a physical or a software experiment. Subsequently, an iterative process in the fashion of a genetic algorithm mutates and matches parameters via mathematical operators to fit the experimental data as well as possible. For example, if an equation for the Oswald factor is desired, then a database with the Oswald factor (property) and the wing geometry

1.4 Outline

parameters (characteristics) is used as the input for the symbolic regression. In addition, the permitted mathematical operators such as addition, subtraction, division, multiplication, and cosine, are specified. A genetic algorithm generates new sets of equations from the characteristics and operators and further modifies the most promising ones. The result is a Pareto front that includes both the accuracy and the complexity of the equations.

Finally, a new equation is the output of the regression. Unlike other regression approaches, symbolic regression returns human-interpretable equations that are not bound to a certain form, e.g., as polynomials. In this study, the multi-fidelity workflow is proposed to address the issues of the information gap between requirements and physics-based analysis and the high computational cost during the early design phases. The following main challenges need to be overcome to validate the applicability of the proposed approach:

- Establishment of a closed multi-fidelity design loop between conceptual design and preliminary design.
- Exploration of a global design space in an efficient and stable way.
- Generation of a surrogate model that reflects the behavior of a physics-based analysis while maintaining low computational cost and high transparency.

1.4 Outline

This document is organized as follows: The present chapter (chapter 1) describes the current situation in aircraft design and derives the problem formulation. It also presents an initial overview of the developed process. Chapter 2 describes the state of the art in conceptual and preliminary design. In addition, it provides an overview of existing approaches for multi-fidelity and surrogate modeling in aircraft design. The proposed process and its components are outlined in chapter 3. This chapter discusses newly developed components such as the conceptual design model. Chapter 4 applies the proposed body of methods to two design studies of a conventional wing in an unconventional domain of definition for the Oswald factor and the wing mass estimation. In both cases new equations are derived and compared to pre-existing design methods. Furthermore, an example

of a strut-braced wing configuration is discussed to prove that the multi-fidelity workflow is applicable to unconventional aircraft configurations. Subsequently, chapter 5 discusses the findings of the design studies. Finally, chapter 6 draws a conclusion and provides an outlook on promising future research topics.

2 State of the Art

Much of the development of a new aircraft concept involves not the design of the configuration itself, but the design of methods by which the concept can be analyzed and evaluated.

(Ilan Kroo)

In 2004 the AIAA Aircraft Design Technical Committee [133] acknowledged the fact that most of today's aircraft design is based on computer simulations. The previous era of try and fail, and experimental design have been overcome due to the increased understanding of physical effects and computing power. Despite the fact that physical testing is still necessary, design time and cost decrease significantly.

As stated by Kroo et al. [66], no design program is valuable without good analysis methods. Two distinctive sources for new analysis methods can be identified: First, if a new product technology, e.g., carbon-fiber-reinforced polymers, emerges then analysis methods are usually available from principal research. The introduction of these technologies and their associated analysis methods poses a challenge for the aircraft design process. Second, new analysis methods arise from new models of known physical phenomena, e.g., direct numerical simulations in aerodynamics.

In an integrated aircraft design process the mentioned analysis methods spread along different dimensions. Van Tooren and La Rocca [69] first published on these dimensions; figure 2.1 is similar to their representation. First, the *multi-disciplinary* nature of aircraft design needs to be mentioned. Different physical effects that are inherent to the functionality of the aircraft, e.g., the lift generated by a wing shaped surface and the bending of this surface due to the lift forces, need to be analyzed. Usually, these physical effects are spread throughout different disciplines, in this example aerodynamics and structures, and they are more or less intensively coupled.

The complexity and number of physical effects that need to be taken into account determine the necessary modeling effort and level of detail. Dur-

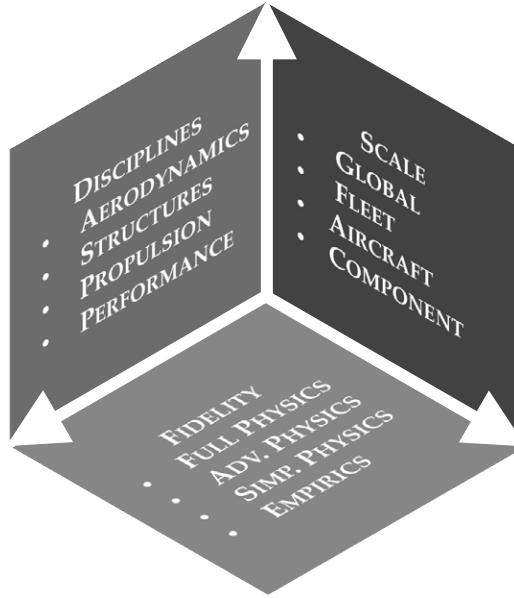


Figure 2.1: Dimensions of aircraft design

ing the course of the aircraft design the level of detail changes, and hence, *multi-fidelity* is a further dimension in the design process.

Finally, analysis methods stretch across the different scales of the air transportation system. Ticks on the *multi-scale* axis of the design process include components, sub-systems, and systems. At the initial stage of the evaluation of a new aircraft concept, the large scale effects are of greatest interest. Only a benefit for several stakeholders of the air transportation system justifies further research. However, reliable results on overall system level can only be given if the technology at survey is sufficiently modeled, often on component level.

The following sections elaborate on the state of the art of analysis methods during the different stages of the aircraft design process. Initially, an overview of **conceptual design** (section 2.1) methods is provided. On-going from conceptual design, the level of fidelity increases and multi-disciplinary analysis is split up into several separated analysis models com-

bined in a **design environment** (section 2.2). At this stage of the design, computational cost may be cumbersome. Therefore, **multi-fidelity** (section 2.3) procedures or **surrogate models** (section 2.4) need to be applied.

Each section lists not only state of the art publications on the topic but also tries to arrange publications into context. For this reason, each section outlines a set of performance criteria that aid in estimating the gains of the cited approaches. As a quantitative assessment of the performance criteria is not always sensible and in most cases beyond the scope of this study, a qualitative evaluation is provided.

2.1 Conceptual Design

In the previous chapter, figure 1.2 shows that conceptual design is a synthesis process. The top level aircraft requirements are defined prior to the conceptual design, and hence, they are the only information available on the new product at this stage of the design. The subsequent steps in the design process are preliminary and detailed design.

The goal of conceptual design is the selection and sizing of an aircraft configuration that fulfills the top level aircraft requirements and delivers as much benefit in terms of design goals, e.g., fuel burn or cash operation cost, as possible. Furthermore, analysis cycles need to be short as several design evaluations are necessary. Hence, as evaluation times need to be short and only little information is available, conceptual design applies rather coarse methods in comparison to advanced physics-based analysis models.

The most simple methods applied in conceptual design base on empirics, i.e., characteristics of the aircraft are determined from other characteristics by statistical, historical observations or correlations. Although physical dependencies may be at hand, the models are too simple to fully reflect these. For example, Raymer [105] provides equation (Eq. 2.1) to determine the thrust specific fuel consumption (SFC) of an engine. The equation depends on the bypass ratio (BPR).

$$SFC_{cr} = 0.88e^{-0.05BPR} \quad (2.1)$$

The equation is valid for a BPR up to 6, and hence, it is not applicable to

today's engine concepts. Furthermore, the SFC depends on several other factors. Section 3.1 provides further details on this aspect.

Slightly more complex methods base on simplified physics-based assumptions with empiric corrections. These equations can usually be solved analytically and are derived from more complex, physical models. For example, some wing mass estimation models use simplified beam theory or at least reflect similar sensitivities. These assumptions are still subject to simplifications, e.g., isotropic materials or static deflections. Hence, care needs to be taken when these methods are applied to assess the impact of new technologies. In addition, corrections that base on historic data are introduced to overcome the short comings of the simplified physics-based assumptions. For example, if the simplified physics-based estimation of the wing mass is only suitable to quantify the mass of the primary structure then empiric corrections include the masses of systems and secondary structures.

Shevell [127] provides a method (Eq. 2.2) to estimate the wing mass that fits into the described scheme. The second part of the equation multiplied by K_2 reflects the physical effects of bending moments acting on the wing. The first part of the equation introduces empiric corrections scaled by the wing's reference area S .

$$m_{wing,Shevell} = K_1 S + K_2 \frac{n_{ult} b \sqrt{m_{TOM} m_{ZFM}}}{(t/c) \cos(\varphi)^2 S} \frac{1 + 2\lambda}{1 + \lambda} \quad (2.2)$$

As can be seen from the examples above, conceptual aircraft design relies heavily on the use of empirics, and these are mostly derived from databases of existing aircraft. The dependency of the empirical methods on a database also leads to the term *historical-based* methods, as a lot of the information for a new design is based on information about pre-existing, i.e., historical designs. The use of empirics leads to several drawbacks:

- Availability of data
- Limited design space
- Limited technology options
- Non-optimum designs

First and most important, the data available for a database is limited. De-

tailed information on the aircraft characteristics and performance are the knowledge assets of each aircraft manufacturer and airline, and hence, only limited amounts of data are available on the overall aircraft performance, e.g., payload range diagrams and geometric characteristics. However, detailed information, e.g., the wing mass, is not publicly accessible. Even if the quality of the publicly available data is high, a hypothetical statement, whether enough data can be gathered in the first place remains questionable.

As already mentioned in chapter 1, conceptual design is supposed to be a diverging phase of the design, i.e., a variety of different concepts and technologies needs to be assessed. Whether reliable assumptions on new aircraft configurations, e.g., forward swept wings, are possible if these rely upon historical-based methods, which only include backward-swept wings, is arguable.

Furthermore, empirical methods are limited to existing technologies, and hence, they are inappropriate to predict the properties of a new aircraft configuration. Technology factors may be applied to circumvent this shortcoming. However, chapter 1 already outlined the drawbacks of this approach.

Finally, a database reflects rarely all the design decisions that influenced the aircraft design. In this context, non-optimum aircraft describe aircraft that are not sized by any of the classical design goals such as fuel burn or cash operating cost or aircraft where the rating between different design goals is unknown. For example, product families generate several points in a database. However, these designs are usually driven by manufacturing issues and not by classical design decisions. For example, all aircraft of the A320 family rely on the same wing⁵. From a manufacturer's point of view this is a sensible solution and it also allows for lower aircraft prices and maintenance, repair and overhaul (MRO) for the airline. If empirics are applied that rely upon a database featuring non optimum designs then the decisions that influenced their design need to be included in the empirics and the later design process.

Several computer codes for conceptual aircraft design exist. These have their origins both in academic and industrial developments. The present

5 The high-lift system of the A321 differs from all other aircraft of the family. However, this change occurs at a level of detail that is rarely available in conceptual aircraft design.

Criterion	Description
Flexibility	The ability to adapt the solution path of the conceptual design
Transparency	The capability to trace qualitative and quantitative physical dependencies
Extensibility	The ability to further extend the calculation methods and hence increase the number of physical effects taken into account
Automation	The capability to automate most of the design steps to allow an efficient exploration of the design space

Table 2.1: Conceptual aircraft design performance criteria

study examines some of the publicly available codes. Several additional solutions may exist within aircraft manufacturers⁶. Table 2.1 outlines major performance criteria for conceptual design codes. However, the presented list makes no claim to be exhaustive.

Flexibility is a key requirement for conceptual aircraft design codes as the design tasks can drastically change. For example, the calculation of the aircraft payload-range capabilities is often subject to changes. The payload-range capabilities are either the boundary conditions for a new aircraft design, or they need to be derived for a refitted design, e.g., in case of a new engine option. In each case the flight performance calculation needs to be evaluated in different ways.

Simplifications are an insurmountable characteristic of conceptual aircraft design. Physical effects are neglected due to these simplifications, and the results of a conceptual aircraft design need to be critically evaluated. Hence, transparency is an important criteria for conceptual design, the solution path needs to be (re-)traceable, and the applied calculations need to be well documented to verify the results.

Furthermore, a conceptual design code needs to be extensible. New technologies often influence the aircraft design process. Hence, means to extend the conceptual design code to reflect these technologies are important.

6 Given the fact that a manufacturer has a large amount of data on aircraft designs available, the accuracy of these codes is supposedly high. However, these codes are of course not available and may even be biased towards single design concepts due to the design philosophy of the manufacturer.

Examples include the application of technology factors or the replacement of existing design methods.

Finally, during the conceptual aircraft design step, several design evaluations are necessary and automation is important. Parameter studies and design optimizations benefit from a code that can be operated in batch mode.

From the aircraft design textbooks by Roskam [114], DarCORP developed the conceptual design software *Advanced Aircraft Analysis (AAA)*. AAA follows a classical approach to conceptual aircraft design that is separated into a first weight sizing, class I and II weight analysis and several disciplinary models. With the aid of an extended graphical user interface it is possible to interact with all parameters. When compared to other solutions, AAA captures an extended range of parameters and provides detailed feedback via plots and tables.

McCuller [86] coupled a set of tools at NASA Langley to create the *Flight Optimization System (FLOPS)*. It comprises a combination of previously developed codes and new developments. Apart from the conventional conceptual aircraft disciplines, FLOPS includes also extended performance, noise and cost analysis models. FLOPS is run by namelist inputs and can easily be automated. As the database of FLOPS includes fighter aircraft as well as jet transport, it is suited for the design of several types of aircraft.

Research at the Institute of Aeronautics and Astronautics at RWTH Aachen resulted in the *Multidisciplinary Integrated Conceptual Aircraft Design and Optimization (MICADO)* environment. It is described in several publications by Risse, Lammering, Anton, Franz, Peter, Sahai et al. [109, 7, 38, 39, 70, 71, 72]. The code focuses on a white sheet approach that enables the design of a new aircraft based only on design requirements⁷. The calculation flow is mostly conventional, but also includes parallelized elements. The development focuses on a modular and extensible architecture. MICADO follows a central model approach that splits product and process information. The aircraft is modeled in a data exchange file, whereas all analysis models receive their tool-specific inputs via configuration files. The analysis models are fully parametric and object-oriented.

⁷ Given the fact that MICADO emphasizes on conceptual design, it is listed in this section of the literature review. In addition, MICADO features the characteristics of a design environment. Section 2.2 further elaborates on this topic.

Criterion	AAA	FLOPS	MICADO	PASS	RDS
Flexibility	+	+	++	+	+
Transparency	+	-	+	+	+
Extensibility	-	-	++	o	+
Automation	-	+	+	+	o

Table 2.2: Qualitative comparison of conceptual design models

In 1988 Kroo and Takai [132, 66] initiated the development of the *Program for Aircraft Synthesis Studies (PASS)* at Stanford University. Antoine et al. [6] show that PASS is also part of ongoing multi-disciplinary design analysis and optimization (MDAO) studies. PASS includes a knowledge-based system that supports the designer during the design process as it checks several design rules. An outstanding feature is the path generator, that enables the calculation of certain parameters throughout various levels of the code. This is established by tracing variable names in the code’s documentation.

Partly based on the text book by Raymer [105], the Conceptual Research Cooperation developed the *Raymer Design Software (RDS)* for conceptual aircraft design. Raymer [106] carried out an extensive study on the applicability of RDS in MDAO applications. One of the outstanding features of RDS is the emphasis on an aircraft specific computer aided design (CAD) system, the *Design Layout Module*. Zhang et al. [139] showed that a transition from models created in RDS to computational fluid dynamics (CFD) meshes is possible. Hence, initialization for higher-fidelity processes is partly included. Other characteristics of RDS are advanced models, e.g., for trimmed flight, and a focus on the easy execution of trade studies.

Table 2.2 summarizes the cited conceptual aircraft design codes with respect to the performance criteria outlined above. It is close to impossible and certainly out of the scope of this literature review to derive a quantifiable metric. Hence, the table provides only a qualitative comparison.

In conclusion, the present section outlined the basics of conceptual aircraft design and listed existing computer codes. However, the listed conceptual design codes suffer from few drawbacks that prohibit their application in

the proposed multi-fidelity loop. The main drawback is their lack of sufficient multi-fidelity capabilities, i.e., means to initialize and integrate models of higher fidelity. Hence, a new conceptual design code, VAMPzero, is introduced in section 3.1.

2.2 Design Environments

As outlined in the previous section, it is rarely possible to reliably derive the properties of new aircraft configurations by so called handbook methods, especially if the design process includes unconventional configurations. In most cases, higher order physic-based analysis is necessary, as no reliable database is available for empirical methods. With a rising level of detail of the analysis models, e.g., from vortex-lattice up to Navies-Stokes, designers need more experience and expertise to master a) the underlying physical principles and b) the complexity of the simulation tool. It is obvious that a single person can and should not handle more than one or two disciplines in a physics-based design environment. Since neither is it desired, nor does the trend call for a "super-user" of monolithic codes, the next logical step is collaboration in MDAO to facilitate an environment of several, distinctive experts. Kroo [65] defines the term 3rd generation MDAO to describe these collaborative, distributed design environments.

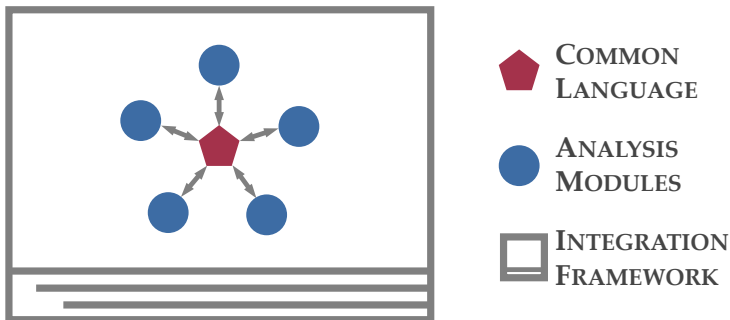


Figure 2.2: Design environment

Design environments are subdivided in three components, as shown in figure 2.2. These cover the integration framework for process control and optimization, a data model for the exchange of information, and various, disciplinary analysis models.

An **integration framework** consists of two parts: First, the editor and visual environment for the creation, modification and access control of analysis tool chains. This graphical user interface provides some kind of workspace and enables process designers to interact with workflows. This encompasses the coupling of analysis models as well as interactions with the data model representations, regardless of whether textual, structural or geometric. In addition, there is the core logic that provides data transfer between remote components, management of intermediate and resulting data sets, and extraction and merging of partial data with the central data model. Further duties of the framework are convergence control and optimization.

Disciplinary expertise, and therefore, analysis capabilities are spread across the boundaries of institutions and locations. Hence, it is necessary to provide resources so that analysis models can be triggered remotely, e.g., designers must be able to interface an analysis model for aerodynamics at DLR in Braunschweig from a desktop in Hamburg. Design teams in distributed institutions benefit, as not only the product description is standardized but the coupling of analysis models is also similar. Furthermore, process information, as often coded in from of analysis chains, is exchangeable.

A **common namespace** is a key feature for efficient data exchange. The structure of the coupling of analysis models has a significant effect on the number of interfaces as shown in figure 1.4. Not only does the number of interfaces decrease but the analysis models also become more independent. Hence, changes in one model do not necessarily impact other models. The common namespace reflects the central information model of the design team and can be seen as the meta-model for all of the deduced analysis models.

A central model for a design environment, as described above, consists of two aspects: a) the schema definition specifies elements, attributes and their structural dependencies, and b) the data set holds the explicit content which is conform to the schema definition. Whereas the data set is mainly

Level	Description
0	Empirical, historical-based models for conceptual design
1	Low order, disciplinary, physics-based, e.g., beam representations, or semi-empirical models
2	Medium order, physics-based models, e.g., shell representations
3	High order, state of the art, physics-based models, e.g., RANS; execution can hardly be automated

Table 2.3: Level of fidelity classification

used for the exchange of information, the schema definition is applied for the documentation, model validation and model generation.

In accordance with the design task, a specific set of **analysis models** is required. These analysis models represent different physical effects that need to be taken into account. A common use case in MDAO is the interaction of fluids and structure for the design of a wing. The analysis models need to be compatible to the underlying data model. Furthermore, in most cases batch operability is preferred to enable an automatic execution. The analysis models return their results to the central data model. In addition, the analysis models need to enable an easy interpretation of the results by discipline specific representations, e.g., by plots such as pressure or skin thickness distributions.

Design environments are mostly applied at the preliminary stage of the aircraft design. The level of fidelity of the applied analysis models is therefore beyond the often empiric based calculations executed in conceptual design. How to specify levels of fidelity is a highly discussed topic in the research community⁸. Bartholomew [9] developed a classification that is applied in the scope of this study and table 2.3 shows Bartholomew's classification that is extended by an additional level 0 to take into account conceptual design methods⁹.

- ⁸ The terms *order* and *fidelity* need to be distinguished: An analysis of high order describes a physical effect in high detail. Conversely, an analysis of high fidelity predicts properties accurately. Despite the establishment of the term multi-fidelity, the former interpretation is in fact more common, even though an analysis with low order might return results of high fidelity.
- ⁹ Robinson and Martin [113] present a classification that is also grouped by different disciplinary levels of fidelity. However, their classification extends beyond the scope of this study as the design studies that are outlined in chapter 4 only addresses few disciplines.

As already mentioned, the expertise and experience of a single user is rarely sufficient to handle a complete design environment. Various analysis models are a part of the design process and demand detailed knowledge. In addition, the process itself is a complicated representation of engineering knowledge. Hence, the definition of a design environment needs to be extended to include the roles of the different experts. Berends et al. [10] and Moerland et al. [91] developed schemes for user roles in design environments. The definition of Moerland et al. [91] defines three key user roles: system expert, process integrator and operator.

System experts have detailed disciplinary knowledge about a system of the aircraft. They usually provide access to one or more analysis models related to their field of expertise. Furthermore, system experts discuss interfaces with each other. They deliver input for design decisions and aid in the interpretation of the design process results. For example, an aerodynamic system expert provides an analysis model at the appropriate level of fidelity for the aircraft configuration under examination. In addition, the expert interprets the aerodynamic properties of the configuration and may suggest changes to the configuration.

Process integrators create, guide, and survey the design process. They have a general understanding of the affected disciplines, physical effects, and good communication skills to exchange information with system experts. The process integrator's task is to couple analysis models of different disciplines to cover all physical effects relevant to the aircraft configuration under examination.

Operators are the product owners in the design environment. They define requirements, constraints and target functions for the design process. In the hierarchy of the design team, operators are superior to process integrators and system experts, hence they need to foster and support their collaboration. While a general disciplinary knowledge similar to the process integrators is necessary, no detailed technical skills are required for operators.

Influenced by the works of LeDoux et al. [73], table 2.4 presents a set of performance criteria for design environments. The criteria are supplemented by the experiences gained in the *Virtual Aircraft Multidisciplinary Analysis and Design Processes* (VAMP) project of DLR, see Nagel et al. [94]. The following paragraphs introduce several existing design environments, both

Criterion	Description
Scalability	The capability to fit available schedule requirements and computing resource availabilities for the optimization problem
Flexibility	The ability to choose from a variety of solvers and other computer aided engineering tools
Extensibility	The capability of the system to grow through refinement of existing capabilities and the incorporation of new ones
Accessibility	The ability easily operate and retrieve information about the system at all stages of the execution
Transparency	The capability to document and further derive information from a given design process

Table 2.4: Design environment performance criteria

from research and industrial background. Subsequently, a qualitative comparison is provided.

Heinze [46] is the initial developer of the PrADO design environment. Despite the rather monolithic structure of PrADO, it is still in use in several academic aircraft design projects. PrADO couples up to 17 disciplinary analysis models via a central data model. The analysis models are classified from level 0 to level 1. An interaction with higher order analysis and PrADO is outlined in section 2.3. Information in the data model is either calculated by PrADO, input from the designer, or takes on a default value. A distinguished execution of analysis models is possible. Designers can interact with PrADO via a graphical user interface that can be seen as the integration framework. PrADO is not capable of multi-user operations and distributed computing. As all code is compiled into a single program the flexibility is low.

Rizzi et al. [111, 110, 112] develop the *Computerised Environment for Aircraft Synthesis and Integrated Optimisation Methods* (CEASIOM). The initial deployment was founded within the European 6th Framework Programme *Simulating Aircraft Stability And Control Characteristics for Use in Conceptual Design* (SimSAC). CEASIOM is a framework tool for aircraft design that integrates several disciplinary analysis models and focuses mainly on stability and control. In addition, analysis models for aerodynamic analysis of level 1-2 and aeroelastics are included. In recent developments [18], CEASIOM adapts to CPACS as the central information model, and hence,

CEASIOM becomes more extensible. CEASIOM is available under a free-ware license and most of the code is written in Matlab. Hence, accessibility and transparency are outstanding.

Alonso et al. [2] introduce the *pyMDO* design environment that is completely coded in Python. The initial focus was to enable an unique interface to several disciplinary tools. As Python is utilized, the design environment can be created in a modern, object-oriented fashion while it maintains the possibility to include faster codes such as C++ or Fortran. The level of detail in the presented studies is high. For example, the design of a supersonic business jet aircraft is based on a coupling of CFD and FEM computations. Recent work, as published by Martins et al. [78], suggests that the development focus is set on optimization problems and algorithms.

OpenMDAO is another integration framework from the Python community. OpenMDAO is published under open source licenses and the core developers are funded by the *National Aeronautics and Space Administration* (NASA). Gray et al. [42] outline some details of the integration framework. However, an application of OpenMDAO in aircraft design yet remains to be published.

Herling et al. [47] present a design environment in commercial use, namely at Boeing. LeDoux et al. [73] further developed the *3-Dimensional Design Optimization Code* (3DOPT) into the *Multi-Disciplinary Design Optimization Framework* (MDOPT). The MDOPT environment enfolds aerodynamics, structures and stability & control and is set up modular to enable the integration of further disciplines. Most of the integrated analysis models comply with level 2. A dedicated data management facility handles the data model. All information is stored in a Structured Query Language (SQL) database and can be accessed via different libraries. Finally, a graphical user interface (MDO Manager) enables the designer to interact with the design environment.

Given the fact that the developers of MDOPT also published parts of the performance criteria in Table 2.4, MDOPT performs well for scalability, flexibility and extensibility. As there is a clear distinction between the three components of a design environment and some additional interface layers are available, the accessibility is high as well. Distributed computation is possible. However, with a low number of incorporated analysis models no distinctive focus for transparency can be identified.

Another design environment in commercial use is PACElab Suite. Schneegans and Ehlermann [124] published the only available literature. Further information can be obtained from the developers homepage¹⁰. PACElab Suite represents a blank design environment without analysis models. A highly customizable graphical user interface serves as integration framework. Data is stored in an internal XML representation. This data is filtered and depending on the use case only selected parts are presented to the designer. Customers may either integrate their own analysis models or buy prepared sets for aircraft design or flight performance from PACE. Common examples for analysis models in PACElab Suite can be classified as level 0 or 1.

In PACElab Suite designers design no workflows. Instead an advanced version of a solution path generator¹¹ is implemented. Each analysis model needs to define its in- and outgoing parameters. PACElab Suite tries to find a computationally efficient execution order that depends on these settings. One prerequisite for this solution is that analysis models can be reversed. From a mathematical point of view this is possible for all analysis models that can be solved analytically and are uniquely defined. If a numerical solution is necessary then an iterative approach is possible. Hereby, it needs to be taken into account that the iterative approach might fail if no suitable starting point can be found. From an engineering perspective not all analysis models can be reversed. For example, it is possible to empirically determine the wing's mass from the maximum takeoff mass but questionable whether this correlation may be used to determine the maximum takeoff mass from the wing's mass. Hence, in the author's opinion care needs to be taken when solution path generators are applied in conceptual aircraft design.

PACElab Suite is a state of the art design environment. Current development targets for a much better scalability. Flexibility and accessibility are supported by a well designed user interface, as expected from a commercial software. Accessibility is generally high, although data and analysis models can only be interfaced via different layers. The already mentioned

¹⁰ <http://www.pace.de/products/preliminary-design/pacelab-suite>

¹¹ Rudolph and Bölling [116] show an application for a solution path generator in airship design. Ait-Aoudia et al. [3] give further information on the details of solution path generators. The details of the implementation in PACElab Suite are not available.

solution path generator is the only drawback on a in other respects high transparency.

The development of an aircraft design environment within DLR started in 2005. During the initial TIVA project Liersch and Hepperle [75] developed the foundations. Nagel and Zill [93, 141] outline the evolution of the design environment in the VAMP project that collected various analysis models from throughout DLR and established processes for multi-disciplinary collaboration.

The common namespace of the environment is the already mentioned CPACS definition that is available as open-source. As CPACS is the standard for aircraft design information exchange among DLR's aeronautical institutes, a long list of disciplinary analysis models is connected to the design environment. Chapter 4 outlines some of these models as they are included in the design studies presented in this study.

Seider et al. [125] develop the integration framework *Remote Component Environment* (RCE). The framework is published under open source license and specialized for a design environment utilizing CPACS. It supports collaborative and distributed work. Current DLR projects extend RCE and CPACS to include the uncertainties that are an inherent component of every model-based design process.

DLR's aircraft design system covers all levels of fidelity and has been extended during the last years. Given the fact that the analysis models have been developed in the heterogeneous environments of several institutes and departments, the accessibility can not be compared to CEASIOM but it remains higher than in a commercial design environment. The aircraft design system benefits from the support of several professional software engineers and hence is superior in scalability and flexibility.

Finally, table 2.5 provides a qualitative comparison of the previously mentioned design environments. The comparison is based on the publicly available information and may be out of date but it is presented as means to clarify this literature review.

Given the fact that the VAMP design environment is based on a central model approach, it is the design environment of choice in the present study, as an initialized data set may be applied in several design studies. Furthermore, the multi-fidelity loop benefits as the different, disciplinary analysis

Criterion	PrADO	CEASIOM	MDOPT	PyMDO	PACelab	VAMP
Scalability	0	0	+	0	+	++
Flexibility	-	+	+	+	-	++
Extensibility	-	+	+	+	++	++
Accessibility	-	++	-	++	++	+
Transparency	0	++	0	+	++	+

Table 2.5: Qualitative comparison of design environments

models of higher fidelity can be triggered independently, and hence, computational overhead is avoided.

2.3 Multi-Fidelity

Different levels of fidelity are an inherent phenomenon of model-based aircraft design. Figure 1.1 shows a simplified design process from conceptual, preliminary and detailed design up to the entry into service of the aircraft. Obviously, as the design process evolves, the amount of information that describes the aircraft increases. The previous section describes different levels of fidelity for analysis models applied in a design environment, see also table 2.3.

Design engineers need to work across the borders of different levels of fidelity to establish a design process that is as continuous as possible. Hence, multi-fidelity has become a substantial part of MDAO. This section derives a classification for multi-fidelity and outlines applications in aircraft design.

A difference in the level of fidelity occurs in two types of models, physical and product, and is associated with changes in cost. First, the fidelity of the analysis model describes the complexity of the underlying **physical model**. With a rise in the complexity, more physical effects are taken into account and an increase in computational cost is likely. Furthermore, fidelity expresses the difference in complexity of the **product model**. The amount of information that describes the product model varies drastically, as can

be seen from the different stages of design, i.e., conceptual, preliminary and detailed design. A change in the fidelity of the product model can but must not be necessary to enable the application of a different analysis, i.e., physical model.

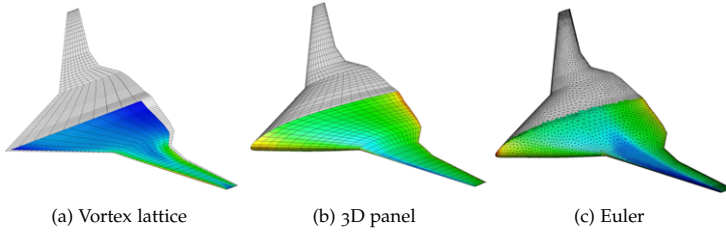


Figure 2.3: Levels of fidelity in aerodynamic analysis of a BWB

Figure 2.3 provides an example for different levels of fidelity both in product and physical models. All representations of the blended wing body (BWB) configuration have different levels of fidelity when the physical models are compared. The level of physical model fidelity increases from Vortex Lattice via 3D Panel to Euler calculations. However, the product model for figures 2.3b and 2.3c is identical. Both analyses base on the same geometric information¹².

It is difficult to translate between different levels of fidelity in the *product model*. A fine product model defined in a space with dimensionality m where m is greater than the dimensionality n of a coarse model can be reduced to the coarse model as a subset of the fine model, as shown in equation 2.3.

$$\mathcal{R}^n \subset \mathcal{R}^m \text{ with } n < m \quad (2.3)$$

During the translation process from the fine to the coarse model, information is lost. Buckingham [23] developed the Π -Theorem (Eq. 2.4); an algorithm that can be used for model reductions. The Π -Theorem states that a functional relationship f of physical quantities (x_1, \dots, x_n) can be reduced

¹² Of course, both analyses apply different meshes, i.e., discretizations of the product model. However, for a CFD calculation different levels of fidelity in the physical model, e.g., the turbulence model, are possible that base on the same mesh, i.e., the same product model.

to a functional relationship F of dimensionless quantities (π_1, \dots, π_m) . The difference between m and n is hereby defined through r as the rank of the dimensional matrix. The dimensionless quantities that now define the model are found from:

$$\pi_j = x_j \prod_{i=1}^r x_i^{-\alpha_{ij}} \quad (2.4)$$

Rudolph [115] applies the Π -Theorem to several product models. Obviously, the information lost is the physical scale of the product model. Any further reductions of the product model lead to a further loss of information.

The translation from coarse to fine product models can not be achieved without the use of assumptions. As assumptions often base on general engineering knowledge it can be possible to capture these in form of design rules. Hence, La Rocca [68] shows that it is possible to “*automate the generation of models*”. Design rules are grouped in so called Knowledge Based Engineering (KBE) frameworks and can aid engineers in the deduction of a finer model from a coarse product model.

As many evaluations of physical models are necessary during the conceptual design stage, e.g., in optimizations, it is preferential to reduce computational cost. In this context, a multi-fidelity algorithms applies for most of the evaluations a coarse analysis model, and only few evaluations of a finer analysis model are necessary to refine the results. A further decrease in the runtime can be achieved if surrogate models for either one or both of the analyses are applied. Section 2.4 provides an overview on this topic.

A distinctive group of multi-fidelity simulations is **mono-disciplinary**. These studies are related to a specific discipline, often aerodynamics, and focus on two or more levels of fidelity of physical models.

Oesterheld et al. [97] present a study that examines the influence of aeroelastic effects during the early design stages. A fine model for aerodynamics and structures, *Structural and Aeroelastic Analysis Module (SAM)*, is included in the *Preliminary Aircraft Design and Optimisation Program (PrADO)*. The SAM model is based on static and dynamic analysis using finite-element method and several analyses models for aerodynamic and aeroelastics.

Heinze [46] outlines the details of the coarse model in PrADO that is based on a beam representation.

Leifsson et al. [74] provide an example for the use of multi-fidelity for the evaluation of the transonic behavior of airfoils. In the course of their study, a coarse physical model is used for most of the optimization runs and the model is corrected by a cost-intensive fine physical model. The authors state that a 90% reduction in the number of model evaluations in comparison to direct optimization could be achieved. No change in the fidelity of the product model occurs.

In addition, March and Wilcox [77] published a study that focuses on the multi-fidelity evaluation of airfoil properties. In their study, several surrogate models of the fine physical model are examined, and a solution is developed that includes Bayesian calibration models. In this way, the number of calls to the fine physical model can be further reduced.

March and Wilcox participated also in a study that is presented by Kroo et al. [67]. The study focuses on multi-fidelity optimization of a supersonic transport aircraft. The models of different fidelity are A502/Panair, Cart3D and simple area rule estimations to quantify and minimize the resulting wave drag of the supersonic configuration. The study is further extended to take into account the uncertainty that arises if the optimization is based on surrogate models.

A different group of studies focuses on **inter-disciplinary** simulations in multi-fidelity research. These studies consider different phases of the design, i.e., conceptual and preliminary design, and hence, they are not only influenced by changes in the level of fidelity of the physical model but also by changes of the product model.

Choi and Alonso [26, 25] published studies that concern the multi-fidelity optimization of supersonic jets. The conceptual design model PASS, already described in section 2.1, represents the coarse model. The calculations in PASS base on experimentally derived data and a vortex lattice model. The study uses two fine models: The first increase in fidelity is established using the A502/Panair supersonic linearized panel code, and for even higher fidelity an Euler analysis is included. PASS encompasses a product model typical for the conceptual design level including wing reference area, span, quarter-chord sweep, taper and leading and trailing edge extensions. A 3-dimensional representation of the product model based on

CAD is necessary for the finer models. Surrogates for the fine models are constructed from quadratic response surfaces. It must be noted, that this surrogate is also included (at a later point) in the coarse model to replace the previous assumptions. However, the design space remains limited to the search space of the optimization run, i.e., the surrogate model is only locally valid. Despite the fact that these analyses are only applied to the aerodynamic properties of the aircraft, the change in the level of fidelity of the product model justifies the classification as *inter-disciplinary* work.

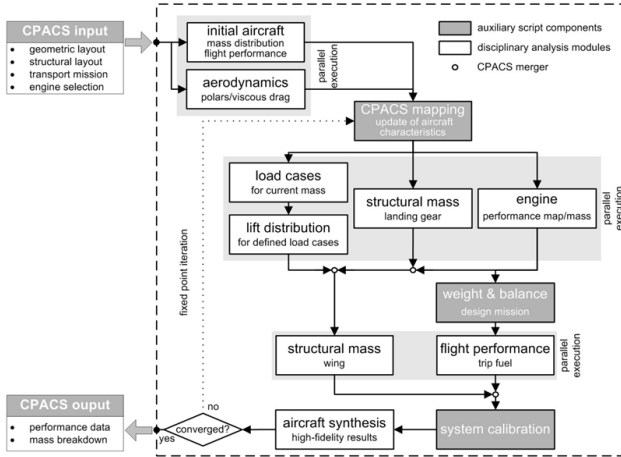


Figure 2.4: Collaborative aircraft design system, [141]

In the course of the VAMP project at DLR, Zill et al. [142] developed variable fidelity optimization techniques. The demonstrated approach includes changes in the level of detail of the product and process model, and it also spans across various physical disciplines. Zill et al. couple a coarse conceptual design model¹³ with a system of fine preliminary analysis models, as shown in figure 2.4. The fine models include aerodynamics, propulsion, wing structures, landing gear and flight performance analyses. Zill executes four different optimization strategies that vary the wing's geometric characteristics of a subsonic jet. In each case a bridge function between

¹³ Zill uses the aircraft design system at DLR and some of the components have been developed in the course of this study. Hence, the conceptual design model applied is VAMPzero and chapter 3 provides further information.

the coarse and the fine model is constructed. With the aid of the variable fidelity approach, the number of evaluations of the coarse model rises quickly from zero to 5112 while the number of evaluation of the fine models decrease significantly from 912 to 35.

While few other examples for multi-fidelity applications exist in the literature, the works from Choi and Alonso [26, 25] and Zill et al. [142] are the ones mostly related to this study. Choi and Alonso present the only study that to some extent re-integrates the fine model behavior into the coarse model. However, the design space they explore is limited and the re-usability of the surrogate model can be neglected due to the specific optimization task. Zill et al. demonstrate the first application that includes significant changes in the level of fidelity of the product model and the process model.



Figure 2.5: Motivations for multi-fidelity

Figure 2.5 identifies three key motivations for the application of multi-fidelity techniques: First, designers try to obtain a higher level of accuracy of their analysis by applying fine models. For example, the approach taken by Oosterheld et al. [97] is mostly driven by this motivation. In addition, the reduction of cost, as intended by Leifsson et al. [74], is a common target. Finally, multi-fidelity can be used to gain further insight as it can be used to make the behavior of the fine model available in the coarse model also at a later point in time. Choi and Alonso [26, 25] addressed this issue in a limited way and this motivation is the main driver for the present study.

While insight is the main driver for this study, the meaning of cost should not be neglected. Multi-disciplinary optimization may be applied to any formulation derived from the proposed multi-fidelity workflow. In this case the optimization may interact only with the conceptual design tool

without any calls to tools of higher fidelity. Any of the monolithic schemes mentioned by Martins et al. [80] can be applied for the optimization.

Hence, the runtimes for the optimization itself can be reduced drastically. However, one needs to take into account that the execution of the proposed multi-fidelity workflow prior to any optimization is time intensive (mostly due to the symbolic regression as will be further outlined in section 3.4), and hence, time benefits will only arise if several optimization tasks are carried out.

An added benefit for an optimization based on any formulation derived by the multi-fidelity workflow is that the formulation is based on an already iterated design. Hence, cost and the risk of non-converged designs is further reduced. This is linked to issues for large scale designs that were already mentioned by Kroo [63] more than two decades ago.

One characteristic that all of the listed approaches have in common is that they apply the multi-fidelity approach locally, often to find a single optimum. In contrast, the goal of the present study is to derive conceptual design methods from the multi-fidelity workflow that are valid in an extended design space, i.e., globally rather than locally. In this way, the results of the multi-fidelity analyses are preserved to permanently improve conceptual aircraft design also in later applications rather than being valid only for a single optimization study.

2.4 Surrogate Models

Section 2.2 introduces design environments that consist of several physics-based analysis models. The execution of these models leads to so called *High-dimensional, Expensive (computationally), Blackbox (HEB)* problems. Especially for applications such as optimization and parameter studies, the computational cost for the evaluation of a model often exceeds manageable time frames.

The previous section discusses multi-fidelity approaches that substitute an expensive, fine analysis model $h(x)$ by a cheaper, coarse analysis model $l(x)$ which reduces the necessary computational time and cost. Certain physical effects may be neglected in the coarse model to reduce the com-

putational time significantly. However, these simplifications contrast with a thorough evaluation of the relevant physical effects.

If the properties of the expensive, fine analysis model need to be preserved but the computational cost is too high then it may be replaced by a surrogate model $s(x)$. The surrogate or meta-model is a mathematical approximation of the original HEB problem. Once a surrogate model is sufficiently trained, it takes the same inputs as the fine model and provides similar outputs¹⁴, but it does not suffer from the computational cost of the original model. Simpson et al. [128] name three motivations to apply surrogate models:

- insight into the relationship between inputs and outputs
- faster analysis for optimization and design space exploration
- independence from computer architectures

The first two arguments, insight and speed, map to the previously mentioned motivations for multi-fidelity techniques. The last argument is still valid for very expensive calculations that require the extensive use of hardware, e.g., computer clusters or cloud applications. Most other analysis models can be ported to today's operating systems due to an ongoing progress in virtualization techniques.

The different kinds of motivations influence the decision for a specific surrogate model. Shan and Wang [126] developed an assessment scheme for surrogate models that is based on a list of performance criteria, see Table 2.6. Criteria like accuracy and flexibility are superior independent from the implementation motivation. A user targeting for reduced cost is interested in a high efficiency and smoothness, for example, if some form of gradient based optimization is a part of the problem. If a surrogate model is applied for reasons of better understanding then interpretability and transparency are the relevant criteria.

In a mathematical notation, the high fidelity analysis model is a function $h(x)$ where x is a vector of k input variables. The surrogate is then described by a function $s(x)$ so that:

¹⁴ Of course, the inputs of the surrogate model may consist only of a subset of the HEB problem inputs. As a matter of fact, the surrogate is (in theory) unable to exactly reproduce the outputs of the HEB problem since the behavior of the HEB problem is known only at selected points in the design space.

2.4 Surrogate Models

Criterion	Description
Accuracy	The capability of predicting underlying functions over a design space
Interpretability or transparency	The ability of proving information and interactions among variables
Flexibility or robustness	The capability to provide accurate fits for different problems
Dimensionality	The amount of data required to avoid an unacceptably large variance that increases rapidly with increasing dimensionality
Computability or efficiency	The computational effort required for constructing the model and for predicting the response for a set of new points by the model
Simplicity	The ease of implementation
Smoothness	The derivative ability of the model function

Table 2.6: Performance criteria for surrogate models

$$y = h(x) \quad (2.5)$$

$$\hat{y} = s(x) \quad (2.6)$$

$$y = \hat{y} + \epsilon \quad (2.7)$$

In this notation ϵ represents the error of the surrogate and therefore the difference between the model response y and the surrogate response \hat{y} . Generally speaking, three different error categories need to be taken into account, and table 2.7 provides the classification by Forrester et al. [36] for different types of experimental errors.

For example, human error arises from mistakes in coding or the handling of input values. Systematic errors occur if the chosen model does not reflect the relevant physical effects. However, the key point with computer experiments, i.e., the conduction of analysis models, is that systematic errors occur in the same fashion every time. Computer models are deterministic. Hence, random errors, as they occur in physical experiments, are neglected

Type	Description
Human	An error introduced simply by the experimenter's mistake
Systematic	An error occurring due to a flaw in the philosophy of the experiment that adds a consistent bias to the result
Random	An error which is due to measurement inaccuracies, e.g., inherent to the instruments being used

Table 2.7: Experimental error classification

when surrogate models are derived¹⁵. This is of importance when more advanced models like Kriging are elaborated.

It is necessary to obtain a set of initial data from the high-fidelity model $h(x)$ to construct a surrogate model $s(x)$. The initial data is gathered by a design of experiments¹⁶ where n samples of $x_{k,n}$ are used to evaluate $h(x)$. In a next step, a surrogate model approach is chosen that is then trained to the data to find $s(x)$.

Forrester et al. [36] introduce the so called *needle in the haystack* function (Eq. 2.8) that is the most simple surrogate model and hardly needs any model fitting. Obviously, the skills of the *needle in the haystack* function to reflect the behavior of the original model $h(x)$ are weak.

$$s(x) = \left\{ \begin{array}{ll} y_1 & \text{if } x = x_1 \\ y_2 & \text{if } x = x_2 \\ \dots & \dots \\ y_n & \text{if } x = x_n \\ 0 & \text{otherwise} \end{array} \right\} \quad (2.8)$$

Therefore, the *needle in the haystack* function serves as cautionary tale for a surrogate model. In the scope of this study, a subset of more sophisticated approaches is highlighted. These approaches include response surfaces,

¹⁵ Whether computer models provide smooth and deterministic inputs for a surrogate model is questionable. Especially, for numerical and iterative analyses the above statements are controversial. Forrester et al. [37] provide more details on this issue that is out of the scope of the present study.

¹⁶ Design of experiments is an essential and far-reaching part of surrogate modeling. Hence, for means of clarity no further information is included at this point. Section 3.3 describes the topic in more detail.

Kriging, and artificial neural networks. Where available, links to studies concerning aircraft design are presented in further detail. For further reading, Simpson et al. [128], Shan and Wang [126] and Queipo et al. [104] developed detailed reviews on surrogate models that include additional approaches. Jones [58] elaborates on a taxonomy for surrogate models in relation to global optimization problems and explains further details out of the scope of this literature review.

Furthermore, section 3.4 outlines symbolic regression, the surrogate model used within the course of this study. Section 3.4 links all presented approaches and symbolic regression to the performance criteria presented in Table 2.6.

Response surfaces

Box and Wilson [20] were the first to implement response surfaces. Usually, response surfaces are created from low, either first (Eq 2.9) or second (Eq. 2.10) order polynomials. Higher order terms are possible but often do not increase the quality of the surrogate due to oscillating behavior of the polynomials and the rising numbers of sampling points necessary to determine the coefficients.

$$\hat{y} = \beta_0 + \sum_{i=1}^k \beta_i x_i \quad (2.9)$$

$$\hat{y} = \beta_0 + \sum_{i=1}^k \beta_i x_i + \sum_{i=1}^k \beta_{ii} x_i^2 + \sum_{i=1}^k \sum_{j=1, j < i}^k \beta_{ij} x_i x_j \quad (2.10)$$

The regression coefficients β are found via least squares estimates that make use of the initially sampled data for x_i and y_i . As outlined by Sasena [119], equation 2.10 results in:

$$\begin{bmatrix} 1 & x_1 & x_1^2 \\ 1 & x_2 & x_2^2 \\ \vdots & \vdots & \vdots \\ 1 & x_m & x_m^2 \end{bmatrix} \begin{bmatrix} \beta_0 \\ \beta_1 \\ \beta_2 \end{bmatrix} = \begin{bmatrix} y_1 \\ y_2 \\ \vdots \\ y_m \end{bmatrix} \quad (2.11)$$

The above equation can easily be solved for β . The minimum number of sampling points n for a set of k design variables in a m order polynomial response surface that is fully determined is provided by the binomial coefficient:

$$n = \binom{m+k-1}{m} m! \quad (2.12)$$

Response surfaces have their most recent application in aircraft design for the quantification of the interference drag of a strut-braced wing aircraft. Duggirala et al. [32] examine several interactions of a strut-strut intersection. The authors explore a larger design space by CFD simulations and make the results available in form of a second order response surface.

Benefits of response surfaces include the low evaluation cost and the high smoothness of the data. On the contrary, response surfaces may not sufficiently capture the shape of the original function $h(x)$, especially for highly non-linear problems. Furthermore, the transparency of a polynomial that describes a reasonably complex physical phenomenon, especially in matrix notation, is low.

Response surfaces are a type of surrogate that is based on regression. Hence, the following sections refer to response surfaces by the term $r(x)$. In combination with interpolating methods that reproduce each sample point exactly, e.g., Kriging, response surfaces can overcome the shortcomings of a regression approach.

Kriging

Kriging¹⁷ surrogates are also known as *Design and Analysis of Computer Experiments (DACE)* from the inaugural paper by Sacks et al. [118]. The basic idea is a combination of the regression approach $r(x)$, as described above, and a correlation $c(x)$ approach. The surrogate is then written as:

¹⁷ Sacks et al. published the first application of the Kriging algorithm in combination with computer experiments. The algorithm is named after Daniël Krige [62], a South African Mining engineer. Matheron [83] published initially about geo-statistics and applied Krige's algorithm.

$$\hat{y} = r(x) + c(x) \quad (2.13)$$

The regression is usually of low order and not dominant in the behavior of the surrogate. The correlation model departs from this regression. As mentioned in the previous chapter, the correlation approach assumes that the error of the approximation model is a function of the design variable x . If one tries to predict the model behavior at a location x_j before any points are sampled then the function value is uncertain. However, it can be assumed that this uncertainty can be described by a random variable $Y(x)$ with a mean value of μ and variance σ^2 . Hence, the function provides a value that is within the range of $\mu \pm u\sigma$, where u is an arbitrary positive number.

Furthermore, it is assumed the function being modeled is continuous. If this is true then the function values $y(x_i)$ and $y(x_j)$ tend to be close for a small distance of x_i and x_j . This statement transfers to the statistic considerations in a way that the correlation of $Y(x_i)$ and $Y(x_j)$ is high if the distance of x_i and x_j is small. In Kriging this is usually expressed by the following basis function:

$$\text{cor}[Y(x_i), Y(x_j)] = e^{-\sum_{l=1}^n \theta_l |x_{i,l} - x_{j,l}|^p} \quad (2.14)$$

Equation 2.14 nicely reflects the behavior demanded above. If x_i equals x_j then the correlation of $Y(x_i)$ and $Y(x_j)$ is 1. On the contrary, if x_i and x_j are infinitively distant towards each other then the correlation tends to zero. The parameters θ and p assist in describing the model behavior in each of the k dimensions of the design space. θ determines the gradient of the relationship between the distance of the points in k and the correlation of the function value. p typically takes values between 0 and 2 and models the smoothness of the function.

All values for θ and p need to be determined to build a surrogate using the Kriging basis function. Commonly this is done by maximizing the *concentrated ln-likelihood function*. This approach makes use of the assumption that in an interpolating surrogate model of a deterministic computer model the modeling error ϵ can be eliminated. However, the further construction of

a Kriging model is complex and out of the scope of this literature review. Jones [58] gives an excellent explanation of the process.

Further details on Kriging can be found from Simpson et al. [128] and Sacks et al. [118]. In an earlier work Simpson et al. [129] compare response surfaces and Kriging approaches for the multi-disciplinary design optimization of an aerospike propulsion system. While both models return at a similar quality, the Kriging model is constructed on a linear base, where as the response surface needs a computationally more expensive second order polynomial.

A further application for Kriging in the field of aircraft design is presented by Koch et al. [60]. The authors build a model from FLOPS (see section 2.1) to evaluate the design of a high speed civil transport (HSCT) aircraft. The number of variables for the approximation models is large given the fact that several design variables and uncertainties are included in the study. The authors further argument that for these large numbers of variables Kriging is more suitable as response surfaces would require too many samples to determine all coefficients. Of course, this argument is valid only if the regression model of the Kriging approach is of lower order. However, the key argument remains valid: If too many evaluations are necessary to create a surrogate model then the cost savings may not be achievable.

Zhang et al. [140] apply Kriging to determine an aerodynamic database of the X-31 aircraft configuration. The database consists of a Kriging model that is build up from low- and high-fidelity aerodynamic analysis. Hence, their study can be classified as a mono-disciplinary, multi-fidelity analysis that is based on surrogate models. As Euler and RANS are the corresponding analyses methods, the level of fidelity is comparably high.

In comparison to response surfaces, Kriging models provide a significantly higher accuracy and robustness. Their key advantage is that each sample point is exactly reproduced. The argument of cost, i.e., computability and dimensionality, depends on the characteristics of the original model. However, the implementation of a Kriging model is rather complex. Furthermore, transparency is low as the number of basis functions and coefficients quickly increases and becomes unmanageable.

Artificial Neural Networks

Scientists model the human brain as a form of a biological neural network. It consists of a set of neurons that are interconnected via synapses. Through synapses signals are transferred from one neuron to one or several other neurons. Once the input at a neuron surpasses a threshold, the neuron sends further information by itself. Artificial neural networks try to model the workings of biological neural networks in a formalized and executable process.

McCulloch and Pitts [87] provide the initial description of a neuron for an artificial neural network. This simplification of a biological neuron is also known as a Threshold Logic Unit (TLU). A TLU takes a set of inputs ($x_i = x_1, \dots, x_k$). The inputs are summed up and if the sum exceeds a certain threshold then a signal (y) is passed on to the next neuron. Otherwise, no signal is emitted. Hence, a TLU is fairly similar to a transistor unit in a computer.

In comparison to the previously outlined approaches, an immediate advantage becomes obvious: While response surfaces and Kriging models try to model continuous data, an artificial neural network can easily describe a non-continuous behavior, e.g., a step function. For example, the fuselage diameter is a step function that depends on the number of seats abreast and the corresponding number of aisles.

Hebb [45] extends the TLU by a set of weighting factors. The weighting factors ($w_i = w_1, \dots, w_k$) are multiplied to each input value x_i . A set of exercises must be at hand to train the neuron, so that the inputs and outputs can be checked against the actual and expected behavior of the neuron. If the weighting factors and the threshold value change then a training or learning effect is established. Figure 2.6 displays a single TLU with inputs x_1, \dots, x_3 that is enhanced by weighting factors w_1, \dots, w_3 and a threshold value σ .

A full artificial neural network, as shown in figure 2.7, is constructed from a set of layers of neurons that interact with each other. The first layer of the neural network is the input layer where upon several hidden layers follow. Finally, the last layer delivers the output $s(x)$. Rummelhart and McClelland [117] established the most well known method to train neural networks, namely back propagation. In back propagation the measured er-

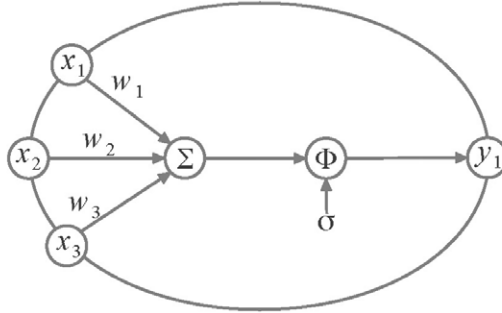


Figure 2.6: Artificial neuron

ror of the output of the neural network ϵ is propagated backwards through each hidden layer. At each layer the weighting factors and summation functions are altered to decrease the error.

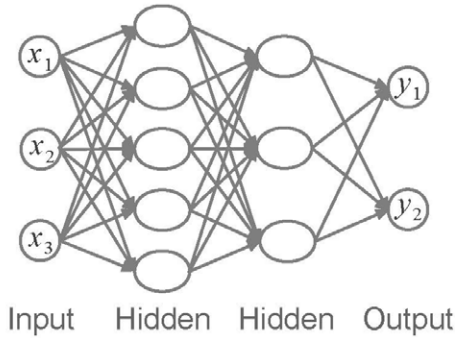


Figure 2.7: Artificial neural network

Patnaik et al. [98] apply artificial neural networks for the multi-disciplinary design optimization of a high speed civil aircraft. The analysis model replaced by the artificial neural network is the already mentioned FLOPS model. Extensive reductions of the computational cost could be achieved by the application of the outlined mechanism. However, due to the ever-

increasing computational power this part of Patnaik's paper is most probably outdated by now.

A recent application for artificial neural networks in aircraft design maps the pressure distribution from a CFD simulation to a FEM model of a UCAV model. Mazhar et al. [84] exploit the benefits of the artificial neural network to overcome the boundaries that arise from different meshing schemes in the high-fidelity analysis tools.

Finally, artificial neural networks benefit from the fact that effective training algorithms are available and that their evaluation can easily be parallelized. For example, each neuron could be hosted on a single core of a computer system. To some extent a neural network can be used as a representation of a symbolic function, and hence, neural networks are connected to symbolic regression as outlined in section 3.4. However, in the context of the present study, interpretability and transparency of a surrogate are key factors. An artificial neural network may present a certain transparency as its functionality can be broken down into each neuron. Nonetheless, for larger neural networks a simple representation or evaluation is not possible.

In the scope of the present study, symbolic regression is proposed as a valuable alternative to the described mechanisms for surrogate modeling. It needs to be proved that symbolic regression can outperform the existing approaches in terms of transparency while maintaining a similar or better performance in terms of model error. Hence, section 3.4 of the next chapter applies all mentioned surrogate models to different problems in aircraft design to reliably quantify their performance in comparison to symbolic regression.

3 Multi-Fidelity Workflow

The purpose of computation is insight, not numbers.

(Richard Hamming)

The book “Numerical Methods for Scientists and Engineers” written by Hamming [44] is a benchmark publication on physical models in engineering under the aid of computer science. This chapter outlines the proposed multi-fidelity workflow in more detail. The goal is to create a workflow that enables a better understanding of design problems in aircraft design, and hence, a workflow that results in insight rather than a set of numbers.

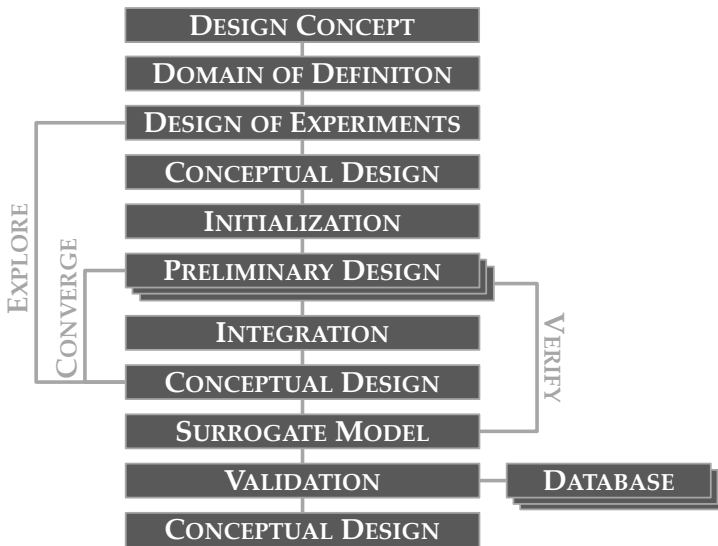


Figure 3.1: Multi-fidelity workflow

The design studies outlined in chapter 4 all follow a pre-defined workflow, as shown in figure 3.1. In the end, the conceptual design model is enhanced and able to describe a certain design aspect, e.g., the wing mass estimation,

by means of physics-based analysis in a given domain of definition at the speed and level of detail of a handbook method.

The first step is the choice of a **design concept**. The design concept describes a topology that is subsequently examined in further detail. For example, the strut-braced wing aircraft design concept consists of a high-wing configuration with a supporting strut, that in subsequent steps is examined parametrically, e.g., for different spanwise locations of the strut-wing intersection. In this stage of the workflow, the relevant physical effects need to be identified, so that appropriate physics-based methods can be selected.

The **domain of definition** describes a set of k design variables, i.e., dimensions in which the design can be explored, $x = (x_1, \dots, x_k)$ with upper and lower boundaries u_i and v_i for each x_i that parametrically describe an aspect of the design concept. The design variables need to be represented at the conceptual design level of detail. Furthermore, the physic-based analysis model (shown as preliminary design) needs to be sensitive to the design variables¹⁸. Of course, the domain of definition may not exceed the domain of definition of the physical model. The **design space** is the combination of the design concept and the domain of definition.

In a subsequent step, the domain of definition needs to be explored by means of a **design of experiments**. The DOE specifies a set of n samples $X = (x_{(1,1)}, \dots, x_{(k,n)})$ within the design space. The distribution of samples must cover the design space as completely as possible while keeping the number of samples as low as possible. Section 3.3 outlines the details of this step.

Subsequently, at each location in the DOE a first **conceptual design** is performed. The characteristics of the derived concept are identical to the values of the design variables. The methods applied in this step are still coarse and often historical-based equations. Section 3.1 outlines the principles of the conceptual design model used in this study.

As can be seen from figure 1.2, the conceptual design is a necessary step to derive initial information before a physic-based analysis model can be

¹⁸ It is not necessary for the conceptual and preliminary model to share identical inputs. During the initialization step the coarse design variable may have an impact on the product model that is forwarded to the preliminary design model. However, this connection must exist to circumvent unnecessary computational cost

triggered. Without sufficient information on the characteristics of the configuration, it is not possible to execute physics-based analysis. For example, if the wing mass needs to be calculated by physics-based means then it is necessary to calculate the loads acting on the wing. Hence, in this case global information, e.g., on overall aircraft masses, is an essential input parameter.

Obviously, the information available at the conceptual design stage is not sufficient to trigger any physics-based analysis model during preliminary design. For example, it is not possible to develop a reasonable finite element model from the few design variables that describe the wing geometry in conceptual design. Hence, **initialization** is a necessary next step in the workflow. During the initialization knowledge based engineering techniques are applied to derive sufficient information for a physics-based analysis. Initialization and integration are described in section 3.2.

In accordance to the design problem, one or more physics-based analysis models are triggered during the **preliminary design** phase. For each design study chapter 4 introduces these models, e.g., a vortex lattice method to determine the induced drag of the aircraft. Physics based methods benefit from the fact that their domain of definition is usually larger than that of historical-based methods.

However, the disciplinary analysis updates only some properties of the aircraft configuration and it is still necessary to take the effect of these changes into account. **Integration** is necessary to make use of the results of the preliminary design at the conceptual design stage. The integration enables the conceptual design to enhance its own calculation by the higher fidelity results obtained. Section 3.2 elaborates on two different approaches for integration: a) parameter replacement, and b) method replacement.

In the next step, the **conceptual design** is updated. It is important to note that an update in the conceptual design can lead to a change in the input set for the preliminary design. For example, if the preliminary design calculates a different wing mass, the overall masses of the aircraft will change, and hence, the loads on the wing change as well. As every other numerical design process, the multi-fidelity loop needs to be repeated iteratively. Once the multi-fidelity loop is converged, the outer loop continues with the next point of the design of experiments.

Finally, once all points in the DOE are examined, a **surrogate model** is

constructed. For this purpose, this study applies symbolic regression and section 3.4 provides further information on this step. It is important to **verify** the derived surrogate, i.e., ensure that the behavior of the surrogate is similar to that of the physics-based analysis. Therefore, additional evaluations are necessary to check the quality of the symbolic regression, and if necessary, introduce changes to the density of the design of experiments. The additional evaluations are placed at random locations within the domain of definition. The verification step is necessary from an academic point of view as it, at least to some extent, ensures that the surrogate model reflects the behavior of the physical model. However, in the course of an HEB problem, every expensive evaluation should be “spent” to train the surrogate model. Chapter 5 discusses this topic in further detail.

Of course, the surrogate model replicates only the behavior of the preliminary design models. As no a-priori validation of the multi-fidelity loop exists, in a next step further **validation** is necessary to prove the applicability in conceptual design. Hence, it must be shown that the disciplinary, physical behavior described by the surrogate model provides reasonable results in the context of overall aircraft design. For this purpose a database, as can be found in appendix B, is used to validate the surrogate model. The database holds details about civil aircraft from publicly available sources. The geometric characteristics and TLAR of these configurations serve as input for the conceptual design model enhanced by the surrogate model. In a subsequent step a conceptual design for all configurations is conducted that includes the derived surrogate model and the outputs for m_{TOM} and σ_{EM} are compared to the database. If the overall error remains within reasonable bounds then the surrogate model is included permanently in the conceptual design model.

As a matter of fact, the validation is only possible within the already existing boundaries of the historical-based methods. A validation in the extended design space is only achievable if further aircraft configurations are available.

Finally, the surrogate model is included in the conceptual design model to enhance the validity at the early design stage. For future applications, it is important to note the valid domain of definition for the newly developed method, a common shortcoming among available design literature.

The following sections highlight some of the necessary implementations to

carry out the above described workflow. Subsequently, chapter 4 describes three design studies that apply the workflow. The design studies substantially increase the domain of definition for aerodynamic and structural analysis of wing geometries in conceptual aircraft design. Furthermore, the last design study examines the properties of a strut-braced wing aircraft and it facilitates the design of such a configuration during the early design stages. Chapter 6 provides an outlook of other possible applications of the multi-fidelity workflow.

3.1 Conceptual Design

As the goal of this study is to enhance aircraft design by supplying physics-based analysis methods at the conceptual design stage, a conceptual design model is one of the core elements of the development. This section defines several requirements that a conceptual design model needs to fulfill to supplement the goals of this study. Subsequently, details of the implementation are highlighted.

Requirements

Primarily, a conceptual design model needs to fulfill three main requirements to be applied in the course of this study. It needs to provide means to:

- reflect the results of the study, i.e., include the physics-based surrogate models in the conceptual design model.
- examine the difference to existing methods, i.e., enable a comparison between physic- and historical-based analysis.
- close the multi-fidelity loop, i.e., initialize and integrate information from different levels of fidelity.

The surrogate models that the design studies (chapter 4) derive need to be included in a conceptual design model to enable design studies in the extended design space. Technically speaking, the source code must be adaptable. From a legal point of view this further implies that it must be allowed to change the code. This is only possible in self-written or open-source codes.

Furthermore, it must be possible to compare the physics-based surrogate models with pre-existing historical-based methods. The goal is to highlight qualitative changes, i.e., in the number of dependencies as well as quantitative changes, i.e., the magnitude of sensitivities at different locations within the design space.

Section 3.2 outlines the interaction of the conceptual design model with the higher fidelity, physics-based analysis models. While it is possible that a separate model initializes¹⁹ the multi-fidelity loop, the integration necessarily needs to be included in the conceptual design model as it influences the dependencies in the synthesis process. For example, if instead of a simple handbook equation a complex engine performance map is applied as means to quantify the thrust specific fuel consumption then several, additional parameters are necessary that need to be provided by the conceptual design model.

Section 2.1 examines several available conceptual design models and it can be seen that none of them fulfills the outlined requirements. Therefore, a new conceptual design model, namely VAMPzero, has been developed. VAMPzero is published under an open source license and the following section outlines some of the implementation details. Further information can be obtained from a previous publication [16] or the online documentation²⁰.

Object-Oriented Structure

Apart from the already mentioned requirements, VAMPzero is supposed to fulfill the requirements of a conceptual design model for the needs of MDAO to support the distributed design environment VAMP mentioned earlier. These requirements include a clear decomposition of components and disciplines of the aircraft so that VAMPzero is able to close gaps in higher fidelity MDAO processes. Furthermore, transparency, flexibility and

¹⁹ The initialization provides the necessary information for analysis models, and hence, most of the information is geometry related. Therefore, a separate initialization code might perform decently, e.g., it transforms a wing from conceptual to preliminary level of detail. However, further information is necessary for some of the operations during the initialization, e.g., weight and balance information to locate the landing gear and size control surfaces. This information becomes available at the conceptual design stage and for this reason the initialization is included in the conceptual design model.

²⁰ <http://software.dlr.de/p/vampzero/>

easy maintenance are required to enable a sustainable development. Therefore, the code uses an object oriented structure, as shown in figure 3.2.

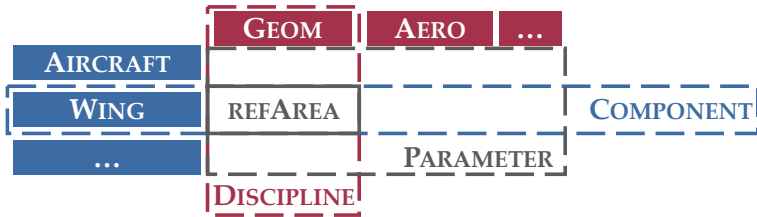


Figure 3.2: Object oriented structure of VAMPzero

Components in VAMPzero resemble selected physical systems of the aircraft, also the aircraft is listed as a component. Like systems of systems, components may be nested within each other, e.g., an aileron within a wing within the aircraft, resulting in the hierarchy of the calculation process. In each component the properties of the component are evaluated within several disciplines. Either a complete calculation or a component- or discipline-wise calculation is possible due to this setup.

At the intersection of disciplines and components, parameters are introduced in VAMPzero. For example, in the above figure 3.2 the component *wing* and the discipline *geometry* overlap. One of the parameters at the intersection is the *reference area* of the wing. While components and disciplines serve as means to organize the calculation, parameters hold the design knowledge coded as calculation methods.

As the design space of a calculation method is usually limited to a specific domain of definition or design concept, multiple calculation methods need to be available for the same parameter. For example, a different calculation method for the fuselage mass is necessary if the engines are wing or fuselage mounted (design concept) and if the slenderness ratio of the fuselage is either large or small (domain of definition). Furthermore, the design task specifies the order in which parameters need to be calculated. For example, whether the design range is an input or a desired result of the calculation, determines the way the mission fuel mass is calculated. VAMPzero includes several calculation methods in a parameter via a monkey patch. A monkey patch enables the dynamic exchange of functions

during the runtime of the code, i.e., VAMPzero always calls the *calc()* function of all parameters but the parameter itself is capable of exchanging its own *calc()* function. For example, the parameter reference area of the wing holds three different calc methods:

- *calc*: to decide upon the correct calculation method and replace itself.
- *calcGeometry*: to calculate the reference area from the span and aspect ratio.
- *calcWS*: to calculate the reference area from the maximum wing loading and the maximum take off mass.

If the *calc()* function of the wing's reference area is called then it determines whether the aspect ratio and the span are given as inputs, and subsequently, it exchanges itself with the correct *calc()* function. In the static code, both *calc* functions have different names. The first function is initially named *calc* and called by the overall calculation during the first iteration. It then decides depending on the input parameters to dynamically exchange itself with, for example, *calcGeometry()*. In the next iteration the overall calculation calls *calcGeometry* instead of *calc*. Pilgrim [100] and Hetland [48] provide detailed information on this process of dynamically changing the behavior of a code element during runtime. The inaugural paper on VAMPzero [12] highlights further details of the implementation.

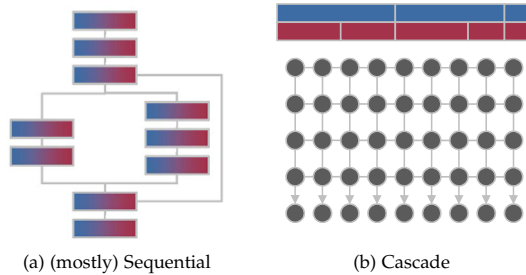


Figure 3.3: Calculation approaches in conceptual design

The object-oriented structure of VAMPzero implies that its calculations follow a different calculation scheme as conventional conceptual design models. As of before, conceptual design calculations followed a sequential ap-

proach over different stages such as a first weight sizing, a class I and II weight analysis, and other disciplinary models such as aerodynamics I and II. The sequential approach, as can be seen from figure 3.3a, suffers from two drawbacks: First, the structure of the calculation is rigid. It is therefore difficult to change the combination of input and output parameters. In accordance to the design task, e.g., design a new aircraft or determine the properties of an existing aircraft with re-fitted engines, the rigid setup can be cumbersome. Second, the convergence control of a sequential approach usually monitors only a few parameters, e.g., the maximum takeoff mass and the mission fuel mass. These parameters have a large influence on the properties of the aircraft configuration, and therefore it is questionable, whether the complete calculation is converged if a code monitors only these few parameters. For example, it is likely that the direct operation cost, an important parameter in many optimization studies, converges several iterations later, as it depends on both of the aforementioned masses.

VAMPzero provides a cascade-like calculation, as shown in figure 3.3b. During one iteration all parameters are calculated once. As all parameters can interact with each other at the same time, no issues from fixed in- and output settings occur. The calculation proceeds iteratively until all parameters are converged. Hence, the convergence of parameters that are downstream in the design process is ensured. It is likely that the cascade like calculation has a higher computational cost²¹. However, which of the approaches, sequential or cascade, provides the better overall convergence performance remains an item of future research.

Qualitative Dependencies

The object-oriented structure of VAMPzero enables it to automatically examine the dependencies between parameters. As the *calc()* functions can be replaced to fit to the design task, dependencies are dynamic and can not be found from static code analysis²². Whenever a parameter's *calc()*

²¹ The overall runtime of VAMPzero remains under a second on a standard desktop computer and can be further reduced for optimization tasks so the cost increase seems to be manageable.

²² For example, the design rules that Kroo [66] extracts from the documentation of PASS base on a static analysis. However, dynamic changes in the code can not be traced in this way. These dynamic changes become necessary either if the design task changes or if multi-fidelity operations are included.

function obtains the value of another parameter, VAMPzero logs this as a dependency. The result is a complete list of qualitative dependencies for the design process.

Figure 3.4 shows the qualitative dependencies for the reference area of the main wing. In the middle, the parameter under examination is shown. The right hand side shows all parameters on which the calculation of the central parameter relies, i.e., the wing's span and aspect ratio. The left hand side provides all parameters whose calculation relies on the value of the central parameter. If the wing's reference area changes then all parameters on the left hand side change as well. It is crucial to deliver this information to the designer to ensure his acquaintance of implications to the design due to changes he introduces.

The right hand side information can easily be gained from any textual representation of an aircraft design process, e.g., by looking up the method for calculation of the wing's reference area in a design handbook. The determination of all the influences of the wing's reference area is more challenging as it would require to examine the complete handbook for appearances of the reference area within an equation. Nonetheless, these observations are static as well, and hence, they are overloaded with unnecessary information.

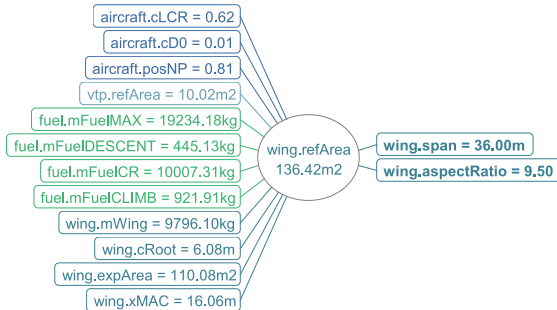


Figure 3.4: Qualitative dependencies of the reference area

Quantative Dependencies

If a designer knows about the qualitative dependencies in a design process then he can determine which parameters influence each other, and hence, he is able to judge whether the calculation method is appropriate for the design problem at hand. If the dependencies are not in agreement with his professional experience then the calculation method might be improper for the design task as it neglects certain physical effects. In a next step, it is important to examine the magnitude of the influence, i.e., the quantitative dependencies. Hence, information about the sensitivities at the design point is necessary. There are several possibilities to derive the sensitivity of a quasi-numerical calculation method.

Finite differences are a conventional method to determine sensitivities. Equation 3.1 is a forward-difference implementation of finite differences for a function $f(x)$ with step-width h and truncation error O . It is obvious that the result depends on the step-width. If the step-width is too large then the error of the sensitivity increases. Contrary, if the step width becomes too small then subtraction errors occur on a computer. Given the large bandwidth of numerical scales in conceptual aircraft design, it is hard to find a suitable step-width to estimate the sensitivities off all calculation methods.

$$\frac{\partial f}{\partial x} = \frac{f(x+h) - f(x)}{h} + O(h) \quad (3.1)$$

VAMPzero applies complex-step derivative approximation (CDA) to overcome these shortcomings. In the context of engineering applications, Martins et al. [82, 81, 79] first described this technique. It benefits from the fact that the analysis is independent from the magnitude of the step-width. At first the function, i.e. the calculation method under examination, is written as $f = u + iv$ and the complex variable $z = x + iy$ is defined. If f is analytic, i.e., differentiable in the complex plane then Cauchy-Riemann (Eq 3.2 and 3.3) can be applied:

$$\frac{\partial u}{\partial x} = \frac{\partial v}{\partial y} \quad (3.2)$$

$$\frac{\partial u}{\partial y} = -\frac{\partial v}{\partial x} \quad (3.3)$$

If equations 3.1 and 3.2 are combined then the derivative for u is written as:

$$\frac{\partial u}{\partial x} = \lim_{h \rightarrow 0} \frac{v(x + i(y + h)) - v(x + iy)}{h} \quad (3.4)$$

Given the fact that the quantitative analysis in VAMPzero targets for real values, equation 3.4 is further simplified by $y = 0$, $u(x) = f(x)$ and $v(x) = 0$. The following equation is therefore noted as complex step derivative approximation:

$$\frac{\partial f}{\partial x} \approx \frac{\Im[f(x + ih)]}{h} \quad (3.5)$$

As complex operations become necessary, the implementation effort of equation 3.5 is of course substantially higher than for equation 3.1. However, as VAMPzero is programmed in a dynamically typed language²³, the development overhead is low.



Figure 3.5: Sensitivities of the reference area

Figure 3.5 shows the sensitivities of the reference area of the wing as given by Equation 3.6. Obviously, the wing span has a larger influence due to

²³ <https://www.python.org>

3.2 Multi-Fidelity

the exponent. Furthermore, the reference area increases if the span rises. Hence, the span's bar in the above plot is larger than the bar of the aspect ratio.

$$AR = \frac{b^2}{s} \quad (3.6)$$

3.2 Multi-Fidelity

In the present study, the conceptual design model closes the multi-fidelity loop. Hence, it must be able to transfer information from its own coarse product model with a dimensionality n to a finer, mono-disciplinary product model with a higher dimensionality m and vice-versa.

The conceptual design model interacts with the physics-based analysis models via a central data model to close the multi-fidelity loop, see figure 1.3. In the direction of increasing fidelity it is necessary to initialize these models with the required product and process information. For example, initialization includes the generation of a 3-dimensional geometry definition as well as flow conditions for aerodynamic analysis.

In addition, in the direction of decreasing fidelity, the higher fidelity results need to be reduced to the level of detail available in conceptual design. For example, a conceptual design model works with discrete SFC values at certain points of the mission profile (climb, cruise, etc.) so that a detailed engine performance map needs to be reduced to the SFC values at these points. In this case, the coarse model can still access all information from the model of higher fidelity, and hence, no further error is introduced into the design. However, if not all information can be transformed to the coarse model then the coarse and the fine model need to be compared to quantify the arising error.

Initialization

The initialization of higher fidelity analysis models from VAMPzero's own data model requires a transition from $\mathfrak{R}^n \rightarrow \mathfrak{R}^m$ which can not be achieved without the use of assumptions. For this upward process La Rocca [68] pro-

poses the application of knowledge based engineering (KBE) techniques²⁴. These techniques are suitable if sufficient design knowledge in an engineering domain is available that can be coded in a set of rules. The next paragraphs provide an example for the initialization of the main wing geometry.

The main wing within VAMPzero is a single trapezoid, planar wing. Most available literature in handbooks gives equations for the analysis of such a simple concept. Within the equations correction factors balance the geometric inaccuracy. However, for the further analysis of jet transport concepts by means of physics-based analysis, a realistic double trapezoid wing including twist and dihedral is required.

Figure 3.6 shows the higher fidelity wing. The wing span (b_W), the leading edge sweep (φ_{25}), the aspect ratio (AR), the taper ratio (λ), and the kink ratio (η_k) describe the wing planform. The trailing edge from root to kink is perpendicular to the fuselage. The twist angle (ϑ) is applied in a linear distribution from root to tip. The thickness to chord ratios are varied in accordance to Schmidt [123] from root to tip. The dihedral folds the wing from the fuselage intersection onward.

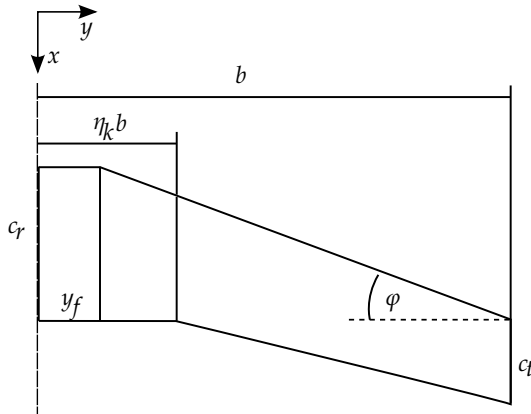


Figure 3.6: Double trapezoid wing planform

²⁴ A previous publication [17] on VAMPzero provides further details on the implemented knowledge based engineering approach.

Table 3.1 lists dimensionless parameters for the description of the geometry of the wing with the help of the Π -Theorem by Buckingham [23]. The complete process is outlined by Jepsen [55] in full detail. During the mapping to the fine product model, Π_1 to Π_4 are constant to assure geometric similarity to the single trapezoid wing. Π_5 and Π_6 are then derived for a constant wing reference area ($S = f(c_i, c_a, b, \eta_f, \eta_k, \varphi)$) and the provided fuselage diameter.

$\Pi_1 = \varphi$	$\Pi_2 = \tau$	$\Pi_3 = \lambda = \frac{c_a}{c_i}$
$\Pi_4 = AR = \frac{4b^2}{S}$	$\Pi_5 = \eta_k = \frac{y_k}{b}$	$\Pi_6 = \eta_f = \frac{y_f}{b}$

Table 3.1: Dimensionless constants

Similar approaches are applied to other parts of the geometry. Figure 3.7 shows an example for a geometry that is initialized by VAMPzero and exported to CPACS. For example, the fuselage in VAMPzero is modeled as a combination of cylinders for nose, cockpit, cabin, and tail. The fuselage is transformed by KBE technologies to standard geometry as it is usually employed in preliminary aircraft design.

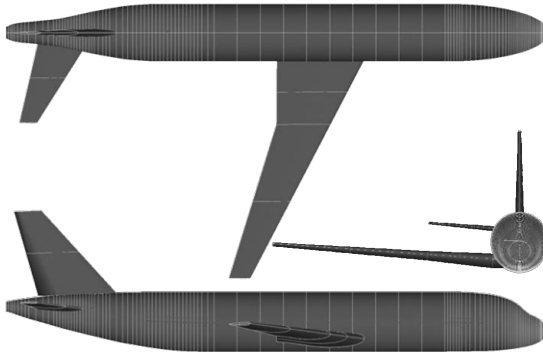


Figure 3.7: Three-dimensional geometry initialized by VAMPzero

Integration

While information based on engineering knowledge needs to be added in the process of initialization, integration reduces the dimensionality of the described information and hence information is lost ($\mathfrak{R}^n \leftarrow \mathfrak{R}^m$). However, the loss of information is still justified as it is the only way to enable conceptual design, and hence, a synthesis in the multi-fidelity loop. Two different approaches enable integration in VAMPzero; they are termed parameter replacement and method replacement.

In a **parameter replacement**, the information from a higher fidelity analysis model simply overwrites one of the parameters in the conceptual design model. In this case, the information is handled as an input parameter, and hence, the calculation of the conceptual design model for the specific parameter is overwritten. During the runtime of the conceptual design model no further calculations are necessary. For example, in VAMPzero the horizontal tail mass is quantified by a method from Raymer [105]. If more accurate information is available, e.g., from finite element analyses then the value for the mass is overwritten. The integration process needs to filter the appropriate value for the relevant cruise condition.

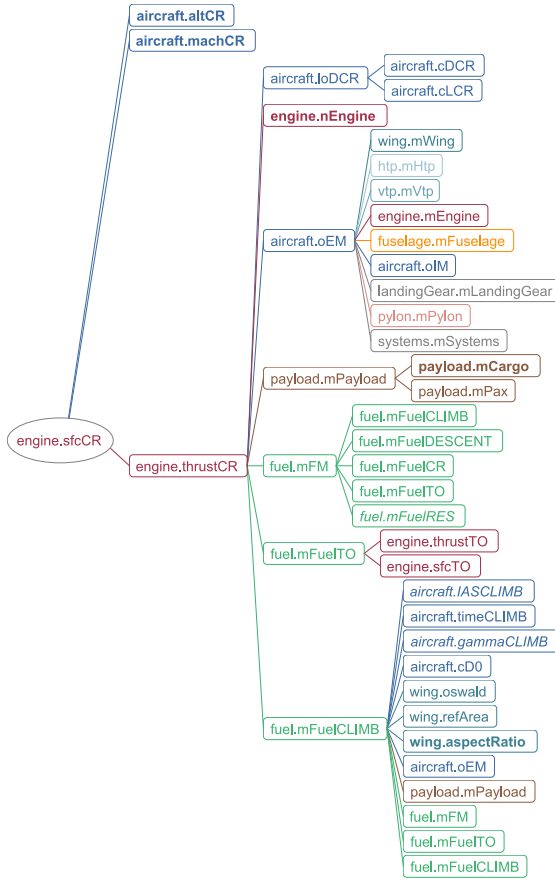
As the parameters in VAMPzero are fixed by a parameter replacement, similar to a user input, no right hand dependencies exist while the level of precision increases due to the higher fidelity of the imported data. If a **method replacement** is applied then it will change the right hand dependencies in the calculation. For example, mission analysis in conceptual design is based on a constant thrust specific fuel consumptions (SFC) in each segment. Equation 2.1 shows a dependency between the SFC and the bypass ratio of the engine. The equation, as mentioned earlier, is introduced by Raymer [105] and valid for bypass ratios up to 6. Obviously, the equation is based on simple empirics and not applicable for modern engine concepts, as these usually rely on much higher bypass ratios. Figure 3.8a shows the limited number of dependencies.

From a higher fidelity analysis model engine performance maps are available via CPACS. While the level of detail in the mission analysis remains unchanged the import of the engine performance map increases the fidelity of the calculation. The performance maps provide the SFC in relation to the altitude, Mach number and thrust. As VAMPzero makes use of a constant SFC, most of the information in the performance map is unused. How-

3.2 Multi-Fidelity



(a) Historic based



(b) Physics based

Figure 3.8: Comparison of level of detail of the SFC

ever, the qualitative dependencies increase (see figure 3.8b) and therefore the feedback that is provided to the designer is enlarged. In this exam-

ple, the thrust is a parameter that constantly changes during the iterative loop, and hence, it is not possible to include the SFC via a static parameter replacement.

3.3 Design of Experiments

One of the first steps in the multi-fidelity workflow after the design space has been chosen is to determine how the experiment is designed, i.e., determine the locations where analyses need to be conducted in the selected domain of definition. Historically, Fisher [34] is deemed to have first introduced the term *Design of Experiments*. This section provides a short introduction on different DOE algorithms and warrants the Latin-Hypercube approach applied in this study.

Given a function or computer model $f(x_1, \dots, x_k)$ with x_k input values the goal of a design of experiments is to examine the function in a domain of definition $x_i \in \mathfrak{R} | v_i \leq x_i \leq u_i$ in a representative way so that the behavior of f is sufficiently observed while maintaining an as low as possible number of samples to minimize computational cost. Thereby, u_i and v_i are the upper and lower boundaries of the domain of definition. Hence, the design of experiments results in an input matrix $X = (x_{1,1}, \dots, x_{k,n})$ with n samples. Generally speaking, two different ways for design of experiments exist: Deterministic and random sampling.

While deterministic sampling ensures an even distribution over the domain of definition, the number of samples usually rises quickly. One example for a deterministic design of experiments is a **full factorial** sampling plan²⁵ that examines for each dimension (x_1, \dots, x_k) a number of levels m . The number of samples results in m^k . Hence, $n = 64$ samples are necessary to examine the outer boundaries of a $m = 6$ level design for a simple two dimensional design space, say wing area and aspect ratio. If two additional dimensions are introduced to the domain of definition then the number of samples rises to $n = 4096$. Obviously, limitations due to computational cost may arise even if the cost of a single analyses run is low.

²⁵ Several deterministic alternatives to full factorial sampling plans exist. For example, Box and Behnken [19] introduce fractional factorial or Box-Behnken sampling plans. As full factorial design of experiments are a well arranged example, this review focuses only them as a representative for deterministic sampling plans.

In the context of the Manhattan Project, Metropolis and Ulam [90] introduced **Monte Carlo** simulation, a well-known example for a random sampling design of experiments. In a Monte Carlo simulation, the input values for $f(x_1, \dots, x_k)$ are randomly selected without further constraints. One of the benefits of the completely random sampling is that additional points can be added to the experiment at any time. On the contrary, it is not guaranteed that the random sampling spreads evenly across the domain of definition, i.e., whether it is *space-filling*. Hence, a large number of evaluations might be necessary to obtain a representative evaluation of the domain of definition.

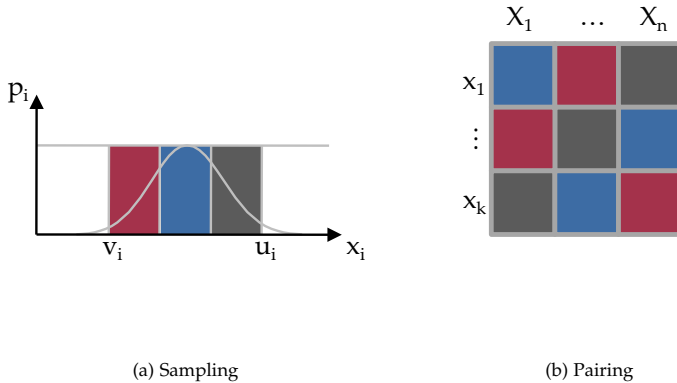


Figure 3.9: Latin square with three elements

In a later development, McKay et al. [88] and later Iman et al. [53] propose a random sampling technology that explores the domain of definition more evenly and is termed **Latin hypercube**. First, each dimension is sampled separately. The sampling is also based on random numbers but it divides the domain of definition of each parameter $v_i \leq x_i \leq u_i$ into n intervals. In each interval a random number is chosen that takes into account the probability density function of the parameter. As the input parameters in the scope of this study are based on characteristics of the product, e.g., the

wing span and the aspect ratio, a constant distribution of the probability density is assumed. If the input parameters include environmental factors, e.g., the crude oil price, then a non-constant distribution is advised. Figure 3.9a shows the sampling process both for a normal as well as for a constant distribution of the probability density function.

In the next step, the samples from each parameter are paired to form the input sets for $f(X)$. The n intervals of the k parameters are then combined via a permutation or pairing algorithms. Figure 3.9b shows a Latin square that illustrates the method applied in Latin hypercube sampling. For each input set $X = [x_{1,1}, \dots, x_{k,n}]$ different intervals from each factor x_i are chosen.

The core benefit of the Latin hypercube sampling is a distributed sampling across the domain of definition, at a relatively low number of samples. One drawback remains: As the number of intervals needs to be known in advance, additional points can not be added to the experiment posteriori. Current research in the field of design of experiments suggests that this drawback may be overcome, and chapter 6 briefly explains in which way the proposed multi-fidelity workflow may benefit from this research.

Assessment of Design of Experiment Algorithms

Three exemplary sampling plans X_{FF} , X_{MC} , X_{LH} for three design variables x_1, x_2, x_3 are introduced to enable a comparison of the different design of experiments algorithms full factorial, Monte Carlo and Latin hypercube. Hereby, the domain of definition is limited from 0 to 1 in each dimension. Each of the sampling plans, regardless of the design of experiment algorithm, holds $n = 64$ samples, and hence, it causes a similar computational cost. Appendix C lists all sampling plans.

On a side note, the sampling plans can be displayed in a three-dimensional plot, as shown in figure 3.10. However, this form of representation lacks clarity both for a higher number of samples and even worse for a higher number of dimensions. Hence, in the further course of this study scatter-matrix plots visualize higher dimensional contents. Figure 3.11 displays the same sampling plans in a scatter-matrix that shows data for a combination of two parameters, e.g., x_1 over x_2 and x_2 over x_1 . Despite the fact that for each plot one dimension is hidden, it is still the most clear way to dis-

play higher dimensional data, especially necessary for the design studies presented in chapter 4.

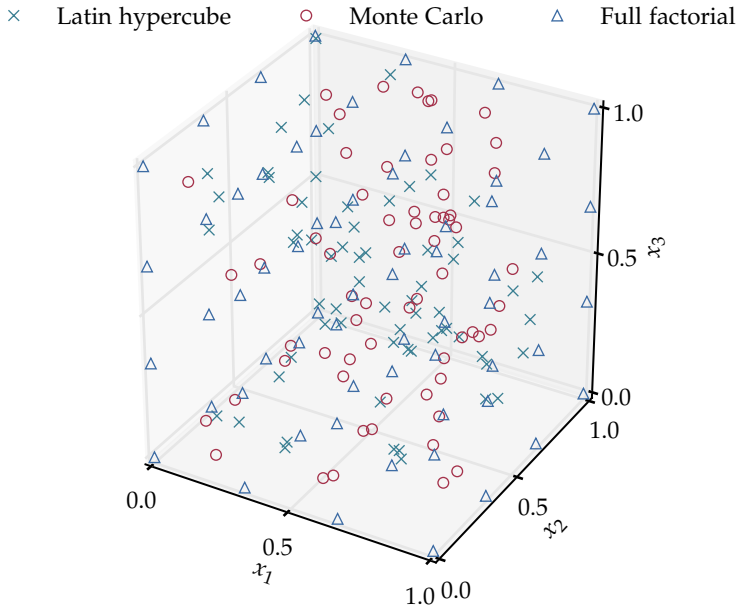


Figure 3.10: Design space coverage as three dimensional plot

As it can be seen from both diagrams (figure 3.10 and 3.11), the full factorial sampling plan evenly distributes the samples but only covers a small number of discrete values within the design space. The Monte-Carlo sampling plan targets for different locations, and hence, it seems to cover the domain of definition better than the full factorial design. However, at some locations a very tight clustering can be observed, e.g., at $x_2 \approx 0.8$ and $x_3 \approx 1.0$. Finally, the Latin hypercube provides an apparently similar design to the

Monte Carlo sampling plan, but no tight clustering occurs as the design space is subdivided into distinct intervals.

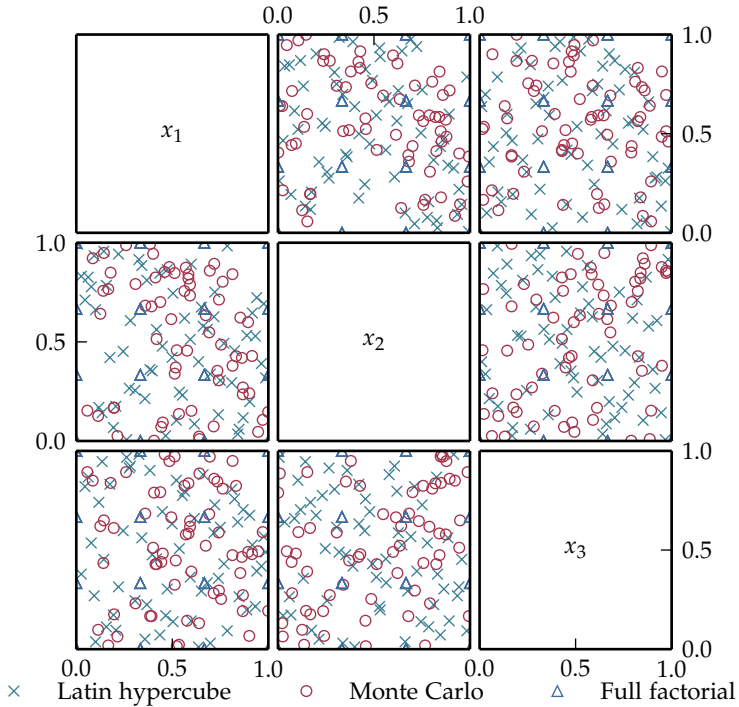


Figure 3.11: Design space coverage as scatter-matrix plot

An important criteria for the quality of a design of experiments is its *space-fillingness*. While this topic opens the view on a complete field of research, far beyond the scope of this study, some clarifications are necessary to justify the application of a certain design of experiments algorithm over another. Graphically, the space-filling abilities of a distribution can be visualized by a histogram. Figure 3.12 displays the histogram for the distribution of samples across the design variable x_1 from the previous example. The plot subdivides the design space $(0, \dots, 1)$ into 16 intervals.

The full factorial sampling plan places samples at four different locations on x_1 and each one holds $n = 16$ samples. Plainly, it will be hard to grasp the behavior of $h(X)$, if only samples from four positions within a dimension are known. On the contrary, the Monte Carlo and Latin hypercube sampling plans distribute samples more evenly along x_1 . In comparison, the Latin-Hypercube appears to be superior as it places four values within each of the sixteen intervals.

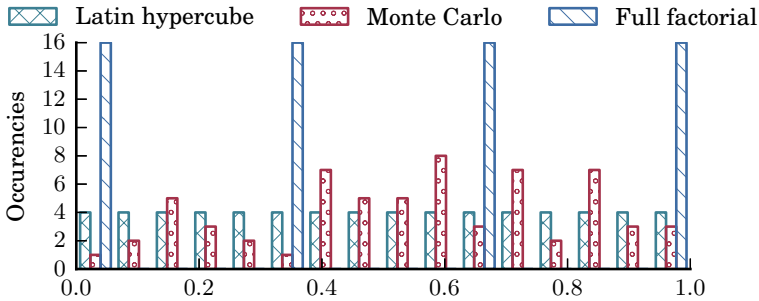


Figure 3.12: Histogram of x_1 distribution

Certainly, a graphical evaluation of design of experiment algorithms either via scatter matrix plots or histograms becomes cumbersome for larger design spaces and sampling plans and is further unsuitable for an exact comparison. Johnson et al. [57] propose the *maximin* criterion as numerical means for the evaluation of the space-fillingness of a sampling plan X . The criterion is based on the set of unique distances $d_{1,\dots,\mu}$ between all pairs of points within the sampling plan and the number of pairs of points $J_{1,\dots,\mu}$ at equal distance. The most common way to determine the distance between a pair of points is the Euclidean norm (Eq. 3.7).

$$d(x_1, x_2) = \sqrt{\sum_{j=1}^k |x_{j,1} - x_{j,2}|^2} \quad (3.7)$$

Johnson et al. then define that a *maximin* sampling plan is the sampling plan among all available plans that maximizes d_1 and minimizes J_1 . Mor-

ris and Mitchell [92] further extend the definition by Johnson et al. to include all distances and occurrences, i.e., the *maximin* sampling plan among all available sampling plans maximizes d_1 and minimizes J_1 and further maximizes all subsequent d and for each minimizes the related J .

While both *maximin* criteria may be applied to compare and subsequently optimize sampling plans, this approach is neglected within the research community for various numerical reasons. Instead, Morris and Mitchell propose equation 3.8 for the comparison of sampling plans where a smaller value of Φ_q , i.e., the Morris-Mitchell criterion, indicates a better space-fillingness.

$$\Phi_q(X) = \left(\sum_{j=1}^u J_j d_j^{-q} \right)^{1/q} \quad (3.8)$$

Forrest et al. [35] explore various values for q and due to high numerical cost they fail to deliver full proof but advise higher values of q to obtain sample plans that also fulfill the above mentioned *maximin* criteria. Hence, table 3.2 displays the results for d_1 , J_1 and Φ_{100} for each of the provided sampling plans.

	Full Factorial	Monte Carlo	Latin Hypercube
d_1	0.3333	0.0373	0.0477
J_1	63	1	1
Φ_{100}	3.1522	26.8016	20.9773

Table 3.2: Space fillingness of DOE algorithms

In terms of the Morris-Mitchell criterion, the full factorial sampling plan is superior to the random sampling methods due to its large distances between pairs of points²⁶. However, as seen from the above plots, and given the fact that J_1 is large, the full factorial sampling remains an inferior choice. The comparison of the Monte Carlo and Latin hypercube sampling plans is straightforward both for the Morris-Mitchell criterion and the *maximin* criterion. Latin hypercubes are the algorithm of choice in the present

²⁶ The higher values of J for the full factorial sampling plan are almost neglected due to high values of q .

study due to a higher value of d_1 , i.e., the shortest distance between a pair of points, and lower values of Φ_{100} .

3.4 Symbolic Regression

A common drawback of the surrogate models, as outlined in section 2.4, is their predefined model structure. Given a parameter set X of a function $h(x)$, a surrogate model is represented by a function $s(x)$ that delivers similar outputs as $h(x)$. Hereby, $s(x)$ is constructed from experiments that apply X to $h(x)$ and measure the result. If the structure of $s(x)$ is predefined, e.g., a polynomial of m^{th} order, then this implies that a certain knowledge about the structure of $h(x)$ is available. If no knowledge about the structure of $h(x)$ is available then the (most probably inappropriate) structure of $s(x)$ should not be fixed.

It is assumed that no prior knowledge about the model structure is available due to the complexity of the applied higher fidelity models $h(x)$ in this study, and hence, a surrogate model without predefined structure is preferred. A technology that enables the construction of a surrogate without a predefined structure is symbolic regression; it is based on genetic algorithms and -programming.

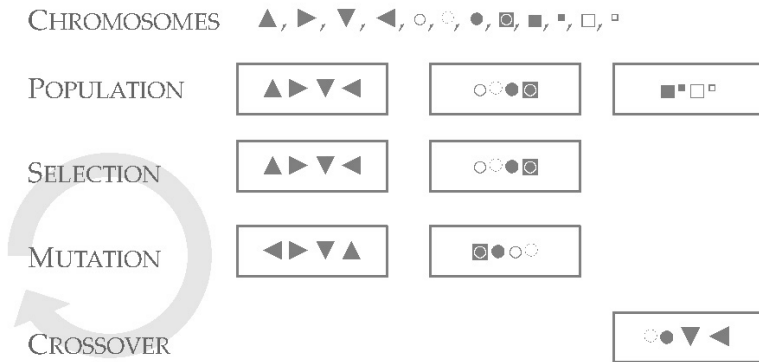


Figure 3.13: Evolutionary algorithm principle

Genetic algorithms are the core of genetic programming as well as symbolic regression. They describe means to model evolutionary processes with the aid of executable computer models. Fraser and Burnell [40] outline the key elements, population, chromosomes, selection, mutation, and crossover, as shown in figure 3.13. In short, a genetic algorithm tries to find an individual out of a generated population that best fits the metrics of a given fitness function. Each individual of the population is described by a set of chromosomes and their order among each other. The genetic algorithm is able to mutate each individual. A mutation exchanges certain chromosomes or reshuffles their order. Furthermore, new individuals are created by crossing over parts of two or more other individuals.

From an initial set of random individuals, the genetic algorithm creates new individuals in an iterative process and applies mutation and crossover. In a subsequent step, the fitness function is applied to each individual. In this step, the equivalent to nature's selection of the fittest, only the best individuals are chosen for further development.

As a further subset of genetic algorithms, Koza [61] and Forrest [35] developed genetic programming. In genetic programming the evolutionary approach is taken to create computer programs. Thereby, each chromosome is an executable statement, often a function. Most relations lead to functional programming languages such as LISP. Symbolic regression is one of the siblings of genetic programming.

In a symbolic regression the chromosomes are the parameters of an input set $X = [x_1, \dots, x_k]$ and mathematical operations such as addition, subtraction, and division or functions such as sine and cosine. While adhering the laws of mathematics, a genetic algorithm combines these chromosomes and tries to find a function $s(x)$. The fitness function for the symbolic regression is some kind of error metric, e.g., the root mean square error (Eq. 3.9). The goal is to minimize the error ϵ so that $s(x)$ becomes as similar as possible to $h(x)$.

$$\epsilon = \sqrt{\frac{\sum_{i=1}^n (h(X_i) - s(X_i))^2}{n}} \quad (3.9)$$

The present study applies the symbolic regression algorithm Eureqa pub-

lished by Cornell University²⁷ and developed by Schmidt and Lipson [121, 122, 120]. In their studies, they show that symbolic regression is capable of finding the Lagrangian and Hamiltonian descriptions of physical systems such as a double pendulum.

Physical systems are described by invariants such as the afore mentioned Lagrangian and Hamiltonian notations of energy in the system. When searching for these invariants from a given set of data, the problem arises that several more trivial invariants exist. Schmidt and Lipson propose the use of a predictive ability criterion to determine suitable and non suitable invariants: *“We define a potential law equation to be nontrivial if it can predict differential relationships between two or more variables.”* The predictive ability is therefore the comparison of partial derivatives. If the experiment is described by two variables x and y then the partial derivatives can be calculated by local polynomial fits and are noted as:

$$\frac{\Delta x}{\Delta y} = \frac{dx}{dt} / \frac{dy}{dt} \quad (3.10)$$

For any equation found by the symbolic regression algorithm the same information can be found from basic calculus. For example, for an equation $f(x,y)$ over variables x and y :

$$\frac{\delta x}{\delta y} = \frac{\delta f}{\delta y} / \frac{\delta f}{\delta x} \quad (3.11)$$

Schmidt and Lipson further apply a mean log error to compare the results of equations 3.10 and 3.11. Equations found from the symbolic regression that lead to a small number for the error are further developed. Hereby, the mean log error is written as:

$$\epsilon = -\frac{1}{n} \sum_{i=1}^n \log\left(1 + \left| \frac{\Delta x_i}{\Delta y_i} - \frac{\delta x_i}{\delta y_i} \right| \right) \quad (3.12)$$

Hence, the implementation by Schmidt and Lipson further reduces the number of possible solutions and the identification of meaningful candidates becomes easier.

²⁷ In 2013 Schmidt created a spin-off from Cornell University and Eureka is now published by Nutonian Inc. The name and licensing of the software have changed various times, but the software is still available for academic purposes.

Assessment of Surrogate Models

Chapter 2, while outlining the state of the art in surrogate modeling, introduced an assessment scheme for surrogate models by Shan and Wang [126]. In the following paragraphs the categories of Table 2.6 are applied to symbolic regression. A quantitative holistic assessment of the various criteria for surrogate models is hard to achieve and is out of the scope of this study. However, some numerical studies are outlined in the next paragraphs to back up the qualitative assessment. The goal of this assessment is to justify the application of symbolic regression as the surrogate model of choice in the present study by means of a comparison against other commonly applied surrogate models.

Selected surrogate models are applied to two different handbook methods for the estimation of the wing mass. The number of samples n is increased and the error of the surrogate model is monitored. This experiment is conducted to answer the following questions:

1. How many samples are necessary for a good fit?
2. Which surrogate provides the lowest error?
3. Which surrogate provides the lowest complexity?

Question 1 relates to the numerical effort necessary to create a surrogate model. If a high number of samples is necessary to create a good surrogate then the computational cost might become insurmountable. As outlined in the previous section, samples are created via Latin hypercubes .

Question 2 relates to the numerical error introduced into the design due to the use of a surrogate model. It may be assumed that for a certain number of samples the error of the surrogate behaves asymptotically, i.e., more samples not necessarily improve the precision of the surrogate model. Kriging models are exempt from this assumption as they are interpolating methods and each additional sample still increases their precision. The error is measured as the root mean square error (Eq. 3.9) divided by the mean of all function evaluations. The result of the surrogate is compared to the result of the examined function for ten thousand samples that are derived by a Monte-Carlo simulation.

Question 3 relates to the computational cost of the surrogate model and its transparency, i.e., the possibility for an engineer to implement and interpret

the surrogate model. The goal of this study is to include the surrogate model in a conceptual design code and in such a code analysis methods are usually implemented in one or few equations per parameter. Furthermore, evaluation times must remain low to justify the replacement of a slower, higher fidelity analysis.

Complexity is expressed as the sum of cost of mathematical operators and operands. A different cost is allocated for each operator. For example, $f(x) = x + 1$ has a complexity of 3; 1 is the cost of each variable or constant, plus a cost of 1 for the addition operator. In comparison, trigonometric operators have a higher cost, and hence, $f(x) = \cos(x + 1)$ has a complexity of 6. Appendix A lists the cost of all mathematical operators.

Subsequently, the computational cost necessary to derive a surrogate model needs to be taken into account, especially as it poses one of the main drawbacks of symbolic regression. While it is possible for the symbolic regression to derive the perfect fit for the deterministic models posed in this assessment, the computational cost and runtime are high. Hence, the maximum computational cost granted to the symbolic regression is limited to one core hour. Of course, for a high fidelity task this is not a sensible boundary condition, but it serves as means to enable a comparison of the different surrogate models:

- Linear Response Surface,
- Quadratic Response Surface,
- Universal Kriging with Constant Regression,
- Universal Kriging with Linear Regression,
- Universal Kriging with Quadratic Regression,
- Artificial Neural Network,
- Symbolic Regression.

If the number of samples is too low and results in an under-determined solution then response surfaces are not trained. Despite several approaches to fit polynomial terms for an under-determined number of samples exist, this study neglects these approaches due to their high numerical cost and low precision. Conn et al. [27] provide detailed information on this subject. It may be assumed that a decent fit is only possible for a number of samples equal or higher than the number of necessary coefficients.

The Kriging models use the response surfaces as regression models. Nielsen et al. [96] published a state of the art implementation of the DACE approach from Sacks et al. [118]. This study uses the Scikit²⁸ version of Nielsen’s implementation.

The artificial neural network is based on the PyBrain²⁹ framework. It consists of an input layer with k nodes. The next layer is linear with $k - 1$ nodes. Subsequently, a linear layer with $k - 1$ nodes is added. Finally, a single node provides the output. The artificial neural network is trained via a back propagation trainer. Despite the fact that the linear layers may not aid in refactoring very complex mathematical constructs, they are chosen in this example due to their low complexity³⁰.

The symbolic regression is based on the Eureqa³¹ toolbox. As already mentioned, a complete holistic comparison of surrogate models lies beyond the scope of this study. Hence, conservative, best practice approaches are chosen for the above mentioned surrogate models.

The first experiment is based on the wing mass estimation method (Eq. 2.2) by Shevell [127], already introduced in chapter 2. Under the assumption that m_{ZFM} is proportional to m_{TOM} all exponents of the equation are natural numbers. Hence, it is expected that all surrogate models reflect most of the behavior of the equation.

Figure 3.14a shows the error for each surrogate model plotted for an increasing number of samples while the number of design variables is kept constant at four. The first observation is that all surrogate models, except the linear response surface, provide an error of less than 5% even for a low number of samples. It can be observed that the Kriging models still increase their precision with a rising number of samples, albeit slowly. The Kriging model with the regression model of highest order, i.e., quadratic, provides the smallest error.

Furthermore, figure 3.14b displays the complexity for each surrogate again over the number of samples. The fixed form linear and quadratic response

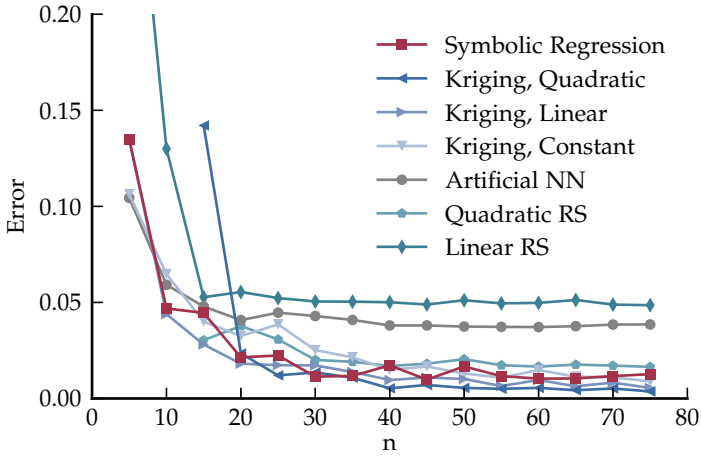
²⁸ www.scikit-learn.org, v0.14

²⁹ www.pybrain.org, v0.3.2

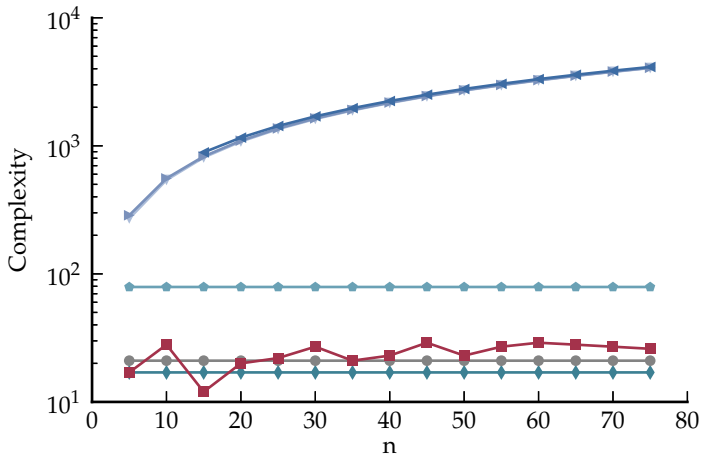
³⁰ In a further step, not only the type of layer could be adjusted but also the number of layers and nodes within each layer may be subject to an optimization. However, this optimization rises significant numerical cost while it increases the complexity and is hence excluded in the comparison

³¹ www.nutonian.com, v0.99.6

3.4 Symbolic Regression



(a) Error over n : Shevell



(b) Complexity over n : Shevell

Figure 3.14: Surrogate models for Shevell

surfaces have a constant complexity. Given the fact that for each sample added to the Kriging model the complexity increases, the complexity rises quickly. The complexity of the symbolic regression varies at a low number between the linear and quadratic response surface.

Given the fact that Shevell provides a (mathematically) simple equation, the same experiment is repeated for the wing mass estimation method (Eq. 3.13) by Raymer [105]. It neglects the influence of m_{ZFM} . Additionally, it introduces the controls surface area S_{cs} . The exponents of Raymer's equation are real numbers and it is assumed that especially the response surfaces face difficulties to reflect their behavior. The ultimate load factor n_{ult} is kept constant at 3.75.

$$m_{wing, Raymer} = 0.0051 \frac{(m_{TOM} n_{ult})^{0.557} S^{0.648} AR^{0.5} (1 + \lambda)^{0.1} S_{cs}^{0.1}}{\cos(\varphi)(t/c)^{0.4}} \quad (3.13)$$

Figure 3.15a displays the error of the surrogate models for Raymer's equation. The overall behavior is similar to figure 3.14a. Apparently, the surrogate models can cope with the more difficult mathematical formulation. However, the error levels are slightly higher. This is most obvious for the linear response surface. The behavior of the complexity in figure 3.15b is similar to the first experiment.

These first two experiments lead to the conclusion that adequate error levels can be obtained for a low number of samples n . From a precision point of view, the Kriging model in combination with the regression model of quadratic order yields the best results, while the linear response surface has the lowest complexity. The vertical axis needs to be displayed on a logarithmic scale to include the complexity of the Kriging model. The symbolic regression provides a balance between both criteria.

In a further step, not only the impact of the number of samples n but also the impact of the number of dimensions k needs to be examined. Hence the three surrogate models, linear response surface, Kriging, and symbolic regression, are trained to Raymer's wing mass estimation again. The number of samples is now a function of k . As a conservative assumption, twenty samples per dimension are evaluated. The number of dimensions increases from two to six, in ascending order from the taper ratio to the wing sweep, the thickness to chord ratio, the maximum take-off mass, and the reference

3.4 Symbolic Regression

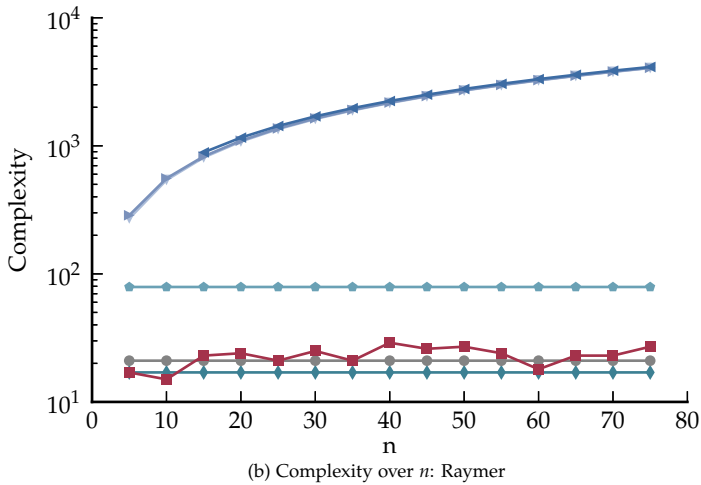
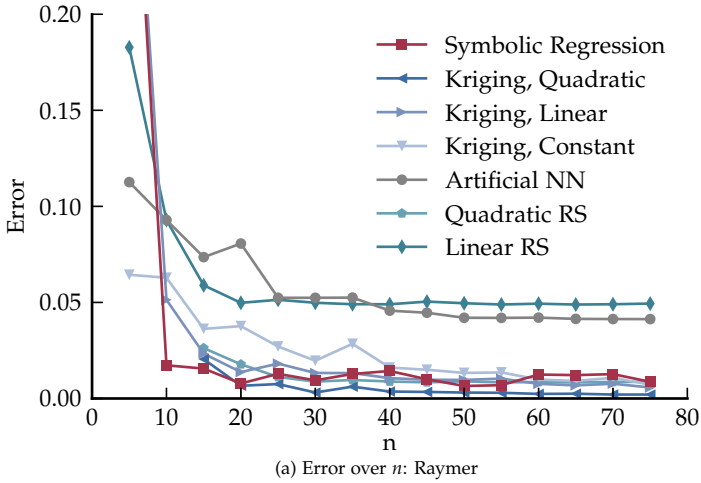


Figure 3.15: Surrogate models for Raymer

area. The goal of the experiment is to determine whether the results obtained from the previous experiment are also valid for higher and lower numbers of design variables.

Figure 3.16a shows the error of the different surrogate models over the number of dimensions k . The linear response surface shows a large error for the low number of dimensions which is due to the non-linear behavior of the equations. The Kriging model and the symbolic regression provide small errors in comparison to the two previous experiments. It must be stated that the error is slightly increasing for a higher number of dimensions, which is likely due to the number of samples. However, the error remains far below 5%.

In addition, figure 3.16b details the complexity of the surrogate models over the number of dimensions k . The linear response surface has a slight increase in complexity compared to the Kriging model. The symbolic regressions is again within an order of magnitude of the linear response surface and even finds solutions with a lower complexity at a higher number of dimensions.

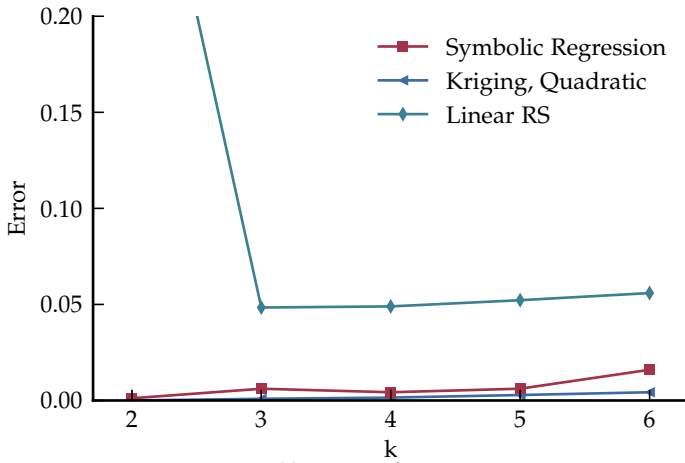
With the insight provided by the above experiments a qualitative assessment of surrogate models based on Table 2.6 is possible.

The **accuracy** of symbolic regression is shown by Schmidt and Lipson and the conducted numerical studies where the relative error remained significantly below five percent, and hence, the level of confidence in the results is high. However, it must be noted that symbolic regression on the contrary to Kriging does not reflect each sample. Furthermore, the sample points are subdivided in a training and a validation set, and hence, they are taken into account for different purposes.

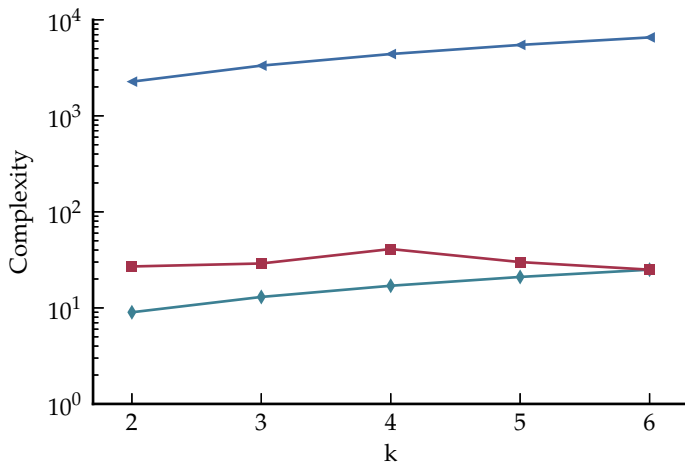
Interpretability and transparency of the symbolic regression approach are generally high as the result is an interpretable equation. For some physical problems it was shown that the resulting equation reflects the well known mathematical description of physical laws, as in the inaugural paper by Schmidt and Lipson [121]. In addition, the optimization of the regression algorithm can be configured to take into account the complexity. Hereby, the number of applied building blocks is kept at a low number.

In comparison to Kriging and artificial neural network approaches that rely on larger mathematical constructs and can easily occupy several kilo- to

3.4 Symbolic Regression



(a) Error over k : Raymer



(b) Complexity over k : Raymer

Figure 3.16: Surrogate models for Raymer

megabytes in a computer code, the transparency of a surrogate created via symbolic regression is outstanding. However, in accordance to the problem formulation, results may include representations that are hard to interpret. Linear response surfaces, the only surrogate model with a lower complexity, return results at an unsatisfying error level.

The **flexibility and robustness** of symbolic regression benefit from the genetic algorithm approach. First of all, the structure of the surrogate model is not predefined and hence flexible. In addition, the genetic algorithm explores a large population of possible structures to further increase the chance to find a suitable representation for the surrogate model.

In comparison to surrogate models of predefined structure, it is hard to characterize the **dimensionality** of symbolic regression. With a predefined structure, where the maximum order of the response surface is known, a minimum of sample points can be derived. For a symbolic regression no minimum number of sampling points exist. However, too little information influences the accuracy of every surrogate model.

The **computability** of symbolic regression may be cost intensive. Especially, for a new fit a large number of evaluations is usually necessary. Benefits in time arise from the good support of parallelization. Hence, calculations can be accelerated by supplying additional computational power.

If pre-existing knowledge about the behavior of $f(x)$ is at hand in the domain of definition then symbolic regression may be accelerated by seeding. Seeding describes the definition of a set of individuals before the genetic algorithm tries to create the surrogate model. In the present study limited knowledge is available in from of handbook methods. These methods may be fed to the symbolic regression to reduce computational cost.

However, just in time computations can hardly be achieved by symbolic regression, and hence, the iterative execution of the multi-fidelity loop is neglected in the present study. Further information on this topic is provided in chapter 6. Adaptations to new design points come at relatively low cost as these can be added to an existing database and the symbolic regression approach can be started with the previously most successful populations.

The **simplicity** of symbolic regression is higher than for all other named surrogate models due to the availability of the Eureqa toolbox from Schmidt

Criterion	Response Surface	Kriging	ANN	Symbolic Regression
Accuracy	-	++	+	+
Interpretability	-	--	-	++
Flexibility	--	+	++	++
Dimensionality	o	+	o	++
Computability	+	++	-	-
Simplicity	+	-	+	++
Smoothness	+	+	-	+

Table 3.3: Qualitative comparison of surrogate models

and Lipson. The symbolic regression algorithm can either be executed from a simple spreadsheet interface or via a batch mode. Cloud and grid computing capabilities are also available. As a drawback, no source code for a symbolic regression analysis is available.

The **smoothness** of an equation derived by symbolic regression depends on the building blocks used during the optimization. Most mathematical operations applied in an engineering background can easily be derived, even analytically. Problems may arise for more complicated building blocks, e.g., hyperbolic functions, or if the derived equation is subject to division by zero errors.

In addition to the already introduced requirements, special attention shall be paid to the application of symbolic regression in multi-disciplinary **optimization**. In comparison to other surrogate models, the time necessary to derive a symbolic regression is large and this must be listed as the greatest con argument. Only if a global surrogate can be found, and hence, it is ensured that the surrogate may be applied for several optimizations significant benefits can be achieved. On the other hand the symbolic regression provides several benefits for an optimization. First, gradient information is in most cases easily accessible for the analytic formulations that are the result of the symbolic regression. Second, the symbolic regression may be based on any grid, and hence, enables dynamic data driven applications. Third, the computation time of the symbolic regression (once it has been derived) is insignificantly short.

Table 3.3 summarizes the qualitative comparison of surrogate models. Cur-

rently, there is no publication available that compares the benefits and drawbacks of the surrogate models in a mathematical fashion. Jin et al. [56] published a valuable approach, but it excludes symbolic regression in the list of compared surrogate models, and hence, the comparison remains an item of future research.

In conclusion, the numerical experiments conducted in this section provide reason that symbolic regression is able to produce surrogates of aircraft design methods at a comparable accuracy to other surrogate modeling techniques commonly applied in MDAO. The sufficient accuracy in combination with the superior transparency, i.e., low complexity, justify its application as surrogate model in the proposed multi-fidelity workflow. The following chapter then applies the multi-fidelity workflow to three design studies.

4 Design Studies

Remember that all models are wrong; the practical question is how wrong do they have to be to not be useful.

(George E. P. Box)

Scientists create models to express the behavior of a certain aspect of reality. However, a model is usually incomplete as it is based on simplifications. These simplifications may have their origin in neglected physical effects. For example, an aerodynamic analysis model that disregards transonic effects. Furthermore, errors in models arise from statistical or numerical approximations. In this chapter, surrogate models of physical models are created by the proposed multi-fidelity workflow and the present study has to prove that this method is useful in the sense of Box and Wilson [20].

Three design studies are presented: First, a design study quantifies the induced drag of various wing geometries. It is comparably simple and serves as a proof of concept. The second design study applies a sophisticated wing mass estimation workflow that includes secondary structures such as control surfaces to quantify the overall wing mass of various geometries. The multi-fidelity workflow takes into account aerodynamics, loads and structures. Finally, the third design study examines the properties of a strut-braced wing aircraft and the mass of the strut and wing combination.

4.1 Oswald Factor

The first design study derives a surrogate model of the Oswald factor and the approach outlined in this section has partially been presented in a previous publication [14]. Contrary to this publication, insight from further research reduces the computational cost as the number of necessary samples is lower than expected.

First, this section introduces a definition of the Oswald factor. Subsequently, it elaborates existing approaches that determine the Oswald factor on a conceptual design level. In a next step, a physics-based multi-fidelity

workflow is set up and applied to create a surrogate model that is based on symbolic regression. Finally, the surrogate model is included in the conceptual design model to enlarge the valid domain of definition and increase the precision.

Induced Drag

A lifting surface in a fluid with free stream velocity V_∞ experiences forces due to pressure and shear. The sum of forces perpendicular to V_∞ is called lift L and the sum of forces parallel to V_∞ drag D . The drag is further subdivided into drag at zero lift D_0 and drag due to lift D_L .

Hence, drag due to lift is a force that is sensitive to lift. In the following, the focus is set on induced drag D_i . However, it is important to note that induced drag and drag due to lift are not exchangeable terms. Induced drag is one component of drag due to lift. Changes in drag due to lift occur also due to different physical effects, e.g., with increasing lift local velocities on the lifting surface change and influence the acting viscous forces.

To enable a clear physical and mathematical description of induced drag and the Oswald factor, the following paragraphs outline some basic aerodynamic principles. As a full introduction into aerodynamics is out of the scope of this study, some principles are taken for granted. Anderson [5] provides a detailed description of the relevant physical effects and modeling approaches.

Prandtl's lifting line theory [101] applies the three basic theorems, *circulation*, *Kutta-Joukowski* and *Biot-Savart*, to a finite wing in an inviscid and incompressible flow. Thereby, a wing, as represented in figure 4.1, is replaced by a single lifting line. The lifting line extends along the y -axis with upper and lower bounds $\pm b/2$. An infinite number of horseshoe vortices is super-positioned along the lifting line. The circulation Γ of each horseshoe vortex is infinite.

Subsequently, the Biot-Savart law is applied to the vortices along the lifting line to find the down-wash velocity w . The down-wash velocity (Eq. 4.1) is the integral of the induced velocities perpendicular to the free stream.

4.1 Oswald Factor

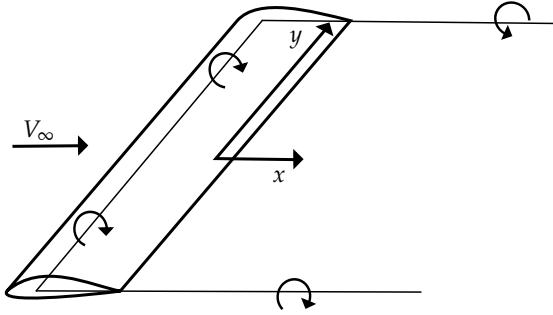


Figure 4.1: Finite wing as lifting line

$$w(y) = -\frac{1}{4\pi} \int_{-b/2}^{b/2} \frac{(d\Gamma/dy)dy}{y_0 - y} \quad (4.1)$$

As some of the stream in proximity to the wing is diverted downwards, the downwash velocity effects the aerodynamics of the finite wing. The actual angle of attack differs from the angle between the wing and the direction of the free stream velocity V_∞ , and the additional angle is called the induced angle of attack α_i . As the velocity components V_∞ and w are known, α_i can be calculated under the assumption that w is much smaller than V_∞ (Equation 4.2). As w is a function of y , the same is true for α_i .

$$\alpha_i = \frac{w(y)}{V_\infty} \quad (4.2)$$

The effective angle of attack α_{eff} is the angle of attack that acts on the finite wing. It equals the difference of the geometrical angle of attack α and the induced angle of attack α_i . As α_i is function of y , α_{eff} is as well. The effective angle of attack is necessary to compute the local lift coefficient c_l for each strip of the finite wing, as in equation 4.3. Furthermore, it is assumed that the local section lift slope equals 2π , and the local angle of attack for zero lift $\alpha_{L=0}$ is introduced.

$$c_l(y) = 2\pi(\alpha_{eff}(y) - \alpha_{L=0}) \quad (4.3)$$

In addition, the lift per unit span is expressed by the local lift of a strip

element (Eq. 4.3) or by Kutta-Joukowski. Equations 4.4 and 4.5 show the respective results for the lift per unit span. Furthermore, the chord $c(y)$, i.e., the extrusion of the wing in x-direction, is introduced as a function of y . For small induced angles of attack the drag per unit span of the wing is equal to the lift per unit span times the induced angle of attack.

$$L' = \frac{1}{2}\rho_{\infty}V_{\infty}^2c(y)c_l(y) \quad (4.4)$$

$$L' = \rho_{\infty}V_{\infty}\Gamma(y) \quad (4.5)$$

$$D' = L'\alpha_i \quad (4.6)$$

Equations 4.4, 4.5 and 4.2 in combination with the definition of the angle of attack and the induced and effective angle of attack provide the fundamental equations of Prandtl's lifting line theory:

$$\alpha = \alpha_{eff} + \alpha_i \quad (4.7)$$

$$\alpha = \frac{\Gamma(y_0)}{\pi V_{\infty}c(y)} + \alpha_{L=0} + \frac{1}{4\pi V_{\infty}} \int_{-b/2}^{b/2} \frac{(d\Gamma/dy)dy}{y_0 - y} \quad (4.8)$$

If an elliptical circulation distribution is assumed for the finite wing then equations 4.9 and 4.10 show that the lift distribution is elliptical as well.

$$\Gamma(y) = \Gamma_0 \sqrt{1 - \left(\frac{2y}{b}\right)^2} \quad (4.9)$$

$$L'(y) = \rho_{\infty}V_{\infty}\Gamma_0 \sqrt{1 - \left(\frac{2y}{b}\right)^2} \quad (4.10)$$

In a next step, y is substituted by $b/2\cos(\Theta)$ and dy by $-b/2\sin(\Theta)d\Theta$ to enable the integration of Eq. 4.10. Hence, the lift of the finite wing L can now be calculated. Furthermore, the wing's lift coefficient C_L and reference area S are introduced in the standard notation (Eq. 4.12).

$$L = \rho_{\infty}V_{\infty}\Gamma_0 \frac{b}{4}\pi \quad (4.11)$$

$$L = \frac{1}{2}\rho_{\infty}V_{\infty}^2C_L S \quad (4.12)$$

4.1 Oswald Factor

The downwash velocity w and the induced angle of attack α_i become:

$$w = -\frac{\Gamma_0}{2b} \quad (4.13)$$

$$\alpha_i = \frac{\Gamma_0}{2bV_\infty} \quad (4.14)$$

If equations 4.11 and 4.12 are solved for Γ_0 and substituted into 4.14 then they provide the induced angle of attack that depends on the lift distribution (Eq. 4.15). Subsequently, equations 4.15 and 4.6 can be solved to find the induced drag coefficient $C_{D,i}$ for the elliptical lift distribution (Eq. 4.16).

$$\alpha_i = \frac{C_L}{\pi AR} \quad (4.15)$$

$$C_{D,i} = \frac{C_L^2}{\pi AR} \quad (4.16)$$

Equation 4.16 provides the induced drag for a finite wing with an elliptical lift distribution in an incompressible, inviscid flow. Hence, the Oswald factor e describes the deviance from the elliptical lift distribution (Eq. 4.17). Anderson [5] states that an approximate value of 25% of the overall drag of the aircraft arises due to induced drag. If aircraft fly at a higher lift coefficient then this value may increase up to 60%.

$$e = \frac{C_L^2}{\pi AR C_{D,i}} \quad (4.17)$$

In an incompressible, inviscid flow an elliptical lift distribution is easily obtained from an elliptical planform of the wing. Several reasons prohibit the design of such a planform. For example, wings are swept to counteract transonic effects. Furthermore, they are built from straight tapered sections to ease production. Finally, an elliptical lift distribution leads to high loads on the outer wing that increase the root bending moment and the wing mass. The negative aerodynamic effects of a non-elliptical planform are usually countered by twisting the wing to establish a close to elliptical lift distribution. Hence, the wings of modern aircraft are designed in such a way that the tip twists (washes) out under high loads to reduce wing bending moments. The wing can either be twisted geometrical by a change

of the incidence angle of local sections or aerodynamically by different local airfoil profiles. However, sophisticated multi-disciplinary optimization is necessary to develop a sensible twist distribution.

Existing Approaches in Conceptual Design

Several approaches exist to quantify the Oswald factor in conceptual aircraft design; Niță and Scholz [95] present an overview paper. Contrary to their work, this section focuses exclusively on the Oswald factor. Hence, the present literature review neglects viscous and wave drag effects as these are hard to quantify at a reasonable computational cost.

The first outlined approach originates from Raymer [105] and is based on the aspect ratio (AR) and the leading edge sweep angle of the wing (φ). Raymer provides two different equations for unswept (Eq. 4.18) and swept (Eq. 4.19) wings.

$$e = 1.78(1 - 0.045AR^{0.68}) - 0.64 \quad (4.18)$$

$$e = 4.61(1 - 0.045AR^{0.68})(\cos(\varphi))^{0.15} - 3.1 \quad (4.19)$$

with $\varphi > 30$

The equations can be evaluated quickly as the number of variables is low. Drawbacks arise as the design space is limited due to the restrictions on the leading edge sweep angle. Brandt et al. [22] present an equation similar to Raymer's second equation that also takes into account the sweep angle.

An approach (Eq. 4.20) by Howe [51] takes into account additional parameters like the flight Mach number (M_N), the taper ratio (λ) and the thickness to chord ratio (t/c). The equations derived by Howe provide drag due to lift, and it is not possible to extract an exact formulation for the Oswald factor. Equations 4.21 and 4.22 are the functions for the taper ratio and aspect ratio:

4.1 Oswald Factor

$$C_{D_i} = \frac{(1 + 0.12M_N^6)}{\pi AR} \quad (4.20)$$

$$\left[1 + g(AR) + \frac{0.142 + ARf(\lambda)(10t/c)^{0.33}}{\cos(\varphi)^2} \right]$$

$$f(\lambda) = 0.005 \left[1 + 1.5(\lambda - 0.6)^2 \right] \quad (4.21)$$

$$g(AR) = \frac{0.1}{(4 + AR)^{0.8}} \quad (4.22)$$

Jenkinson [54, 50] describes a partially physics-based approach for the induced drag that is based on the lifting-line theory. The approach leads to a function (C_1) that depends on the taper ratio and aspect ratio, as shown in figure 4.2.

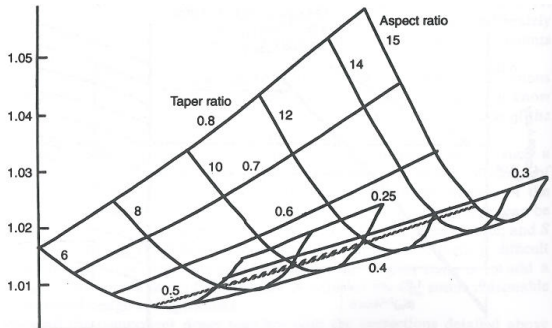


Figure 4.2: C_1 as a function of λ and AR , [54]

Subsequently, the results are corrected for conventional (Eq. 4.23) and CFD (Eq. 4.24) wing designs so that e results in C_2 over C_1 . As can be seen from figure 4.2, Jenkinson's approach returns an optimal Oswald factor for wings with taper ratios of approx. 0.4.

$$C_2 = 1.235 - 0.0245AR \quad (4.23)$$

$$C_2 = 1.113 - 0.0116AR \quad (4.24)$$

Kroo [64] provides equation 4.25 for drag due to lift³² $C_{D,L}$ that takes into account the induced drag, the increase of drag due to viscous forces due to lift³³, and the zero lift drag due to twist³⁴.

$$C_{D,L} = \frac{C_L^2}{\pi ARus} + a_0 \tau C_L v + (a_0 \tau)^2 w \quad (4.25)$$

In the scope of this literature review, the first part of equation 4.25 is important. The Oswald factor equals the product of u and s . Hereby, u represents a theoretical value for the Oswald factor. Kroo states that u should be quantified by physics-based analysis and s defines a correction factor to take into account the aerodynamic effects of the fuselage. The fuselage effect on the induced drag can be found from equation 4.26, where d is the fuselage diameter and b the wing span.

$$s = 1 - 2 \frac{d^2}{b^2} \quad (4.26)$$

Despite the fact that Kroo's formulation may not be applied for a numeric comparison, it is listed for two reasons: First, it supports the overall statement of the present study that physics based analysis is already necessary at the conceptual design stage. Second, it introduces the correction factor in equation 4.26 that is applied in the later course of this design study.

Hörner [49] provides an equation for the Oswald factor that depends on the aspect and taper ratio of the wing. The Oswald factor is described in equation 4.27, and figure 4.3 shows a plot for the included δ over the taper ratio. Furthermore, Hörner outlines corrective terms for the impact of the sweep φ (Eq. 4.28) and the dihedral ψ (Eq. 4.29) angle on the Oswald factor. Similar to Jenkinson's approach, Hörner finds an optimal Oswald factor for unswept, low aspect ratio wings with a taper ratio between 0.3 and 0.4. McCormick [85] and Dubs [31] present similar approaches.

³² Kroo applies the term induced drag for the overall equation. For clarity Kroo's naming convention is changed in this literature review. The physical meaning of the three components of the drag term remains unchanged.

³³ As the lift produced by the wing changes, velocities increase. Hence, viscous drag, usually only taken into account as zero lift drag, rises as well. Conceptual design usually neglects this effect.

³⁴ As a wing with negative and positive incidence angles produces local lift that may result in no overall net lift, induced drag is present that is not a function of C_L

4.1 Oswald Factor

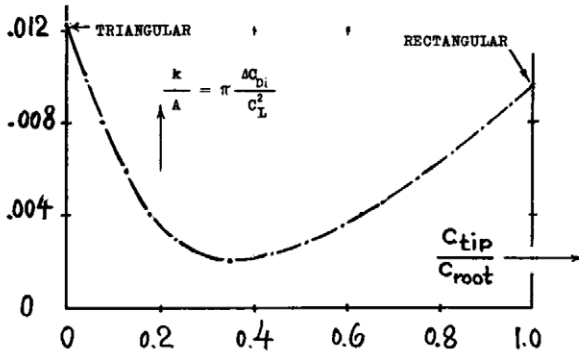


Figure 4.3: δ depending on the taper ratio, [49]

$$e = \frac{1}{1 + \delta AR} \quad (4.27)$$

$$e' = e \cos(\varphi) \quad (4.28)$$

$$e' = e \cos(\psi)^2 \quad (4.29)$$

Table 4.1 summarizes the findings of the literature review on existing approaches to quantify the Oswald factor. It displays the qualitative dependencies for each analysis method. It must be noted, that none of the analysis methods takes into account the twist angle of the wing neither as geometric nor as aerodynamic twist. Furthermore, all approaches are limited to single trapezoid geometries.

Author	AR	φ	λ	t/c	ψ
Raymer [105]	•	•			
Howe [51]	•	•	•	•	
Jenkinson [54]	•		•		
Kroo [64]	•				
Hörner [49]	•	•	•		•

Table 4.1: Existing approaches: Oswald factor

As already mentioned, the method described by Kroo relies on a factor u that needs to be determined from physics-based analysis, and hence, Kroo's approach is usually sensitive to more parameters. Howe's method is listed for completeness. It is not comparable to the definition of the Oswald factor that is applied in this study as it includes several other effects.

Multi-Fidelity Workflow: Oswald Factor

The design space that is covered by the above mentioned methods is limited to few parameters, a common characteristic of conceptual design methods. Hence, in the following paragraphs the multi-fidelity workflow, as outlined in chapter 3, is applied to derive a new conceptual design method to quantify the Oswald factor. The new method is supposed to remain as transparent and cost effective to evaluate as the outlined existing approaches in conceptual design.

The design concept is a low-wing, wing and tube configuration with conventional empennage. It is similar to the aircraft shown in figure 3.7. The wing is a double trapezoid with an inboard rectangular fuselage section followed by trapezoids each in- and outboard of the kink. The wing is linearly, geometrically twisted³⁵ from the root to the tip. Figure 3.6 shows the graphical representation of the parametrization.

Variable	Symbol	Range
Sweep angle	φ_{25}	$-40.0^\circ - 40.0^\circ$
Aspect ratio	AR	5.0 - 25.0
Taper ratio	λ	0.1 - 1.0
Twist angle	τ_t	$-5.0^\circ - 5.0^\circ$
Kink ratio	η_k	0.2 - 0.4

Table 4.2: Domain of definition: Oswald factor

Table 4.2 details the domain of definition that includes wing sweep, aspect

³⁵ For an up-to date commercial aircraft the twist distribution is far more complex. However, such a twist distribution can only be found from detailed studies that include several disciplines. The goal of this study is rather to establish a sensitivity of the aircraft properties towards twist, and enable designers to assess how much twist is approximately necessary for the final design.

ratio, taper ratio, twist and kink ratio. Both forward and backward swept geometries are under examination. Furthermore, the study explores low to high aspect ratio wings; aspect ratios for nowadays aircraft range from 7 to 10. The taper ratio is limited from 0.1 to 1.0, to examine a broad area around the expected optimum of ≈ 0.4 for an unswept wing. Finally, the twist angle and the spanwise location of the kink are taken into account. The study neglects the effects of the fuselage, and instead, it applies the correction as proposed by Kroo, see equation 4.26.

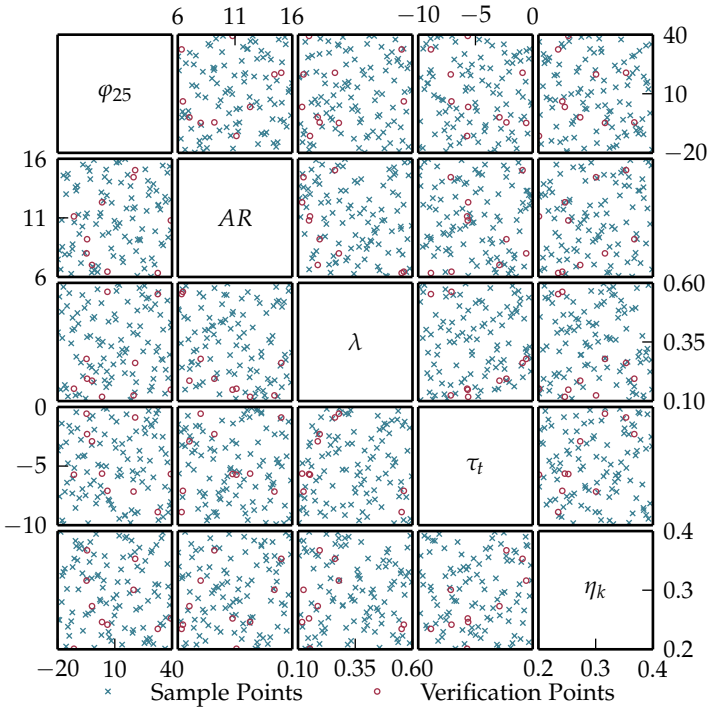


Figure 4.4: Design of experiments: Oswald factor

The design of experiments builds upon a Latin hypercube sampling plan with $n = 100$ samples. As the experiments conducted in chapter 3.3

suggested $n = 10k$ samples, the sampling plan is sized conservatively. Figure 4.4 shows the design of experiments. All points from the Latin hypercube are displayed as blue crosses. Furthermore, red circles mark $n = 10$ verification points that are the result of a Monte Carlo sampling. Appendix D list all results of the multi-fidelity workflow.

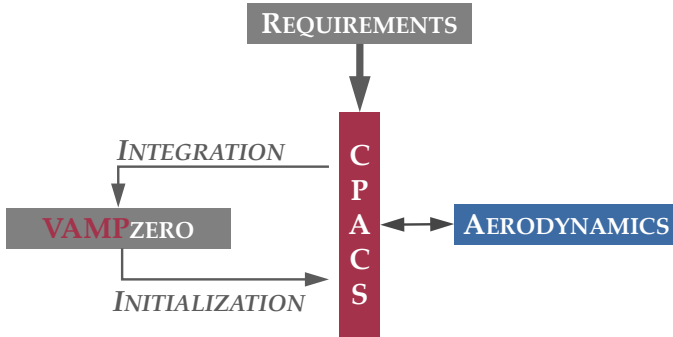


Figure 4.5: Multi-fidelity loop: Oswald factor

The multi-fidelity loop that quantifies the Oswald factor is shown in figure 4.5 which is a special case of figure 1.3. It consists of a set of requirements, e.g., range and cruise Mach number, for the aircraft³⁶ that include the characteristics, e.g., sweep angle and aspect ratio, which are identical to the samples within the design of experiments. This information is forwarded via CPACS to the conceptual design model VAMPzero. Subsequently, VAMPzero derives the concept and creates the necessary information to trigger the physics-based analysis.

A vortex lattice method is applied to quantify the induced drag. Similar to Prandtl's lifting line theory, it is valid for incompressible, inviscid flows. However, it overcomes some of the shortcomings of Prandtl's theory and provides reliable results for swept and low-aspect ratio wings. The theory applies not only one lifting line along the spanwise coordinate, but an infinite number of lifting lines. Therefore, the circulation changes not only in spanwise, but also in chordwise direction, as figure 4.6 shows. Hence, two vortex sheets in x and y exist, where one is due to vortex lines running

³⁶ In this study the requirements are similar to a mid-range, passenger aircraft like the Airbus A320 or Boeing B737.

in spanwise direction $\gamma(x, y)$ and one is due to vortex lines running in chordwise direction $\delta(x, y)$. Subsequently, these distributions are solved for the flow-tangency condition, i.e., the induced velocities summed with the free stream velocity need to be zero on the lifting surface.

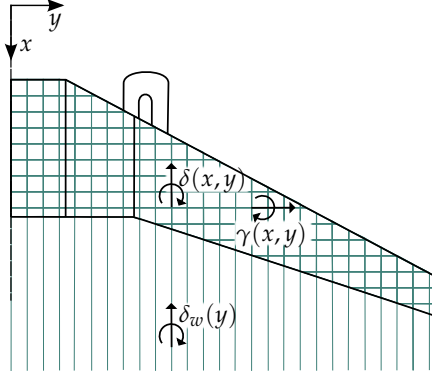


Figure 4.6: Vortex lattices on double trapezoid wing

Several analysis models exist for vortex lattice analysis and are publicly available. Among the most widely known are: Tornado from Melin [89], AVL by Drela [30], and LIFTING_LINE from Horstmann [50]. This study applies Tornado as implemented by Pfeiffer et al. [99].

Subsequently, VAMPzero receives the aerodynamic performance map of the aircraft configuration from Tornado³⁷. The aerodynamic performance map lists, among other parameters, the lift and drag coefficients over the angle of attack of the configuration. VAMPzero groups corresponding pairs of lift and drag coefficients, and it fits them to a polynomial of second order as in Eq. 4.30. The constant part of this equation provides the increase in

³⁷ Vortex-lattice models may only be applied to slender bodies to produce reasonable results. Hence, the fuselage is excluded in the aerodynamic calculation. Furthermore, the empennage is excluded from the calculation to eliminate any side-effect. In a future study, it might be of interest to derive the Oswald factor for a trimmed configuration that includes a sized horizontal tail plane.

drag due to local lift³⁸, the linear part the shift in drag due to the incidence angle of the wing. Both terms may be neglected when the focus is set on the Oswald factor. Hence, equations 4.17 and 4.30 in combination provide the Oswald factor (Eq. 4.31) as an outcome of the vortex lattice analysis.

$$c_D = ac_L^2 + bc_L + c \quad (4.30)$$

$$e = \frac{1}{aAR\pi} \quad (4.31)$$

The values of the Oswald factor at each location within the design of experiments are passed on to the symbolic regression algorithm. The algorithm is forced to include all parameters in the resulting equation even if their influence on the Oswald factor is small. Furthermore, the algorithm is allowed to apply the following mathematical operators: constant, addition, subtraction, multiplication, power, cosine, sine, logarithm, and the e -function. Division is omitted to suppress zero division errors in the resulting equation. However, the algorithm may apply divisions by negative exponents for the power operation, but they come at a significantly higher cost in terms of complexity. Hence, the mathematical solution is not omitted, but limited by a higher cost in terms of complexity.

Equation 4.32 is the result³⁹ of the symbolic regression. It departs from the formulation mentioned above to take into account the further design parameters. Interestingly, the symbolic regression proposes to apply a cosine in the equation. The cosine as well as the Oswald factor may not exceed values greater than one, and hence, the upper limits of the codomain are identical.

$$e = \cos(0.3761\lambda - 2.086/AR + 0.2013AR\eta_k\varphi - 0.2013AR\lambda\tau_t\eta_k\varphi) \quad (4.32)$$

In addition to the initial sample points in the DOE, a Monte Carlo sampling plan with ten samples is evaluated to verify equation 4.32. For this purpose

³⁸ Drag due to local lift arises mostly from a twist of the wing. For a twisted wing incidence angles exist where the wing creates no net lift, because the segments of the wing create equal amounts of negative and positive lift. Despite the zero net lift, drag arises due to the local lift.

³⁹ The cosine is calculated in radians and the sweep and twist angle are also converted to radians to remain compatible with most computer algebra systems.

4.1 Oswald Factor

Metric	Sample points	Verification points
Mean error	-0.16%	-0.70%
Standard deviation	3.3%	1.8%
Root mean squared error	0.11%	0.04%
Standard deviation	0.22%	0.039%

Table 4.3: Verification: Oswald factor

the sample and verification points are compared to the equations proposed by the symbolic regression. Table 4.3 shows both the mean error and the root mean square error averaged over all samples, as in Equation 3.9, and their respective standard deviations. It can be seen that all error metrics have a reasonable low value, in some cases the error is even lower for the verification points than it is for the sample points. Hence, equation 4.32 seems to represent the physical behavior not only at the locations specified in the initial DOE but also at different locations in the design space. Chapter 5 further discusses the results obtained from the design studies.

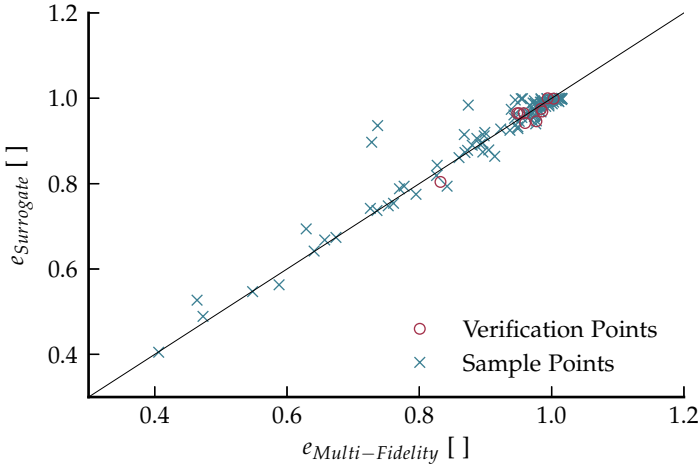


Figure 4.7: Verification: Oswald factor

Figure 4.7 displays the error between the surrogate model and the multi-

fidelity loop. Sample points are indicated by blue crosses; verification points by red circles. The error equals zero if all points are located on the diagonal. It can be seen that the error remains mostly in reasonable boundaries, especially for all verification points.

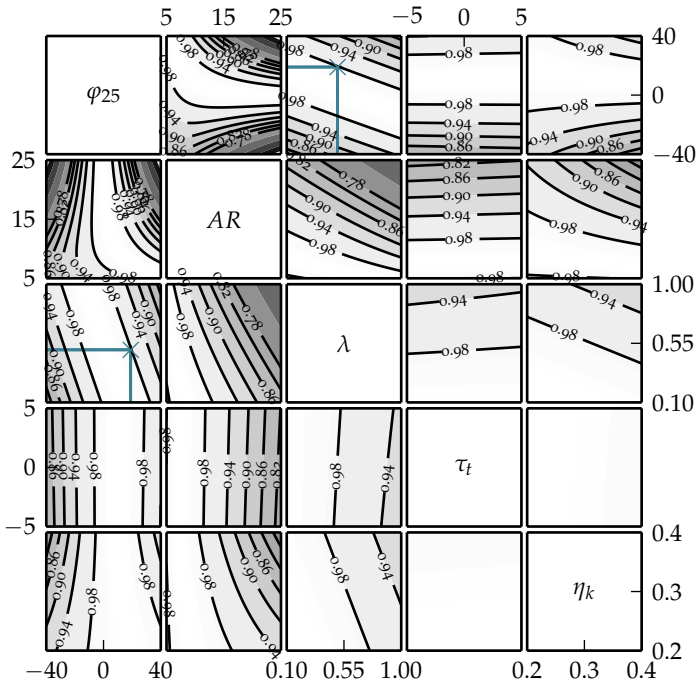


Figure 4.8: Surrogate model: Oswald factor

Figure 4.8 displays the behavior of the surrogate model. The hidden dimensions are set to default values, i.e., $\varphi = 20^\circ$, $AR = 9.5$, $\lambda = 0.25$, $\tau_t = -2^\circ$, and $\eta_k = 0.35$. As a matter of fact, the full behavior of Eq. 4.32 can only be displayed in an infinite number of plots, and hence, the interpretation is limited on this snapshot of the multi-dimensional space.

For clarification, figure 4.8 can be understood as a combination of contour

plots for two dimensions each. Each contour plot is repeated in opposite order. The remaining dimensions take the above mentioned default values. For example, in figure 4.8 two locations for a taper ratio of 0.5 and a wing sweep of 19° are highlighted. The value of the Oswald factor at this location equals ≈ 0.98 .

Generally speaking, figure 4.8 shows that equation 4.32 is highly sensitive to the sweep angle, aspect ratio and taper ratio. The influence of the twist and the kink is significantly lower. The Oswald factor is high for low sweep angles. The tendency towards positive sweep angles is a result of the kink on the trailing edge of the wing. For a forward swept wing the kink increases the inboard area of the wing. On the contrary, the kink decreases the inboard area of a backward swept wing. For a tapered wing, the former effect leads to a lift distribution that is shifted too far inboards.

If the aspect ratio is low then the highest values for the Oswald factor can be obtained. While this seems to be inconsistent with aircraft designers experience (the higher the aspect ratio the lower the induced drag) it must be kept in mind that the Oswald factor describes the deviance of the elliptical lift distribution, and this deviation becomes significant for very high aspect ratios. However, due to equation 4.17 the induced drag is lower for a high aspect ratio of the wing. The same behavior can be observed from Hoerner's and Raymer's formulations for the Oswald factor.

The sensitivity of the Oswald factor towards the taper ratio is comparable to the aspect ratio and sweep angle. If the wing has only little sweep then the taper ratio must be close 0.5 to obtain best values for the Oswald factor. For forward swept wings the taper ratio should be further reduced, again a result of the kink on the trailing edge. The higher the aspect ratio the higher the taper ratio should be to remain within a reasonable range of an elliptical lift distribution.

The influence of the twist angle on the Oswald factor is comparably small. On the one hand, this may be due to the fact that wing is twisted linearly, and hence, the twist acts similar to an increase of the incidence angle of the wing, despite the increased effect towards the tip of the wing. On the other hand, the effect of the twist on the constant part of equation 4.30, i.e., the drag due to local lift, is significant. In a future study, the outlined design study can be applied to deliver means of quantification for this ef-

fect. However, the twist distribution should then be a result of a combined aerodynamic and structural study.

The effect of the spanwise kink location on the Oswald factor is, similar to the twist, small. For high sweep values, a more inbound location of the kink is preferable as it reduces the amount of inboard lift. This effect is higher for forward swept wings. The same effect applies for high aspect ratio wings.

The results presented above serve as means to verify equation 4.32, i.e., ensure that the equation reflects the behavior of the higher-fidelity model in an accurate way. Subsequently, a validation is necessary that demonstrates that the same equation is applicable in conceptual aircraft design. As a matter of fact, the design space during the validation is limited to existing designs, and appendix B lists the 25 reference aircraft.

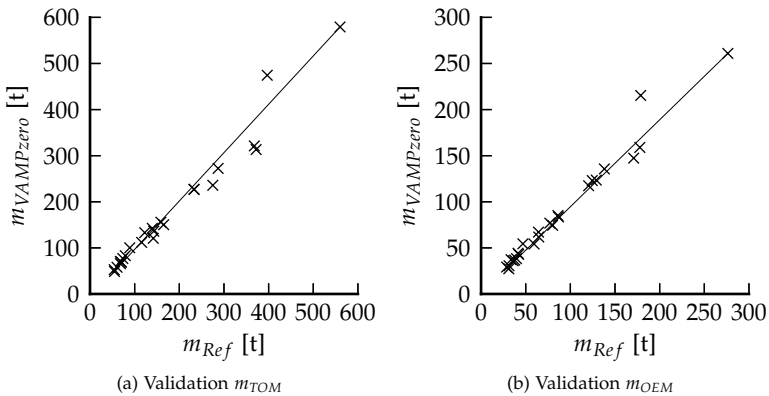


Figure 4.9: Validation: Oswald factor

Usually, the input into a conceptual design code is limited as little information is available. Similarly, the data given in the appendix is sparse and hampers convergence. The initial version of VAMPzero⁴⁰ fails to converge for five of the reference aircraft. If these aircraft remain out of consider-

⁴⁰ The initial version of VAMPzero is based on Raymer's previously mentioned method to estimate the Oswald factor.

ation then the average error is approx. 7.3% for the m_{TOM} and 3.6% for the m_{OEM} . The results improve after equation 4.32 has been integrated into VAMPzero. The average error is now $-2,1\%$ respectively -0.9% and all designs converge. Figure 4.9 compares the results of the VAMPzero calculations and the reference aircraft. Hence, the multi-fidelity workflow enlarges not only the design space, but it also increases the accuracy of the conceptual design model.

4.2 Wing Mass

The second design study quantifies the wing mass of a jet transport aircraft by means of a high-fidelity wing mass estimation process. A predecessor of the study has been published in [13]. Contrary to the Oswald factor, the wing mass is a dimensional parameter, i.e., it is expressed by some means of a mass unit and a conceptual design method for a dimensional parameter may not be scaled as easily. For example, the equation to quantify the Oswald factor is applicable to wings of all sizes. Given the fact that the mass estimation introduces a further physical dimension, the domain of definition that needs to be covered increases significantly. Furthermore, as not all locations within the domain of definition are valid design points, the analysis is hampered, e.g., an analysis for an aircraft with a wing of low reference area, e.g., similar to an Embraer E-195, and high maximum takeoff mass, e.g., similar to an Airbus A380, is likely to fail. Regardless of the “success” of the physics-based analysis, the design concept is most probably inappropriate.

The following sections cover these issues. First, a definition of the wing mass is introduced. Subsequently, the study outlines means for wing mass estimation and existing approaches. Finally, the multi-fidelity workflow that determines the wing mass is processed, evaluated and validated.

Wing Mass Definition

This study applies the wing mass definition of the Luftfahrttechnisches Handbuch [52]. It is similar to the Airbus weight chapter 10 definition. Accordingly, the wing mass equals the sum of:

- skins (including stringers),

- spars,
- ribs,
- pylon attachments (front and rear attachment, fairing attachments, spigot attachment),
- landing gear support (gear beam and ribs, attachments and fittings),
- fixed leading edge (ribs, panels, movable support structures),
- movable leading edge (slat, droop nose, krueger flaps, slat tracks),
- fixed trailing edges (panels, falsework, flap tracks and attachments, spoiler and aileron support),
- movable trailing edges (flaps including flap track rear link and carriages, ailerons and spoiler),
- and miscellaneous (external paint final coat, wing tips, winglets, sealant, fairings, fittings and supports).

It must be noted that the definition above is applied to all calculations in the subsequent sections. However, it may not be taken for granted that all of the existing approaches that are outlined in the literature review follow this definition. The information that is obtainable from these resources is seldom sufficient to extract an exact definition of the wing mass.

Ardema et al. [8] estimate that the total mass of the wing equals the primary wing mass, i.e., the physically sized wing box, times a factor of ≈ 1.73 . Of course, this number is only valid in a very limited domain of definition of a conventional design concept. Hence, special attention needs to be paid to the methods that are applied to quantify the wing mass and whether they take into account secondary structures or not.

Means for Wing Mass Estimation

Several analysis methods exist to quantify the items of the wing mass breakdown listed above and their applicability depends on the design task

at hand. This section outlines different levels of fidelity of wing mass estimations methods⁴¹ and their recommended area of application.

For conventional configurations reliable conceptual design methods exist. These base on historical-based methods and may be enhanced by simplified physics-based terms. Chapter 2 already presented some examples. However, these conceptual design methods suffer from the drawbacks of any historical-based method, and hence, they are usually not applicable for unconventional designs. As it is the goal of this work to replace some of these methods, the following section discusses existing approaches in conceptual design in more detail.

The next higher level of fidelity encompasses lower order physics-based models. For example, Ardema et al. [8] and Elham et al. [33] published representative studies. Their methods require more information as input and are physics-based with the aid of some empirical corrections. Some of the included analyses base on assumptions, i.e., the lift distribution. In the structural analysis, models base mostly on beam representations. Beam models presume that one dimension of the structure is significantly larger than the others. Hence, beam models return reasonable results for high aspect ratio wings. However, beam models suffer from the fact that kinks can hardly be represented and local load introduction, e.g., at the engine location, is also hampered by the physical model.

Higher order physics-based models rely on shell models of the structure rather than on beam models. Dorbath [29] and Rieke [108] published exemplary implementations. Usually, not only the structural representation of these models is more elaborate, but also the loads computation and aeroelastic⁴² couplings go into more detail. Shell models differ themselves from beam models as not only one dimension, but two are significantly larger than the other. These models overcome many of the shortcomings of beam models, and hence, they enable designers to reliably predict the properties of more sophisticated structures, e.g., secondary structures such as control surfaces and pylon attachments. Hence, the change in the level

⁴¹ Concerning higher fidelity models, a detailed treatment of loads and finite element models is out of the scope of this study and only an overview on implementations of these disciplines is given. Lomax [76] is a sound source for detailed information on loads as well as Cook et al. [28] is for finite element analysis.

⁴² However, the aeroelastic coupling remains static for these high level of detail models. For example, most academic aeroelastic applications exclude full control surface kinematics and structures.

of detail of the physical models allows the designer to increase the level of fidelity of the product model. As the works of Dorbath already link to CPACS, this model is applied in the present study.

Existing Approaches in Conceptual Design

The Luftfahrttechnisches Handbuch [52] introduces Equation 4.33 to quantify the mass of the wing. It is valid for conventional, aircraft configurations that range from a maximum takeoff weight (m_{TOM}) of $33t$ up to $400t$. When validated to a broad set of existing designs, the standard deviation of the method is 6.4% .

$$m_{wing} = 2.20013 \cdot 10^{-4} \left(401.146S^{1.31} + m_{TOM}^{1.1038} \right) \frac{AR^{1.5}(t/c)^{-0.5}}{\cos(\varphi)} \quad (4.33)$$

Contrary to the Luftfahrttechnisches Handbuch, Raymer [105] introduces a handbook method (Eq. 3.13) that also includes the ultimate load factor n and the area of the control surfaces S_{cs} . In addition, the taper ratio of the wing λ is taken into account. Chapter 3 already applied Raymer's equation for the comparison of surrogate models.

$$m_{wing} = 0.0051 \frac{(m_{TOM} n_{ult})^{0.557} S^{0.648} AR^{0.5} (1 + \lambda)^{0.1} S_{cs}^{0.1}}{\cos(\varphi)(t/c)^{0.4}}$$

Shevell [127] developed a handbook method (Eq. 2.2), as already mentioned in chapter 2, that quantifies the wing mass and distinguishes between parts that are dependent and independent of the wing bending moment. Therefore, the first part of the equation is completely empirical, whereas the second part is influenced by physical assumptions. Furthermore, Shevell introduces the maximum zero fuel weight m_{ZFM} as a variable to take into account the missing bending relief from fuel stored in the wing tanks.

$$m_{wing} = K_1 S + K_2 \frac{n_{ult} b \sqrt{m_{TOM} m_{ZFM}}}{(t/c) \cos(\varphi)^2 S} \frac{1 + 2\lambda}{1 + \lambda}$$

Toreenbeek [134] developed equation 4.34, and Roskam [114] cites this equation as well. It relies only on m_{ZFM} and leaves out m_{TOM} . Several

Author	m_{TOM}	m_{ZFM}	S	b	AR	t/c	φ	λ	S_{cs}
LTH [52]	•		•		•	•	•		
Raymer [105]	•		•		•	•	•	•	•
Shevell [127]	•	•	•	•		•	•	•	
Toreenbeek [134]		•	•	•		•	•		

Table 4.4: Existing approaches: Wing mass

additional correction parameters can be defined, e.g., for wing mounted engines and aircraft of different weight classes.

$$m_{wing} = \left(\frac{12.55 \cdot 10^{-3} b}{\cos(\varphi)} \right)^{0.75} \left[1 + \left(\frac{6.3 \cos(\varphi)}{b} \right)^{0.5} \right] n_{ult}^{0.55} \left(\frac{bS}{(t/c)m_{ZFM} \cos(\varphi)} \right)^{0.3} \quad (4.34)$$

Table 4.4 lists all dependencies for the named handbook methods^{43,44}. The aspect ratio, span and wing reference area may of course be substituted by each other. It can be seen that Raymer provides the only handbook method that takes into account the control surface area of the wing, i.e., some means to explicitly, yet only simply, address the impact of secondary structures on the wing mass.

Multi-Fidelity Workflow: Wing Mass

As the outlined approaches are limited to statistical observations in combination with simplified physical models, they can hardly be applied to new design concepts or at unconventional locations in the domain of definition. This section elaborates a multi-fidelity workflow to quantify the wing mass that is physics-based, includes some of the secondary masses, and leads to

⁴³ The dependencies of the named handbook methods are not as similar as displayed in the table. For example, the thickness to chord ratio may be the thickness to chord ratio at the root of the wing or the average thickness to chord ratio. This distinction is excluded for clarity but taken into account for the quantitative comparison of the handbook methods.

⁴⁴ As the study takes into account only aircraft that belong to the same regulation category, the load factor is excluded from this list

Variable	Symbol	Range	Unit
Wing loading	W/S	450 - 750	[kg/m ²]
Sweep angle	φ_{25}	-40.0°- 40.0°	[]
Aspect ratio	AR	6.0 - 13.0	[]
Taper ratio	λ	0.2 - 0.6	[]
Thickness ratio	t/c	0.1 - 0.16	[]

Table 4.5: Domain of definition: Wing mass

a surrogate model that can be applied in conceptual aircraft design. The schematic of the multi-fidelity workflow is again similar to figure 3.1 introduced at the beginning of chapter 3.

The design concept remains unchanged to the previous design study on the Oswald factor: A low-wing, wing and tube aircraft with a parametrization similar to figure 3.6. Two engines are located on the wing outboard of the kink. The wing box is created from two spars. The wing features all control surfaces of a today's aircraft, i.e., ailerons, flaps, slats, and spoilers.

The domain of definitions is similar to the previous design study. Twist is now excluded and set to standard values as the detailed twist distribution that includes twist angles at several locations should be determined by a separate optimization at a later design stage. The thickness ratio is included as an additional parameter, as it has a major impact on the wing mass. The thickness to chord ratio is a non-dimensional parameter that describes the maximum thickness of the wing in terms of its chord. The provided thickness to chord ratio is the thickness to chord ratio at the root of the wing. The thickness to chord ratio is identical at the root and the fuselage-wing intersection. As the wing thins towards its tip, the thickness to chord ratio at kink and tip is lower.

As the design of experiments consists of five design variables and again for each design variable twenty samples are taken into account, the DOE of the previous design study can be reused. As a matter of fact, the scaling of the design variables changes but the overall layout is similar to figure 4.4. Furthermore, appendix E provides all results of the multi-fidelity workflow.

As already mentioned, several difficulties arise from the fact that the wing mass is a dimensional parameter. Instead of analyzing several aircraft of

different weight categories this study remains its focus on a mid-range, narrow-body aircraft and alters the wing loading W/S . The wing loading is the ratio of the maximum takeoff mass to the wing's reference area. Hence, in the multi-fidelity workflow the wing area remains constant and the maximum takeoff mass changes. The result of the multi-fidelity workflow is an equation f_0 , as in equation 4.35. In a subsequent step, f_0 is scaled by the reference area to extend the domain of definition of the newly developed conceptual design method. For this purpose the wing mass data that has been used to derive the LTH wing mass estimation equation is combined with the initial equation to find f_1 as a function of f_0 and the wing's reference area.

$$f_0 = f(AR, \varphi_{25}, \lambda, (W/S), (t/c)) \quad (4.35)$$

$$f_1 = f(S, f_0) \quad (4.36)$$

Figure 4.10 shows the multi-fidelity loop for the wing mass design study which is again a special case of figure 1.3. In contrast to the Oswald factor design study, it includes further analysis models. These are loads, aerodynamics and structures, i.e., mass estimation. In the initialization, VAMPzero derives not only the outer wing shape but also the location of inner structures as well as the control surfaces and wing tanks. The area of the control surfaces is determined by empirical correlations in VAMPzero; the initialization defines the outer shape of the control surfaces in accordance to the overall wing layout. All values are provided in a relative spanwise coordinate ζ and a relative chordwise coordinate χ .

In accordance to empiric rules, two spars and four ribsets, where each ribset may either hold a fixed number of ribs or several ribs at a fixed distance, are placed within the wing. The first ribset is located within the rectangular fuselage section and holds four ribs. The second ribset extends from the fuselage up to the engine. It is combined with a single rib so that one rib is equidistant to the engine pylon on the right and left side. Finally, a last ribset stretches from the engine on outward close to the tip of the wing.

Three tank volumes are defined within the wing where the boundaries of the tanks are provided by the spars and ribs. Again, the first tank is in the rectangular section within the fuselage, the second extends from

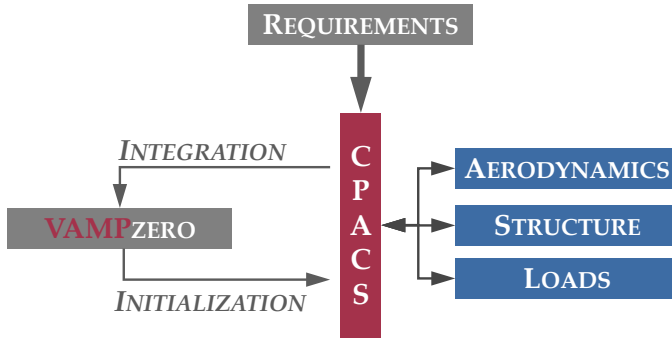


Figure 4.10: Multi-fidelity loop: Wing mass

the fuselage up to the engine, and finally the last tank is outboard of the engine.

In a subsequent step, VAMPzero positions the control surfaces (ailerons, flaps, slats and spoilers) on the wing. The positioning encompasses the definition of the outer shape as well as the internal structure of the control surfaces and the connections to the overall wing structure. The area of each control surface is determined by the inner loop of VAMPzero, the shape is subject to knowledge based engineering rules as outlined in the following paragraphs.

Ailerons are placed from the outer tip of the wing inwards. As the chord of the aileron is a function of the span, the layout needs to be determined in an iterative process. The aileron starts at $\zeta = 0.96$ and is extended inboard with a constant relative chord offset to the rear spar of the wing. Actuators of the aileron are placed at a relative aileron span position of thirty and seventy percent, respectively.

Flaps are divided in inner flaps that are inboard of the kink and outer flaps outboard of the kink. The initialization starts with the inner flaps. All remaining area⁴⁵ is forwarded to the outer flaps. The inner flaps have a constant absolute chord which is determined by the spar offset at the kink. The inner flaps extend between the kink and the wing-fuselage intersection. The outer flaps have a constant relative spar offset. The spar offset

⁴⁵ At the conceptual design stage only the overall flap area is quantified. Hence, the initialization must distribute the flap area across the wing in a reasonable manner.

decreases, if the outer flaps overlap with the aileron. If the remaining area is not sufficient then the rear spar positioning needs to be changed. Flaps are split up into several flaps if the aspect ratio of a flap exceeds 9.

Similar to the flaps, spoilers are grouped into inner and outer spoilers with respect to the kink. The outermost ζ location of the spoiler is identical to the outermost position of the flaps. The chord of the spoilers is 5% of the kink chord length plus 50% of the inner flap length. All spoilers have a rectangular shape. Spoilers are split up if their aspect ratio exceeds 3.

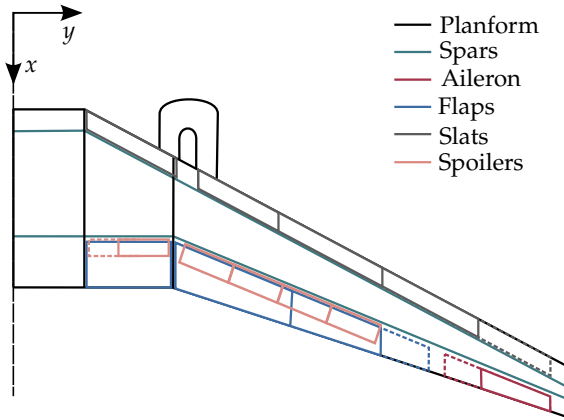
Finally, slats are defined on the wing's leading edge. Slats have a constant absolute chord, and a $\zeta = 0.05$ gap is inserted at the engine location. The outboard position of the slats may not exceed $\zeta = 0.95$. They are split up for aspect ratios higher than 5.5. If the chord of the slats exceeds $\chi = 0.075$ at the wing-fuselage intersection then the front spar locations need to be revised.

Figures 4.11a and 4.11b show a schematic of the wing including control surfaces that is initialized by VAMPzero and an example representation of the finite element model in WINGmass, developed by Dorbath [29]. All the control surfaces that are defined by VAMPzero include structural information on the material and the thickness of the skin, the spars, and the ribs. The initialization is not expected to deliver a sufficiently designed aircraft, e.g., a sized skin thickness distribution, but enables the use of higher-fidelity analysis. Hence, the design may be sized and altered as more detailed information becomes available.

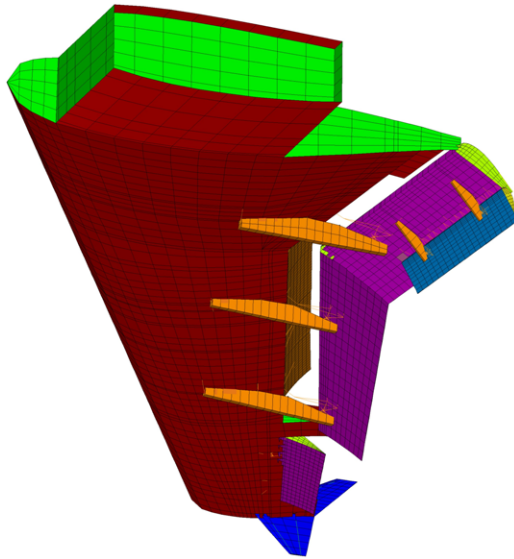
WINGmass is one of the components of ELWIS that encompasses all higher fidelity analysis models applied to determine the wing mass⁴⁶. ELWIS serves as a preprocessor and communicator between the already mentioned disciplines loads, aerodynamics and structures. The finite element wing model is generated by ELWIS in a fully automated process from the CPACS parameterization. The ELWIS model generator reads the CPACS file, builds an internal model of the wing and finally writes the ANSYS input file. Skins, ribs and spars are modeled as shell elements. Stringers are modeled in a smeared representation in an additional shell layer. Spar caps are modeled by beam elements with a rectangular cross section.

After the lifting surfaces, the so called additional structures are generated.

⁴⁶ The full detail of the wing mass estimation workflow exceeds the scope of this study. Dorbath [29] is the best source for further information.



(a) Planform of wing components



(b) FEM of wing structure

Figure 4.11: Design concept: Wing mass

These structures are all structural connections between movables and the wing (flap tracks, hinges and actuators), the engine pylon and the landing gear. Compared to the generation of the lifting surfaces, the knowledge-based generation of the additional structures goes one step further. Hereby, the geometry and the computational model are generated by KBE rules. The load carrying structure of the additional structures is modeled three-dimensional, it includes the models of all joints and hinges that are part of the real components. On the one hand, this leads to realistic load paths in the component. On the other hand, the flaps and the landing gear can deflect in a non-linear multi body simulation in ANSYS. This is required, for the accurate modeling of load cases with flaps in landing configuration. Apart from the slat mass and some minor components off the mass breakdown all results of the ELWIS process are physics-based.

The integration of the higher-fidelity wing mass includes an update of the mass breakdown and a parameter replacement within VAMPzero. It is therefore straight forward in comparison to the integration of the Oswald factor. Subsequently, the results of the design of experiments can be forwarded to the symbolic regression.

The building blocks that are available to the symbolic regression to find $f_0()$ include multiplication, division, power, cosine, sine, logarithm, and the exponential function. Addition and subtraction are excluded to extract an equation that can easily be scaled by S and still remains reasonably transparent. Equations 4.37 and 4.38 are the result of two consecutive symbolic regression runs. Obviously, the symbolic regression neglects the taper ratio as the sensitivity of the wing's mass to this parameter is small. The decision of the algorithm seems reasonable in comparison to the literature review. Only two out of four sources include the factor and in Raymer's as well as in Shevell's approach the impact of the taper ratio is small.

$$f_0 = \frac{353.9AR(W/S)^{0.1699}\cos(2.178(t/c)\ln(AR))}{\cos(\varphi_{25})e^{1.96E-7\varphi_{25}AR^{3.452}/(t/c)^{2.918}}} \quad (4.37)$$

$$f_1 = 0.0123f_0S - 0.42f_0 \quad (4.38)$$

Figure 4.12 shows the behavior of equation 4.37 in comparison to the results of the multi-fidelity loop. It serves as means to verify that the surrogate model represents the behavior of the physic-based analysis. As before, the

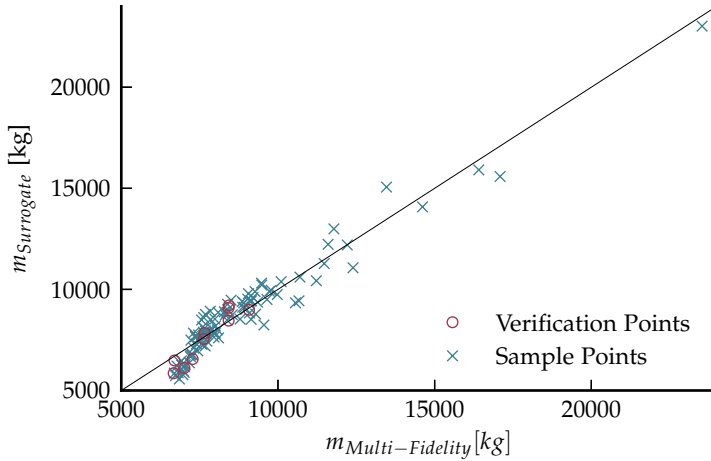


Figure 4.12: Verification: Wing mass

Metric	Sample points	Verification points
Mean error	-0.61%	-2.1%
Standard deviation	7.5%	7.3%
Root mean squared error	0.57%	0.58%
Standard deviation	0.71%	0.61%

Table 4.6: Verification: Wing mass

error of the surrogate model is zero if all points are located on the diagonal. Remarkably, the surrogate as well as the physics-based analysis manage to represent the outlier at $\approx 22t$ in the upper right of the plot. The sample is a high aspect-ratio, forward swept wing with a high wing loading and close to minimum thickness to chord ratio. It is the only sample that made changes to the physics based analysis necessary to converge. However, the changes affected only the numerical solver and not the physical model.

Furthermore, table 4.6 lists the error metrics for the surrogate model. Similar to the previous design study, the values of the sample and verification points are compared to the results of the surrogate model at the same loca-

4.2 Wing Mass

tions. The mean and root mean error are provided as well as their standard deviations. All values are comparably low; the mean error for the verification points is noticeable, but not critical.

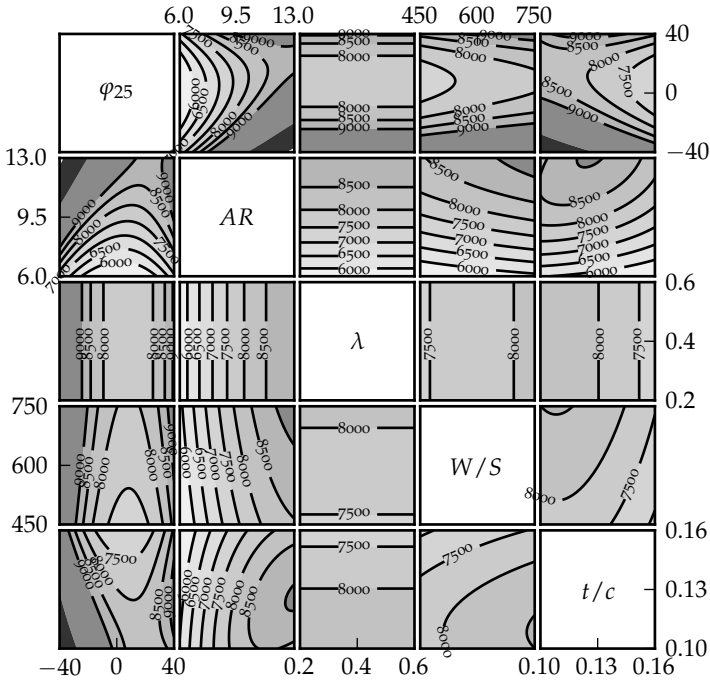


Figure 4.13: Surrogate model: Wing mass

Figure 4.13 displays the behavior of the surrogate model. The hidden dimensions are set to default values, i.e., $\varphi = 20^\circ$, $AR = 9.5$, $\lambda = 0.25$, $(W/S) = 600\text{kg}/\text{m}^2$ and $(t/c) = 0.14$. It must be noted that similar to the previous plot on the behavior of the Oswald factor and due to the high dimensionality of the design space only this single cut-out of the behavior in the five-dimensional design space can be presented.

As the taper ratio is included in the design space but not in the surrogate

model, figure 4.13 is not sensitive to this parameter. Furthermore, the wing loading has the lowest impact on the wing mass. The sweep angle has a large impact on the wing mass. The mass increase is worse for forward swept wings than for backward swept wings. Partially, this is due to wash-in and wash-out effects. Furthermore, the design concept hampers forward swept wings. On the one hand the twist distribution, albeit conservative, is non-beneficial for a forward swept wing. However, as already mentioned, a sophisticated multi-disciplinary optimization is necessary to determine a reasonable twist distribution and while the multi-fidelity loop is capable of this operation the computational cost⁴⁷ is currently not manageable. On the other hand, the kink is beneficial for the wing mass of forward swept wings as additional bending moment is shifted inwards.

As expected, the aspect ratio has the highest impact on the wing mass. Non-linear effects are dominant in combination with the sweep angle of the wing. Furthermore, for high aspect ratios the coupling with the thickness to chord ratio becomes dominant. Minor sensitivities can be observed for the combination of the wing loading and the thickness to chord ratio.

In comparison to the design study on the Oswald factor, the domain of definition has been limited as the structural design concept is only applicable in this limited bandwidth. Both the behavior of equation 4.37 and the outlier in figure 4.12 justify these limitations as they demonstrate the boundaries of the design concept. If considered independently then higher aspect ratios seem to be possible even if they may not be sensible designs. However, the combination of high-sweep angles and high aspect ratios is close to what is manageable by the physics-based analysis⁴⁸ and at least the backward sweep angle should not be reduced any further to still include existing designs.

Finally, equation 4.38 is included in the conceptual design model to validate it in the context of overall aircraft design. Figure 4.14 compares the results of VAMPzero and the reference aircraft. It must be noted that VAMPzero is improved by equation 4.32 (Oswald factor) as well as by equation 4.38

⁴⁷ A single sample of the multi-fidelity loop takes about 7 to 10 hours. The number of samples is 110. Hypothetically, if each optimization demands an additional 20 iteration per sample, the raise in computational cost is insurmountable.

⁴⁸ Furthermore, aeroelastic effects start to have a significant influence on the wing mass as high aspect ratios and sweep angles amplify the effects of wash-out. Hence, for these radical designs a sophisticated twist distribution is necessary which is currently omitted due to the reasons mentioned above.

4.3 Strut-Braced Wing Mass

(wing mass). In combination, both equations improve the average error of the maximum take off mass from -2.1% to -1.4% and the average error of the operational empty mass from -0.9% to -0.6% .

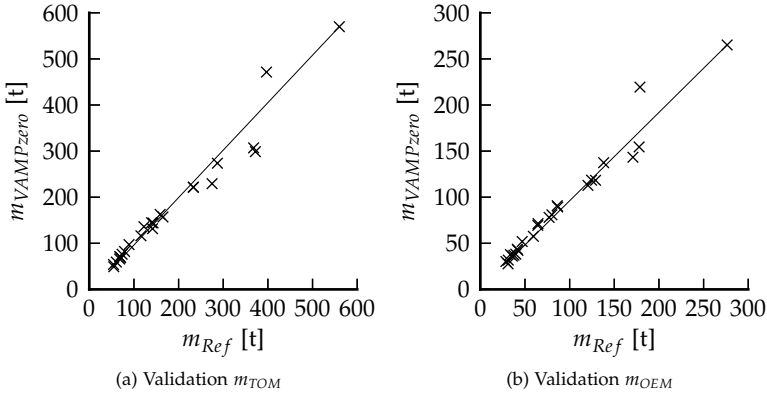


Figure 4.14: Validation: Wing mass

4.3 Strut-Braced Wing Mass

The present study states that conceptual design methods are currently not capable of handling unconventional configurations, and the study aims to enhance conceptual design by means of physics-based analysis at comparable cost and complexity of a conceptual design method. However, the design studies included so far in this chapter show none of the infamous unconventional design concepts such as the box- or strut-braced wing. The design studies explore the properties of a conventional design concept in an unconventional domain of definition rather than an unconventional design concept. Hence, to prove that the workflow is applicable for unconventional designs, this section describes a design study which applies the multi-fidelity workflow to a strut-based wing design. The workflow focuses on the strut and wing mass estimation.

A strut-braced wing is a high wing with a supporting strut that extends from a low fuselage position up to the wing, typically at an outer spanwise

position. The shape of the strut is similar to an untapered wing. If the wing produces lift then it puts the strut under tension. In this way, the bending moment on the wing root is reduced. Several means exist to derive a design that exploits this effect. The wing may be constructed lighter by reducing skin and spar thicknesses. Alternatively, the wing geometry may be altered to increase the aerodynamic properties. For example, high aspect ratio strut-braced wings reduce the amount of induced drag, or the thickness of the wing may be reduced to enable a higher proportion of natural laminar flow, at least on the upper surface of the wing. If the thickness of the wing decreases then the wave drag decreases under the assumption that the aircraft travels at transsonic speeds. Consecutively, the wing sweep can be reduced to further enhance the aerodynamic properties of the wing and reduce the torsion loads. Drawbacks of the configuration arise from the additional strut mass which may exceed the wing mass savings, the additional strut drag, and the interference drag at the strut-wing intersection.

Existing Approaches

Several strut-braced wing configurations have been developed in the research community. Figure 4.15 shows three different configurations from different research institutions. These studies either make use of empirics based assumptions or sophisticated physics-based analysis.

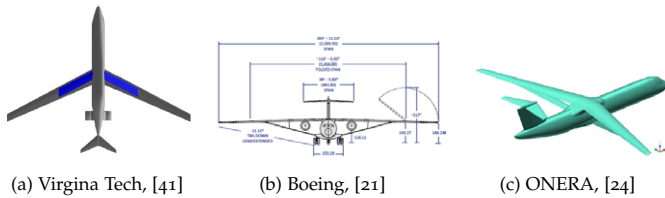


Figure 4.15: Existing approaches: Strut-braced wing

Grasmeyer [41] and Gur et al. [43] outline the research at Virginia Tech on the topic of strut braced wings. The later study examines a jet transport configuration with a design range of 7730 nautical miles and 305 passengers. Some parts of the analysis base on empirics and simple methods while other parts of the analysis, as Ko et al. [59] outline, utilize second

order response surfaces from higher-fidelity analyses. In comparison to a conventional configuration that fulfills the same requirements, the maximum take-off mass decreases by 3,5% and the fuel consumption is reduced by more than 9% percent.

Bradley and Dronney [21] present the subsonic ultra green aircraft concept (SUGAR) that is based on a strut braced wing. However, the main focus of their research is on alternative propulsion concepts. The requirements in their study ask for a configuration with a design mission of 3500 nautical miles and 154 passengers. A comparison of a today's conventional aircraft configuration with the new design at the technology level of the year 2030 results in a reduction of fuel burn by 38,9% on a mission of 900 nautical miles.

Finally, ONERA investigates a strut-braced wing configuration within the Albatros project. Carrier et al. [24] present a design for a design range of 3000 nautical miles and 180 passengers. The results are based on high-fidelity analysis with a focus on aerodynamics and natural laminar flow. Their design bests a conventional configuration by 7% in terms of take-off mass and 5,6% in terms of fuel consumption on a mission of 500 nautical miles.

The cited studies have in common that the calculations are either based on empirics or higher fidelity analysis. As empirics are usually sensitive only to a limited number of design variables (if they are sensitive at all), and higher-fidelity analysis is omitted due to reasons already mentioned in the course of this study, the conventional design of a strut braced wing is hardly possible during the very early design stages.

None of the studies mentioned above present a sophisticated mass estimation method for the strut-braced wing that includes primary and secondary structures. As the mass

Multi-Fidelity Workflow: Strut-Braced Wing Mass

Generally speaking, the multi-fidelity workflow for the estimation of the wing and strut mass is an extension of the previous workflow. Hence, similar components of both workflows are not explained in further detail. Given the fact that no strut-braced jet transport aircraft are in production or have been constructed for the size and speed of this category, a validation

is not possible. Accordingly, the last step of the multi-fidelity workflow can not be accomplished.

Apart from the strut-braced wing arrangement, the design concept changes slightly in comparison to the previous design concept. The empennage is a T-tail as customary for a high-wing configuration that must prevent deep stall scenarios. The engines are fuselage mounted to circumvent the negative impact of wing mounted engines on the natural laminar flow of the configuration. Furthermore, due to the stiff connection inboard of the strut-wing intersection no major gains in bending moment relief are expected from wing mounted engines.

The complexity of the wing is slightly reduced as no kink is necessary to include the landing gear. Hence, the wing consists of a rectangular fuselage section and two trapezoid sections outboard of the wing, where the first section extends up to the wing strut intersection. The wing still encompasses flaps and ailerons.

The strut has a wing like geometry with a symmetric airfoil and a relative thickness of 12%. The root of the strut is mounted at the lower and outer end of the fuselage, close to the expected landing gear position of this configuration. Given the fact that the strut is mostly sized by tension loads, the strut structure is composed of a single spar and a set of ribs. All components of the strut are constructed from carbon fibre materials. The tip of the strut ends in the wing in such a way that the strut spar and the wing's front spar as well as one wing rib intersect.

Additional design parameters for the strut are the position of the strut tip relative to the wing spanwise coordinate η_{strut} , and the depth of the strut c_{strut} as a ratio of the strut chord to the wing chord at the wing's root section. Figure 4.16 shows the parametrization of the strut-braced wing as well as the representation in the finite element model.

The domain of definition includes the sweep, aspect ratio, tip twist, thickness to chord ratio, maximum takeoff mass and reference area already established in the previous design studies as well as the spanwise position of the strut tip and its relative depth. Table 4.7 shows the upper and lower boundaries of the domain of definition. In comparison to the previous studies, the design space is more restricted due to the fact that more design variables are included. Especially, the combination of the maximum

4.3 Strut-Braced Wing Mass

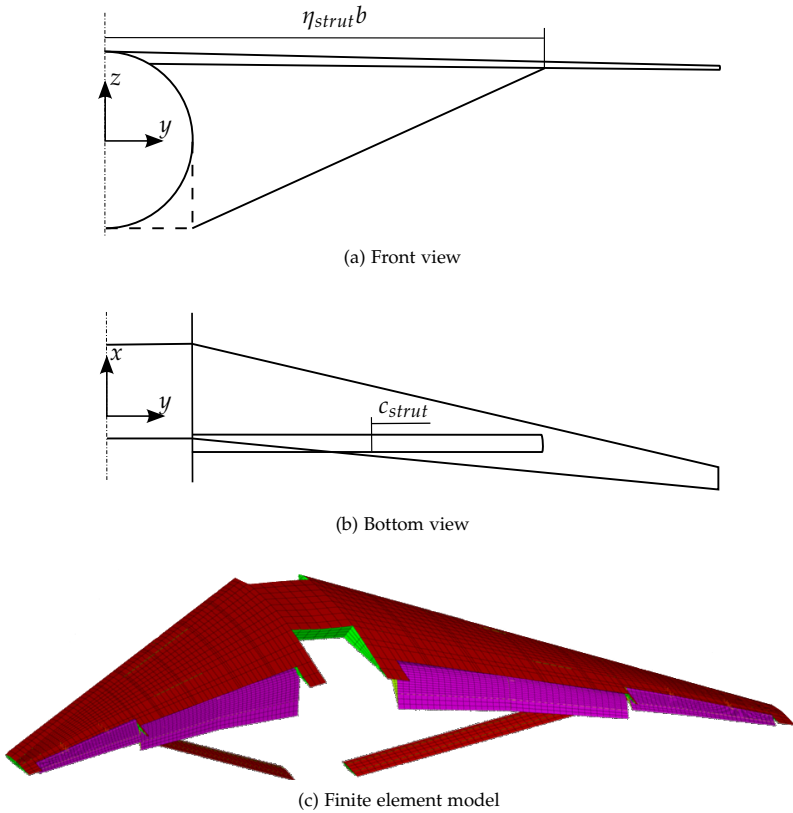


Figure 4.16: Design concept: Strut-braced wing

take-off mass and the reference area may otherwise lead to several unfeasible designs in an extended design space.

The design of experiments is based on a Latin hypercube with 160 samples. Hence, the ratio of 20 samples per design variable is maintained. Given the high dimensionality of the design space, a graphical representation of the DOE is futile, and instead, appendix F lists the corresponding data.

As in the previous design studies, VAMPzero initializes the higher fidelity analyses. Apart from the additional geometric parametrization, VAMPzero

Variable	Symbol	Range	Unit
Reference area	S	100. - 160.	[m ²]
max. take-off mass	m_{TOM}	60.0 - 90.0	[t]
Sweep angle	φ_{25}	5.0 - 20.0	[]
Aspect ratio	AR	12.0 - 17.0	[]
Tip twist	τ_t	-6.0 - 0.0	[]
Thickness ratio	t/c	0.08 - 0.13	[]
Strut position	η_{strut}	0.2 - 0.7	[]
Strut chord	c_{strut}	0.1 - 0.2	[]

Table 4.7: Domain of definition: Strut-braced wing

estimates that the primary wing mass is reduced by approximately 40% compared to a cantilever wing. Carrier et al. [24] published similar results and this study extrapolates their findings. The mass of the strut is constant during the initialization. These estimates are necessary to predict a meaningful aircraft configuration. However, given the fact that the maximum take-off mass is provided by the domain of definition, this simplified mass estimation has no influence on the subsequent loads process and the final results.

The physics-based analysis utilizes the WINGmass tool chain that has been introduced in the previous design study, see also Figure 4.10. As WINGmass is coded accordingly to the CPACS definition that encompasses an abstract definition of wings and their attachments, no further changes to WINGmass are necessary. Furthermore, the integration by VAMPzero requires no additional changes.

The results of the design of experiments are forwarded to the symbolic regression to find separate equations for the mass of the strut-braced wing and the strut. The default mathematical operations are allowed during the symbolic regression. For clarity, the mass estimation is split up for the two components of the strut-braced wing (Eq. 4.39-4.41). The symbolic regression includes all design variables in the equations, albeit, each single equation excludes few design variables.

4.3 Strut-Braced Wing Mass

$$m_{wing} = \frac{1.144E-4AR^2m_{TOM} - 76.91AR}{ARt/c\eta_{strut} - \tau_t\eta_{strut} - 7.698E-3AR} + 39.35S + 130.2\varphi_{25t}/cS \quad (4.39)$$

$$m_{strut} = 0.0206\varphi_{25}m_{TOM} + 87.71\eta_{strut}c_{strut}\sqrt{ARS} + S\eta_{strut}c_{strut}\sqrt{ARS} - 21.790E3\varphi_{25t}/c\eta_{strut} \quad (4.40)$$

$$m_{sbw} = m_{wing} + m_{strut} \quad (4.41)$$

Figure 4.17 shows the behavior of the strut-braced wing mass in the domain of definition. As before, the contour plot matrix only displays one plane out of the domain of definition. In this case, all hidden values are set to the mid point of the domain of definition. Furthermore, the maximum take-off mass, the tip twist, and the the strut chord are excluded from the plot to establish transparency.

Given the fact that the wing section inboard of the wing strut connection is very stiff, this part of the wing is mostly sized by minimum skin thickness. Hence, the reference area of the wing has a large impact on the strut-braced wing mass.

The influence of the wing sweep is comparably low and this behavior is mostly due to the small bandwidth in the domain of definition. Higher sweep values can be excluded as they are only reasonable in combination with high cruise speeds. However, these lead to significant transonic drag at the strut-wing intersection. Furthermore, as the strut attaches to the wing front spar the negative torsion effects of wing sweep are reduced.

In comparison to the conventional, cantilever wing, the influence of the aspect ratio on the strut-braced wing mass is low due to the stiff inboard triangle that consists of the wing, the strut and the fuselage. Hence, a high aspect ratio design of a strut-braced wing appears reasonable. However, the domain of definition should only be extended to higher aspect ratios if a detailed aeroelastic analysis is available.

For a cantilever wing, the thickness to chord ratio has a large influence on the wing mass. With a strut-braced wing the sensitivity is reduced. As before, one of the drivers for this behavior is the triangle arrangement of fuselage, strut and wing. The added stiffness reduces the inboard loads, and hence, the influence from the thickness to chord ratio diminishes. For

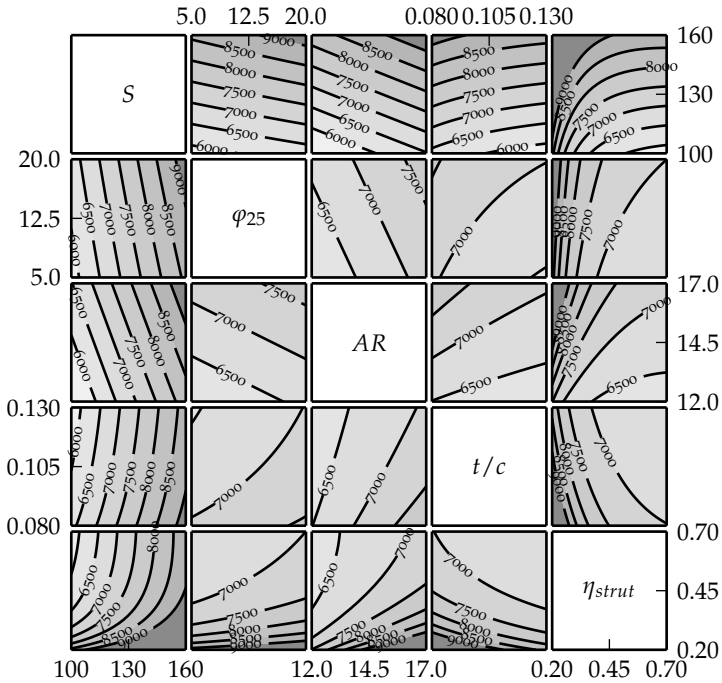


Figure 4.17: Surrogate model: Strut-braced wing

a natural laminar flow design of the strut-braced wing this behavior is beneficial, as low thickness laminar profiles may be selected. Nonetheless, for very low thickness to chord ratios detailed aeroelastic analysis is necessary as well.

The influence of the spanwise strut coordinate on the strut-braced wing mass is outstanding. The bandwidth of η_{strut} includes small values to demonstrate the rise in mass due to a diminishing effect of the strut. In accordance to the overall design of the aircraft the optimum spanwise position of the strut is at ≈ 0.6 . This value is comparable, yet slightly lower than the results by Carrier et al. that have been mentioned earlier.

4.3 Strut-Braced Wing Mass

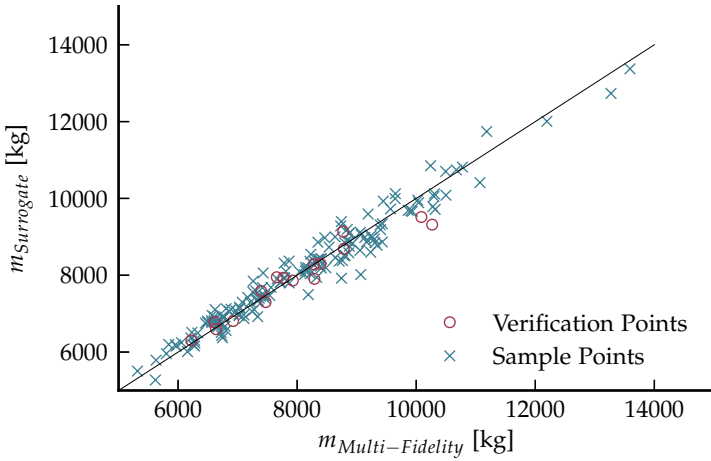


Figure 4.18: Verification: Strut-braced wing

As before, sixteen, i.e., ten percent of the number of sample points, verification points are placed at random locations in the domain of definition and evaluated. Table 4.8 and figure 4.18 show the results of the verification. The quality of the symbolic regression for the wing mass is high. In contrast, the results of the strut mass equation verification are not as precise. However, given the fact the only two parameters are available that describe the actual geometry of the strut, this lack of precision has been predictable. The present design study enhanced the capabilities of conceptual design so that the design of a strut-braced wing configuration is possible at the very

Metric	Sample points		Verification points	
	m_{wing}	m_{sbw}	m_{wing}	m_{sbw}
Mean error	0.39%	1.8%	-0.85%	1.2%
Standard deviation	3.5%	16.0%	3.5%	11.0%
Root mean squared error	0.12%	2.6%	0.13%	1.3%
Standard deviation	0.23%	6.1%	0.29%	1.9%

Table 4.8: Verification: Strut-braced wing

early design stages and at very low computational cost. Future research may look into further configuration-specific details such as the interference drag of strut and wing as well as the landing gear integration.

The findings as well as further sources of error of all design studies are discussed in more detail in the following chapter. Furthermore, chapter 6 highlights areas of future research. The presented topics include further fields of application for the multi-fidelity workflow as well as means to improve the body of methods.

5 Discussion

All models are wrong, and
increasingly you can succeed
without them.

(Peter Norvig)

Norvig [4], in his role as Director of Research at Google Inc., rephrased the previously introduced dictum by Box. He states that in an environment where vast quantities of data are available no actual models are necessary to represent knowledge, i.e., bare correlation is supposedly enough. For example, statistics-based machine translation software that depends on vast sets of translated text requires no additional explicit, a-priori knowledge, e.g., on the grammar of a language.

As the presented study relies heavily on large amounts of data, i.e., the design of experiments conducted on the multi-fidelity loop, and surrogate models that are derived from this data, one might be tempted to follow Norvig's dictum. However, this study is not aligned with this line of thought: The goal of this study to increase the capabilities of conceptual design, an inevitable step in the design process, by the exploitation of a multi-fidelity workflow for speed and precision rather than to replace higher fidelity analysis models. Higher-fidelity analysis models remain a necessity in aircraft design. Currently, non-sufficient, historical-based statistical data and methods hamper conceptual design. An aircraft design that arises only from historical-based methods may be as unconventional as a new language derived from statistics-based machine translation. The symbolic regression algorithm is the only technique applied in the course of this study that requires no a-priori knowledge. As symbolic regression needs to find a new description for an unknown problem structure, it benefits from the fact that it is not bound by a predefined mathematical structure.

This chapter elaborates on the findings of the design studies and highlights results as well as possible sources of error. Subsequently, chapter 6 discusses the body of methods in more detail and reflects upon the initial targets of this study.

The previous chapter presents three design studies that derive new con-

ceptual design methods based on higher-fidelity physical models. The first design study serves as a proof of concept and derives a new equation to quantify the Oswald factor for a double trapezoid wing. The second study overcomes a larger information gap between conceptual and preliminary design as it connects to a high-fidelity wing mass estimation that includes models for primary and secondary structures as well as loads and aerodynamics. It results in a new equation for the estimation of the wing mass. Finally, the third design study establishes a link to unconventional designs and examines the mass of a strut-braced wing aircraft.

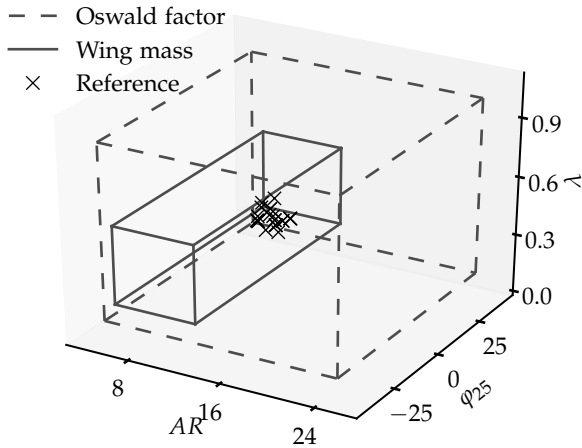


Figure 5.1: Historic vs. physics-based domain of definition

The studies prove that the domain of definition can be significantly extended. As figure 5.1 shows, the design space of existing⁴⁹ jet transport aircraft is limited to a small bandwidth and any predictions on future designs are not possible outside of the narrow design space. All aircraft are grouped in a narrow space when the aspect ratio, sweep angle, and taper

⁴⁹ The domain of definition that is outlined by the plot is not exhaustive. It includes all aircraft that are listed in the validation data set, see appendix B.

ratio are compared. In contrast, the two larger boxes represent the design spaces covered by the first two design studies.

The design space for the wing mass design study is smaller as the design concept is only applicable in a limited domain of definition. On the one hand, this effect is due to the increase in the level of fidelity of the product model (flaps, slats, ailerons, etc.), and on the other hand, this is due to an increase in the level of fidelity of the physical model (aeroelastic convergence). For example, if the taper ratio is small then no sufficient chord depth remains for ailerons and slats and the spar layout needs significant changes. Hence, one insight of these studies is that at a higher level of detail the domain of definition may be limited by the design concept. For example, in a previous study a simpler beam model of a wing has been applied where control surfaces have only been taken into account empirically. With these simpler models it is possible to extend the domain of definition further, yet the precision is worse.

Of course, if sufficient analysis models are available then the multi-fidelity workflow is applicable to further design concepts, e.g., delta- or highly tapered wings. However, one needs to take into account that different design concepts should be handled in different analysis routines, i.e., conceptual design equations. Hence, it is not advisable to force the description of all design concepts into one in-transparent and un-maintainable package but rather perform separate analyses, as outlined for the conventional and the strut-braced wing. Chapter 6 presents an outlook on further design studies.

As the issues of scale diminish, it is far less complex to quantify non-dimensional than dimensional properties of the aircraft. The Oswald factor equation can be found without any reference to the size of the wing and accordingly the size of the aircraft. Conversely, this is not as simple for the wing mass as it is significantly influenced by the size of the wing and the mass of the aircraft. However, a design of experiments, where both the reference area and the maximum takeoff mass change, leads to several infeasible⁵⁰ (and non-converging) designs. Hence, the design study is based on the wing loading and becomes scaled by statistical data. In this way the physical behavior of the higher-fidelity analysis is preserved while a larger

⁵⁰ Of course, given sufficient computational power, it is possible to explore a DOE that includes invalid locations and ignore failed the analysis runs. However, this approach is only valid if *failed* analysis runs can be identified reliably, and hence, the approach is prone to errors and high cost.

design space is covered. The design study on strut-braced wing aircraft circumvented this issue by a smaller domain of definition where unsuitable designs are unlikely.

As seen from the results in the previous chapter, all equations verified to the data from the design of experiments both for the sample and the verification points and behave well within the conventional design space during the validation phase. However, some sources for errors exist and should be included in the discussion. The most outstanding are due to the:

- error of the parametrization.
- error of the surrogate model.
- error of the physical analysis model of higher-fidelity.

When an equation is derived from a multi-fidelity workflow it is important to ensure that a quantity is interpreted equally on all levels of detail. Hence, CPACS as a common namespace is applied in the scope of this study to minimize translation errors. Furthermore, each design study describes the quantities in rich detail, e.g., the wing mass breakdown to minimize errors due to misinterpretation. Furthermore, the validation ensures that the equations return sensible results in the context of conceptual design. However, errors of the parametrization or rather its interpretation can hardly be excluded completely.

The introduction of any kind of surrogate model implies a certain amount of error in the calculation as it will not exactly reflect the behavior of the underlying physical model. One may try to decrease the error as much as possible within the bounds of given resources. However, two distinctive aspects come into play:

First, as it would be necessary to determine the behavior of the underlying model at every possible point within the domain of definition, it is merely impossible to quantify the error exactly. The computational cost rises quickly beyond what is manageable and a verification must end at a reasonable error level. However, the physics behind the underlying models are well understood and hence no singularities are expected that would make an extended effort necessary. The verification based on the Monte Carlo sampling plans ensures that the surrogate model reflects the behavior of the physical model also at locations that are not covered within the initial DOE.

Second, the quantification of the error of a surrogate model is a Sisyphus task. In a verification step, further evaluations of the high cost model are necessary. If one determines these evaluations then they should also be included within the surrogate model to increase the overall quality. It can easily be seen that this loop may be non-terminal.

Finally, the error of the physical model of higher-fidelity has several sources. Apart from error's due to simplifications⁵¹, which are neglected given the fact that the amount of simplification is drastically decreased by advancing from conceptual to preliminary design, systematic and human errors stand out. The higher fidelity models have been checked for systematic errors, as shown in the cited studies. All models that are applied in the course of this study have to be validated to existing aircraft configurations, and hence, systematic errors on a large scale may be excluded. Human error may arise from a wrong application and configuration of the higher fidelity models. At first, the use of a common namespace eliminates several sources of faulty input specification, as it defines the necessary process information to trigger each analysis model. Furthermore, the developers of the preliminary design models aided in the setup of the multi-fidelity loops and ensured correct use. In the end, the validation further reduces the chance of human errors as it shows that the extracted equations return sensible results for a given database of aircraft configurations.

On a final note, the validation suffers from the fact that it is limited to conventional configurations. Yet, this is an inevitable characteristic. If a database for unconventional configurations would exist then another historical-based conceptual design model could be created in the same fashion as before. However, the developed methods foster the design of such configurations and may be validated against higher fidelity results in the future.

51 A model remains a model, and hence, it is always prone to errors. Of course, a higher-fidelity model reflects the physics and design concept in more detail than a coarse model. However, whether any model applied in preliminary design returns the exact value for any aircraft in production remains questionable.

6 Conclusion

If we want to start new things rather than trying to elaborate and improve old ones then we cannot escape reflecting on our basic conceptions.

(Hans Primas)

Despite the fact that Primas focuses on issues in natural sciences and philosophy on a much broader scale than the present study, his dictum reflects the overall problem definition. If present-day aircraft design systems are assumed to accurately predict the properties of unconventional aircraft configurations then historical-based formulations in conceptual aircraft design need to be replaced in as many cases as possible.

Chapter 1 outlined the current design process for a new aircraft configuration and identified conceptual design and preliminary design as inevitable parts that are nonetheless distinguished as elements of analysis and synthesis, respectively. The historical-based nature of conceptual design hereby restricts the design process to a limited domain of definition. Accordingly, two obstacles hamper the design process and the introduction of physics-based analysis in the early stages of aircraft design. Given the fact that both the design phases operate on different levels of fidelity, a seamless exchange of information is not possible. First, it is necessary to bridge the **information** gap between conceptual design and preliminary design. However, in aircraft design a large number of evaluations, for example, in optimization loops, are necessary. Given the high computational cost of preliminary design methods, no benefits are derived from bridging the information gap, as neither sufficient time nor sufficient computing power is available. Hence, even if the information gap is bridged, the obstacle of **time** remains.

The present study proposes a multi-fidelity loop to bridge the information gap. This loop couples a conceptual design model with several preliminary design models via a common namespace. The key steps are initialization, i.e., the creation of sufficient input for the preliminary design models from the results of the conceptual design, and integration, i.e., the feedback of

higher-fidelity results of the preliminary design into conceptual design to evaluate the synthesis of the design.

In the subsequent step, it is necessary to decrease the computational cost. Hence, the multi-fidelity loop is coupled upstream with a design of experiments and downstream with a surrogate modeling algorithm. Design studies explore the multi-fidelity loop on a global scale and construct a surrogate model that can be applied in conceptual design at a low computational cost. Furthermore, the proposed solution attempts to extract a surrogate that has a low mathematical complexity and therefore high transparency. This goal aligns well with another statement of Primas [102]: *“In mathematical and scientific theories the aesthetic dimension plays a decisive role alongside logical correctness.”*

The introduction outlined three main challenges that need to be addressed to enable successful application of the proposed body of methods:

- Establishment of a closed multi-fidelity design loop between conceptual design and preliminary design.
- Exploration of a wide design space in an efficient and stable way.
- Generation of a surrogate model that reflects the behavior of a physics-based analysis while maintaining low computational cost and high transparency.

Chapter 2 presented the state of the art of the various research fields included within the scope of this study. It established fields where further development is necessary and where existing solutions could be applied.

Subsequently, chapter 3 focused on the body of methods necessary to master the above-mentioned challenges. First, a closed multi-fidelity loop is an essential part of the aircraft design system developed at DLR in recent years. The present study contributed to this development as it further enhanced the capabilities of the common namespace that is represented by the CPACS data format. Furthermore, a conceptual design model termed VAMPzero was developed. Of utmost importance for the multi-fidelity loop is VAMPzero’s ability to both initialize and integrate information. It is presently the only conceptual design model that was specifically developed and the only one capable of closing a multi-fidelity loop. By now, several preliminary analysis models are connected to the CPACS data format and some of these have been applied in the course of the design studies.

In contrast to most other works in the field of multi-fidelity, the problem formulation in the present study necessitated a global rather than a local exploration of the design space, as it would be the case for optimization studies that include trust regions. Hence, several algorithms for the design of experiments were outlined and compared. Latin-hypercubes are a state of the art approach and were applied in the course of this study. Even though, several methods for the improvement of Latin-hypercubes exist beyond what has been included in the design studies, satisfying results were obtained. Given the fact that the proposed body of methods was applied for the first time, the number of samples was kept rather high⁵² to minimize the risk of numerical inaccuracies. Hence, an optimization of the design of experiment algorithm might prove valuable only after the overall number of samples has been reduced to a minimum.

Usually, a calculation method in conceptual design seldom covers more than one page of code; often, a single equation is sufficient. The overall size of the code may range from several hundred kilobytes to a few megabytes. As the applied methods are simple, their transparency is of utmost importance to enable the designer to quickly identify dependencies and simplifications. Hence, it is of essential to derive a surrogate model that covers not only the behavior of the physical model but is also transparent and well-arranged. The present study introduced symbolic regression as a surrogate model algorithm. Symbolic regression creates surrogates with a comparably high accuracy that is essential for the solution approach. Unlike most other surrogate models, e.g., Kriging, the symbolic regression combines low complexity and high accuracy.

Finally, the first of the three design studies served as a proof of concept and resulted in a new equation to quantify the Oswald factor. Furthermore, a more advanced multi-fidelity coupling was established that coupled conceptual design with a high-fidelity wing mass estimation. Furthermore, a similar workflow was applied to estimate the mass of a strut-braced wing, and hence, the applicability of the proposed approach for unconventional configuration was proven. The outcomes of these studies were discussed in greater detail in the previous chapter.

⁵² Despite the fact that numerical experiments (as shown in figure 3.15) and general experience within DLR research indicate a factor of approximately ten samples per dimension, a conservative number of twenty samples was applied for the design studies.

Outlook

The present study brought the research to a coherent (intermediate) point. Of course, several topics come to mind that can possibly extend this research in the future. Apart from the fact that the outlined body of methods may be applied to other design problems, e.g., empennage sizing including stability and control analysis, three distinctive research fields are named and discussed here explicitly.

Unconventional design concepts

In the course of this study the case has been made that conceptual design methods are currently not capable of handling unconventional configurations and the goal is to enhance conceptual design by means of physics based analysis at comparable cost and complexity of a conceptual design method. Nevertheless, the design studies in chapter 4 did not include any of the infamous unconventional design concepts such as the blended wing body as no sufficient analysis models of higher-fidelity have been available during the conceptual phase of the present study. The following paragraphs outline which components of the multi-fidelity workflow are subject to changes to extend the design studies to a more unconventional design concept. Hereby, no changes to the overall process are necessary, but adoptions need to be applied to those components that are specific to the design concept.

In a first step a common namespace is necessary which describes the characteristics of any configuration in an unambiguous way, e.g., the aspect ratio of a box wing needs to be defined. Subsequently, all conceptual and preliminary design models that are a part of the multi-fidelity loop need to be adapted to this parametrization.

The conceptual design model can either be extended to take into account further unconventional design concepts or be replaced by a design specific conceptual design code. Given the fact that the level of detail is low at the conceptual design stage, these extensions can usually be achieved without greater effort. The synthesis part of the conceptual design model operates mostly on the properties of a configuration, e.g., lift over drag and thrust specific fuel consumption, and hence is stable to changes of the design concept.

In accordance to the design concept, the effort necessary to initialize a detailed model from the description at conceptual design stage may be substantial. However, for the blended wing body mentioned above the initialization is comparably simple, as the design concept can be represented by a wing-like structure.

Contrary, all analysis models of higher fidelity, i.e., at the preliminary design stage, need to be adjusted to changes in the design concept. For example, the wing mass analysis chain applied in the second and third design study needs to process the unconventional configurations. For higher fidelity physics based models this may also include some amount of calibration and this calibration is hard to achieve given the limited amount of available, detailed, and accurate data.

Once the three major issues specific to the design concept *parametrization*, *initialization* and *higher-fidelity analysis* are overcome, further design studies can be conducted. Current research at DLR and other institutions, e.g., on the topic of the box-wing or the blended wing body, seem to make the extension of the proposed body of methods for more unconventional design concepts possible in the foreseeable future.

Reduction of computational cost

As the body of methods was applied for the first time and hence included several safety factors, means can be identified to reduce the computational cost of the multi-fidelity workflow. First, as mentioned above, the cost of the design of experiments may be reduced significantly. Conversely, the safety factor for the number of samples per dimension may be lowered. Alternatively, the design of experiment algorithm may be improved. A Latin-hypercube explicitly optimized for space-fillingness may allow for a further reduction of the number of samples per dimension. Both these improvements would lead to a smaller number of samples for the multi-fidelity loop and hence reduce the number of higher-fidelity analyses. This would lead to significant reductions in computational cost, for example, in the case of a further study on the wing mass that incorporates costly finite element models.

Another significant factor contributing to computational cost is the symbolic regression. The algorithm developed by Schmidt and Lipson [121]

profits from parallelization, so some of its computational time may simply be reduced by a more intense use of hardware. Furthermore, it is possible to speed the symbolic regression up by seeding, i.e., feeding the genetic algorithm with predefined solutions as initial populations. For example, it is possible to perform seeding using the available historical-based conceptual design methods. However, the usefulness of these seeds for describing the physics-based analysis remains a topic of future research.

Iterative approach

Another possibility for improvement in addition to optimizing parts of the overall process as described above is the exploitation of an iterative rather than a sequential process. Currently, the number of samples is determined a-priori, which leads to the major drawback that it is unknown whether this number of samples is sufficient or perhaps even extraordinarily large. For example, the number of samples needs to be increased if the verification fails. However, this information is obtainable only after a significant amount of computational cost has been incurred.

The alternative approach follows an iterative operation scheme, as sketched in figure 6.1, that is comparable to the trust region approach in multi-fidelity optimization processes. In the trust region approach, the optimization process is based on low-fidelity and high-fidelity models. Most evaluations operate on the low-fidelity model and are corrected by a few evaluations of the high-fidelity model. The optimization process thereby operates initially on a global scale and creates a surrogate that is applicable in a local trust region where the quality of the surrogate model is ensured. In contrast to this scheme, an iterative, multi-fidelity workflow for the creation of a global surrogate model should work from the local scale to the global scale rather than vice versa.

As a first step, the creation of a local surrogate model in a limited domain of definition based on a small number of samples is proposed. It is probable that most physic, or at least most linear (and a few non-linear), effects may already be captured by the local surrogate model. In subsequent steps, the domain of definition is extended with a small number of samples. The symbolic regression in this next step takes into account all available points and becomes seeded with the solution of the previous iteration. The nested

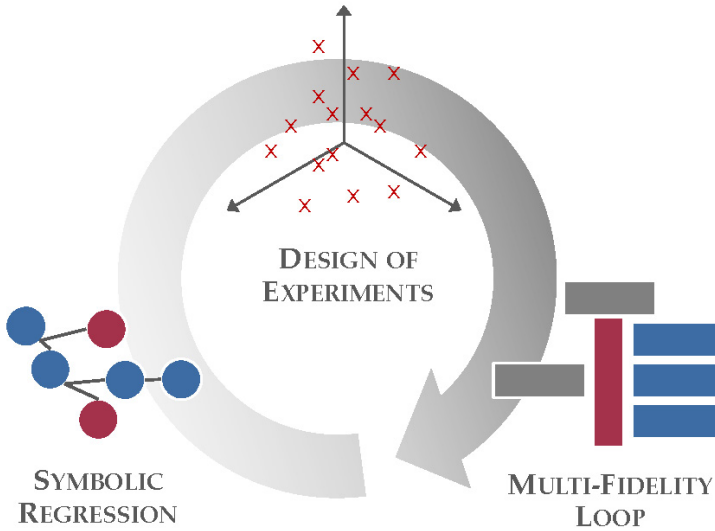


Figure 6.1: Iterative multi-fidelity workflow

Latin hypercubes described by Qian [103] and Rennen et al. [107] might be used for the repeatedly created design of experiments.

Furthermore, the current result of the symbolic regression can be validated against all available sample points to identify locations within the design space where the accuracy is low. If the DOE is then adjusted iteratively to distribute further samples near these locations than the multi-fidelity workflow is able to react to local effects in the domain of definition and capture them sufficiently.

However, only detailed research can demonstrate whether the iterative approach leads to a decrease in computational cost. Even if the small number of samples is taken into account to capture most of the behavior of the physical models, whether the overall number of samples can be reduced remains questionable. Nonetheless, due to the parallelization effects of a combined search for a surrogate model and the next iteration of preliminary designs the overall time may be reduced.

Summary

In conclusion, the information gap has been bridged and conceptual design methods based on physics rather than on historical data have been developed. However, this is a work-intensive task, especially for the initialization. A large amount of design knowledge needs to be coded. For example, the complete structural layout of a wing must be placed in an algorithm that is applicable over a wide domain of definition and needs to generate sensible layouts. Furthermore, expertise is necessary to identify the variables for the domain of definition that a) are design drivers and b) can be included in conceptual design in a reasonable manner.

In addition, the created surrogate models extend the capabilities of conceptual design and will be a major time saver for future applications. Not only is the accuracy of the conceptual design model increased but also less iterations are necessary in multi-fidelity loops as the quality of the initial solution is increased. In the case of the strut-braced wing, no means to perform a conceptual design at low computational cost existed prior to this study.

The introduction of symbolic regression as a surrogate model is one of the key factors for the success of the outlined study. Without symbolic regression the surrogate models would not have been transparent enough for conceptual design. It is especially gratifying to note that to some extent these models perform well in the *aesthetic dimension*.

Bibliography

- [1] ALEXANDER, C. Notes on the Synthesis of Form. *Harvard Paperback* (1964).
- [2] ALONSO, J., LEGRESLEY, P., VAN DER WEIDE, E., MARTINS, J., AND REUTHER, J. pyMDO: A Framework for High-Fidelity Multi-Disciplinary Optimisation. *10th AIAA / ISSMO Multidisciplinary Analysis and Optimization Conference* (2004).
- [3] ALT-AOUDIA, S., JEGOU, R., AND MICHELUCCI, D. Reduction of constraint systems. *Compugraphic, Alvor, Portugal* (1993), 83–92.
- [4] ANDERSON, C. The End of Theory: The Data Deluge Makes the Scientific Method Obsolete. *Wired Magazine* (2008).
- [5] ANDERSON, J. D. Fundamental of Aerodynamics, 4th Edition. *McGraw-Hill* (2006).
- [6] ANTOINE, N., KROO, I., WILCOX, K., AND BARTER, G. A Framework for Aircraft Conceptual Design and Environmental Performance Studies. *10th AIAA/ISSMO Multidisciplinary Analysis and Optimization Conference* (2004).
- [7] ANTON, E., LAMMERING, T., AND HENKE., R. A Comparative Analysis of Operations towards Fuel Efficiency in Civil Aviation. *Applied Aerodynamics: Capabilities and Future Requirements* (2010).
- [8] ARDEMA, M. D., CHAMBERS, M. C., PATRON, A. P., HAHN, A. S., MIURA, H., AND MOORE, M. D. Analytical Fuselage and Wing Weight Estimation of Transport Aircraft. *NASA Technical Memorandum 110392* (1996).
- [9] BARTHOLOMEW, P. The Role of MDO within Aerospace Design and Progress towards an MDO Capability. *7th AIAA/USAF/NASA/ISSMO Symposium on Multidisciplinary Analysis and Optimization* (1998).

- [10] BERENDS, J., AND VAN TOOREN, M. Design of a Multi-Agent Task Environment Framework to Support Multidisciplinary Design and Optimisation. *ASM* (2007).
- [11] BLANCHARD, B. S., AND FABRYCKY, W. J. Systems Engineering and Analysis. *Prentice Hall International Series in Industrial & Systems Engineering* (2010).
- [12] BÖHNKE, D. Python in Conceptual Aircraft Design, in german. *Py-ConDE* (2011).
- [13] BÖHNKE, D., DORBATH, F., NAGEL, B., AND GOLLNICK, V. Multi-Fidelity Wing Mass Estimations Based on a Central Model Approach. *SAWE 71th Annual Conference of Society of Allied Weight Engineers, Bad Gögging, Germany* (2012).
- [14] BÖHNKE, D., JEPSEN, J., PFEIFFER, T., NAGEL, B., GOLLNICK, V., AND LIERSCH, C. An Integrated Approach for Determination of the Oswald Factor in a Multi-Fidelity Design Environment. *CEAS Air&Space Conference, Venice, Italy* (2011).
- [15] BÖHNKE, D., LITZ, M., NAGEL, B., AND RUDOLPH, S. Evaluation of Modeling Languages for Preliminary Aircraft Design in Multidisciplinary Engineering Environments. *DGLR Congress* (2010).
- [16] BÖHNKE, D., NAGEL, B., AND GOLLNICK, V. An Approach to Multi-Fidelity in Conceptual Aircraft Design in Distributed Design Environments. *IEEE Aerospace Conference* (2011).
- [17] BÖHNKE, D., REICHWEIN, A., AND RUDOLPH, S. Design Language for Airplane Geometries using the Unified Modeling Language. *ASME Int. Design Engineering Technical Conferences (IDETC) & Computers and Information in Engineering Conference (CIE)* (2009).
- [18] BÖHNKE, D., ZHANG, M., RIZZI, A., AND NAGEL, B. Towards a Collaborative and Integrated Set of Open Tools for Aircraft Design. *AIAA Aerospace Sciences Meeting, Grapevine, USA* (2013).
- [19] BOX, G. E. P., AND BEHNKEN, D. W. Some New Three Level Designs for the Study of Quantative Variables. *Technometrics* 2 (1960).
- [20] BOX, G. E. P., AND WILSON, K. B. On the experimental attainment of optimum conditions . *Journal of the Royal Statistical Society* 13 (1951), 1-45.

- [21] BRADLEY, M. K., AND DRONEY, C. K. Subsonic Ultra Green Aircraft Research: Phase II. *NASA N+4 Advanced Concept Development* (2012).
- [22] BRANDT, S., A., STILES, R., J., BERTIN, J., J., AND WHITFORD, R. Introduction to Aeronautics: A Design Perspective. *AIAA Education Series* (1997).
- [23] BUCKINGHAM, E. On Physically Similar Systems; Illustrations of the Use of Dimensional Equations. *Physical Review* (1914), 345–376.
- [24] CARRIER, G., ATINOULT, O., DEQUAND, S., HANTRAIS, J., LIAUZUN, C., PALUCH, B., RODDE, A., AND C.TOISSAIN. Investigation of a Strut-Braced Wing Configuration for Future Commercial Transport. *ICAS Congress* (2012).
- [25] CHOI, S., ALONSO, J. J., AND KROO, I. M. Two-Level Multi-Fidelity Design Optimization Studies for Supersonic Jets. *43rd AIAA Aerospace Science Meeting and Exhibit* (2005).
- [26] CHOI, S., ALONSO, J. J., AND KROO, I. M. Multi-Fidelity Design Optimization of Low-Boom Supersonic Jets. *Journal of Aircraft* 45 (2008), 106–118.
- [27] CONN, A. R., SCHEINBERG, K., AND VICENTE, L. N. Introduction to Derivative-Free Optimization. *MPS-SIAM Series on Optimization*, SIAM, USA (2008).
- [28] COOK, R. D., MALKUS, D. S., PLESHA, M. E., AND WITT, R. J. Concepts and Applications of Finite Element Analysis. *John Wiley & Sons 4th edition* (2002).
- [29] DORBATH, F. A Flexible Wing Modeling and Physical Mass Estimation System for Early Aircraft Design Stages. *DLR Forschungsbericht* (2014).
- [30] DRELA, M. Athena Vortex Lattice User’s Guide, v. 3.30. MIT (2010).
- [31] DUBS, F. Highspeed Aerodynamics, in german. *Birkhäuser, Basel* (1975).
- [32] DUGGIRALA, R. K., ROY, C. J., AND SCHETZ, J. A. Analysis of Interference Drag for Strut-Strut Interaction in Transonic Flow. *AIAA Journal* 49 (2011), 449–462.

- [33] ELHAM, A., AND VAN TOOREN, M. J. L. Weight Indexing for Airfoil Multi-Objective Optimization. *Journal of Aircraft* 50 (2013), 1046–1059.
- [34] FISHER, R. A. The design of experiments. *Oliver and Boyd* (1935).
- [35] FORREST, S. Genetic algorithms: Principles of adaptation applied to computation. *Science* 261 (1993).
- [36] FORRESTER, A., SOBESTER, A., AND KEANE, A. Engineering Design via Sourrogate Modelling: A Practical Guide. *Wiley and Sons, Ltd.* (2008).
- [37] FORRESTER, A. I. J., KEANE, A. J., AND BRESSLOFF, N. W. Design and Analysis of Noisy Computer Experiments. *AIAA Journal* 44, 10 (2006), 2331–2339.
- [38] FRANZ, K. Sizing of primary control surfaces in preliminary aircraft design, in german. *60. Deutscher Luft- und Raumfahrtkongress* (2011).
- [39] FRANZ, K., LAMMERING, T., RISSE, K., ANTON, E., AND HOERNSCHEMEYER, R. Economics of laminar Aircraft considering Off-Design Performance. *8th AIAA Multidisciplinary Design Optimization Specialist Conference* (2012).
- [40] FRASER, A., AND BURNELL, D. Computer models in genetics. *McGraw-Hill* (1970).
- [41] GRASMEYER, J. Multidisciplinary Design Optimization of a Strut-Braced Wing Aircraft. *Virginia Polytechnic Institute* (1998).
- [42] GRAY, J., MOORE, K. T., AND NAYLOR, B. A. OpenMDAO: An Open Source Framework for Multidisciplinary Analysis and Optimization. *13th AIAA/ISSMO Multidisciplinary Analysis and Optimization Conference* (2010).
- [43] GUR, O., BHATIA, M., SCHETZ, J., MASON, W., KAPANIA, R., AND MAVRIS, D. N. Design Optimization of a Truss Braced Wing Transsonic Transport Aircraft. *Journal of Aircraft* 47 (2010).
- [44] HAMMING, R. Numerical Methods for Scientists and Engineers. *Dover Publications* (1987).
- [45] HEBB, D. O. The organization of behaviour. *John Wiley & Sons* (1949).

- [46] HEINZE, W. An approach to the quantitative analysis of technical and economical design boundaries of different aircraft concepts for the transport of high payloads, in german. *PhD Thesis Technical University Braunschweig* (1994).
- [47] HERLING, W., LEDOUX, S., RATCLIFF, R., TREIBER, D. A., AND WARFIELD, M. J. 3DOPT - An Integrated System for Aerodynamic Design Optimization. *Applied Aerodynamics Conference, Albuquerque, USA* (1998).
- [48] HETLAND, M. L. *Beginning Python*. Apress (2008).
- [49] HÖRNER, S., F. *Fluid Dynamic Drag*. Dayton Ohio Press (1951).
- [50] HORSTMANN, K. H. A multi-lifting-line method for design and check of nonplanar wing-configurations, in german. *DFVLR-FB 87-51* (1981).
- [51] HOWE, D. Aircraft conceptual design synthesis. *Professional Engineering Publishing* (2000).
- [52] IABG LTH-KOORDINIERUNGSTELLE . Aeronautical Information Publication, in german. *MA 401 12-01* (2011).
- [53] IMAN, R. L., HELTON, J. C., AND CAMPBELL, J. E. An approach to sensitivity analysis of computer models. *Journal of Quality Technology* (1981).
- [54] JENKINSON, L., SIMKIN, P., AND RHODES, D. *Civil Jet Aircraft Design*. Butterworth Heinemann (1999).
- [55] JEPSEN, J. Wissensbasierte Erstellung von Geometrien auf der Grundlage von Handbuchverfahren. *IB-328-2011-07, TU Hamburg-Harburg* (2011).
- [56] JIN, R., CHEN, W., AND SIMPSON, T. Comparative studies of meta-modeling techniques under multiple modelling criteria. *Structural Multidisciplinary Optimization* 23 (2001), 1–13.
- [57] JOHNSON, M. E., MOORE, L. M., AND YLVISAKER, D. Minimax and maximin distance designs. *Journal of Statistical Planning and Inference* 26 (1990), 131–148.
- [58] JONES, D. R. A Taxonomy of Global Optimization Methods Based on Response Surfaces. *Journal of Global Optimization* 21 (2001), 345–383.

- [59] KO, A., MASON, W. H., AND GROSS, B. Transonic Aerodynamics of a Wing/Pylon/Strut Juncture. *AIAA Applies Aerodynamics Conference* (2003).
- [60] KOCH, P. N., SIMPSON, T., ALLEN, J. K., AND MISTREE, F. Statistical Approximations for Multidisciplinary Design Optimization: The Problem of Size. *Journal of Aircraft* 36 (1999), 275–286.
- [61] KOZA, J. R. Genetic programming: On the programming of computers by means of natural selection. *MIT Press* (1992).
- [62] KRIGE, D. A statistical approach to some mine valuations and allied problems at the Witwatersrand. *University of Witwatersrand, South Africa* (1951).
- [63] KROO, I. MDO for Large-Scale Design. *Multi-Disciplinary Design Optimization: State of the Art* (1995).
- [64] KROO, I. Aircraft Design: Synthesis and Analysis. *Desktop Aeronautics* (2001).
- [65] KROO, I. Multi-Disciplinary Design Architectures: History and Status. *Multidisciplinary Design Consortium, Stanford University, USA* (2006).
- [66] KROO, I., AND TAKAI, M. A Quasi-Procedural, Knowledge-Based System for Aircraft Design. *AIAA 6502* (1988).
- [67] KROO, I., WILCOX, K., MARCH, A., HAAS, A., RAJNARAYAN, D., AND KAYS, C. Multifidelity Analysis and Optimization for Supersonic Design. *NASA/CR-2010-216874* (2010).
- [68] LA ROCCA, G. Knowledge Based Engineering Techniques to Support Aircraft Design and Optimization. *Tu Delft* (2011).
- [69] LA ROCCA, G., AND VAN TOOREN, M. Development of Design and Engineering Engines to support Multidisciplinary Design and Analysis of Aircraft. *Delft Science in Design - A Congress on Interdisciplinary Design* (2005).
- [70] LAMMERING, T., ANTON, E., AND HENKE, R. Validation of a Method for fast Estimation of Transonic Aircraft Polars and its Application in Preliminary Design. *Applied Aerodynamics: Capabilities and Future Requirements* (2010).

- [71] LAMMERING, T., ANTON, E., RISSE, K., AND FRANZ, K. Impact of Systems Integration on Fuel Efficiency in Preliminary Aircraft Design. *3rd International Workshop on Aircraft System Technologies* (2011).
- [72] LAMMERING, T., FRANZ, K., RISSE, K., HOERNSCHEMEYER, R., AND STUMPE, E. Aircraft Cost Model for Preliminary Design Synthesis. *50th AIAA Aerospace Sciences Meeting including the New Horizons Forum and Aerospace Exposition* (2012).
- [73] LEDOUX, S., HERLING, W., FATTA, G. J., AND RATCLIFFE, R. MDOPT-A Multidisciplinary Design Optimization System Using Higher order Analysis Codes. *AIAA/ISSMO Multidisciplinary Analysis and Optimization Conference* (2004).
- [74] LEIFSSON, L., AND KOZIEL, S. Multi-Fidelity Design Optimization of Transonic Airfoils Using Shape-Preserving Response Prediction. *International Conference on Computational Science* (2010).
- [75] LIERSCH, C. M., AND HEPPELLE, M. A distributed toolbox for multidisciplinary preliminary aircraft design. *CEAS Aeronautical Journal* (2011).
- [76] LOMAX, T. L. Structural Loads Analysis for Commercial Transport Aircraft: Theory and Practice. *AIAA Education Series* (1996).
- [77] MARCH, A., AND WILCOX, K. A Provably Convergent Multifidelity Optimization Algorithm not Requiring High-Fidelity Derivatives. *Multi-Disciplinary Design Optimization Specialist Conference* (2010).
- [78] MARTINS, J., MARRIAGE, C., AND TEDFORD, N. pyMDO: An Object-Oriented Framework for Multi-Disciplinary Design Optimization. *ACM Transactions on Mathematical Software* 36 (2009).
- [79] MARTINS, J. R. R. A., KROO, I. M., AND ALONSO, J. J. An automated method for sensitivity analysis using complex variables. *AIAA Paper 2000-0689* (2000).
- [80] MARTINS, J. R. R. A., AND LAMBE, A. B. Multidisciplinary Design Optimization: A Survey of Architectures. *AIAA Journal* 51, 9 (2013), 2049–2075.
- [81] MARTINS, J. R. R. A., STURDZA, P., AND ALONSO, J. J. The Connection between complex-step derivative approximation and algorithmic differentiation. *AIAA Paper 2001-0921* (2001).

- [82] MARTINS, J. R. R. A., STURDZA, P., AND ALONSO, J. J. The Complex-Step Derivative Approximation. *ACM Transactions on Mathematical Software* 29 (2003).
- [83] MATHERON, G. Principles of Geostatistics. *Economic Geology* (1963).
- [84] MAZHAR, F., KHAN, A. M., CHAUDHRY, I. A., AND AHSAN, M. On using neural networks in UAV structural design for CFD data fitting and classification. *Aerospace Science and Technology* (2013).
- [85] McCORMICK, B. Aerodynamics, Aeronautics, and Flight Mechanics. *John Wiley & Sons, New York* (1995).
- [86] McCULLERS, L. A. Flight Optimization System (FLOPS) User's Guide. *NASA Langley Research Center* (2009).
- [87] McCULLOCH, W., AND PITTS, W. A logical calculus of the ideas immanent in nervous activity. *Bulletin of Mathematical Biophysics* 7 (1943), 115–133.
- [88] MCKAY, M. D., BECKMAN, R. J., AND CONOVER, W. J. A comparison of Three Methods for Selecting Values of Input Variables in the Analysis of Output from a Computer Code. *Technometrics* 21 (1979), 239–245.
- [89] MELIN, T. Tornado, a vortex lattice MATLAB implementation for Linear Aerodynamic Wing applications. *KTH, Sweden* (2000).
- [90] METROPOLIS, N., AND ULAM, S. The monte carlo method. *Journal of the American Statistical Association* (1949).
- [91] MOERLAND, E., ZILL, T., NAGEL, B., SPANGENBERG, H., SCHUMANN, H., AND ZAMOV, P. Application of a Distributed MDAO Framework to the Design of a Short- to Medium Range Aircraft. *Deutscher Luft- und Raumfahrtkongress, Berlin, Germany* (2012).
- [92] MORRIS, M. D., AND MITCHELL, T. J. Exploratory designs for computational experiments. *Journal of Statistical Planning and Inference* 43 (1995), 381–402.
- [93] NAGEL, B., BÖHNKE, D., GOLLNICK, V., SCHMOLLGRUBER, P., RIZZI, A., LARocca, G., AND ALONSO, J. Communication in Aircraft Design: Can we establish a Common Language? *28th International Congress of the Aeronautical Sciences, Brisbane, Australia* (2012).

- [94] NAGEL, B., ZILL, T., MOERLAND, E., AND BÖEHNEKE, D. Virtual Aircraft Multidisciplinary Analysis and Design Processes - Lessons Learnt from the Collaborative Design Project VAMP. *4th CEAS Air & Space Conference* (2013).
- [95] NIȚĂ, M., AND SCHOLZ, D. Estimating the Oswald Factor from Basic Aircraft Geometrical Parameters. *DLRK* (2012).
- [96] NIELSEN, H. B., LOPHAVEN, S. N., AND SONDERGAARD, J. DACE - A MATLAB Kriging Toolbox. *Technical University of Denmark* (2002).
- [97] ÖESTERHELD, C. M., HEINZE, W., AND HORST, P. Influence of Aeroelastic Effects on Preliminary Aircraft Design. *ICAS Congress* (2000).
- [98] PATNAIK, S., GUPTILL, J. D., HOPKINS, D., AND LAVELLE, T. Neural Network and Regression Approximations in High Speed Civil Transport Aircraft Design Optimization. *NASA/TM 206316* (1998).
- [99] PFEIFFER, T., NAGEL, B., AND GOLLNICK, V. Konfigurationsanalyse im Flugzeugentwurf unter der Berücksichtigung von Unsicherheiten. *Deutscher Luft- und Raumfahrtkongress, Berlin, Germany* (2012).
- [100] PILGRIM, M. Dive into Python. *Apress* (2004).
- [101] PRANDTL, L. Applications of Modern Hydronamics to Aeronautics. *NACA TR 116* (1922).
- [102] PRIMAS, H. The Reality of the Symbol in the Exact Sciences. *Kunst als Wissenschaft* (2001).
- [103] QIAN, P. Z. G. Nested Latin hypercube design. *Biometrika* 96 (2009), 957–970.
- [104] QUEIPO, N. V., HAFTKA, R. T., SHYY, W., GOEL, T., VAIDYANATHAN, R., AND TUCKER, P. K. Surrogate-based analysis and optimization. *Progress in Aerospace Sciences* 41 (2005), 1–28.
- [105] RAYMER, D. Aircraft Design: A Conceptual Approach. *AIAA Education Series* (1989).
- [106] RAYMER, D. Enhancing Aircraft Conceptual Design using Multidisciplinary Optimization. *PhD, Royal Institute of Technology, Stockholm* (2002).

- [107] RENNEN, G., HUSSELAGE, B., AND E. R. VAN DAM, D. D. H. Nested maximin Latin hypercube designs. *Structural Multidisciplinary Optimization* 41 (2010), 371–395.
- [108] RIEKE, J. Bewertung von CFK-Strukturen in einem multidisziplinären Entwurfsansatz für Verkehrsflugzeuge. *Forschungsbericht 02* (2013).
- [109] RISSE, K., LAMMERING, T., ANTON, E., FRANZ, K., AND HOERNSCHEMEYER, R. An Integrated Environment for Preliminary Aircraft Design and Optimization. *8th AIAA Multidisciplinary Design Optimization Specialist Conference* (2012).
- [110] RIZZI, A. Modeling & Simulating Aircraft Stability & Control – SimSAC Project. *AIAA Atmospheric Flight Mechanics Conference, Toronto, Canada* (2010).
- [111] RIZZI, A., AND VON KAENEL, R. CEASIOM: Simulating Stability & Control with CFD/CSM in Aircraft Conceptual Design. *26th International Congress of the Aeronautical Sciences, Anchorage, Alaska* (2008).
- [112] RIZZI, A., ZHANG, M., NAGEL, B., BÖHNKE, D., AND SAQUET, P. Towards a Unified Framework using CPACS for Geometry Management in Aircraft Design. *AIAA Aerospace Sciences Meeting, Nashville, USA* (2012).
- [113] ROBINSON, J. S., AND MARTIN, J. G. An Overview of NASA's Integrated Design and Engineering Analysis (IDEA) Environment. *Joint Army-Navy-NASA-AirForce 6th Modeling and Simulation/4th Liquid Propulsion/3rd Spacecraft Propulsion Joint Subcommittee Meeting, Orlando Fl* (2008).
- [114] ROSKAM, J. Airplane Design. *DARCorporation I-VII* (1989).
- [115] RUDOLPH, S. A Methodology for the Systematic Evaluation of Engineering Design Objects. *PHD Thesis Stuttgart University* (1994).
- [116] RUDOLPH, S., AND BÖLLING, M. Constraint-based conceptual design and automated sensitivity analysis for airship concept studies. *Aerospace Science and Technology* 8 (2004), 333–345.
- [117] RUMMELHART, D. E., AND MCCLELLAND, J. L. Parallel distributed processing: explorations in the microstructure of cognition. volume 1. foundations. *MIT Press, Cambridge, MA* (1986).

- [118] SACKS, J., WELCH, W. J., MITCHELL, T. J., AND WYNN, H. P. Design and Analysis of Computer Experiments. *Statistical Science* 4 (1989), 409–435.
- [119] SASENA, M. Flexibility and Efficiency Enhancements for Constrained Global Design Optimization with Kriging Approximations. *University of Michigan, USA* (2002).
- [120] SCHMIDT, M., AND LIPSON, H. Coevolution of Fitness Predictors. *IEEE Transactions on Evolutionary Computation* 12 (2008), 736–749.
- [121] SCHMIDT, M., AND LIPSON, H. Distilling Free-Form Natural Laws from Experimental Data. *Science* 324 (2009), 81–85.
- [122] SCHMIDT, M., AND LIPSON, H. Symbolic Regression of Implicit Equation,. *Genetic Programming Theory and Practice* 7 (2009), 73–85.
- [123] SCHMITT, D. Exercise Aircraft Design I, in german. *Technical University Munich* (2007).
- [124] SCHNEEGANS, A., AND EHLERMANN, F. Applying KBE Technologies to the Early Phases of Multidisciplinary Product Design. *The Future of Product Development* 11 (2007), 587–595.
- [125] SEIDER, D., FISCHER, P. M., LITZ, M., SCHREIBER, A., AND GERNDT, A. Open Source Software Framework for Applications in Aeronautics and Space. *IEEE Aero* (2012).
- [126] SHAN, S., AND WANG, G. Survey of modeling and optimization strategies to solve high-dimensional design problems with computationally-expensive black-box functions. *Structural Multidisciplinary Optimization* 41 (2010), 219–241.
- [127] SHEVELL, R. S. Fundamentals of Flight. *Prentice Hall* (1988).
- [128] SIMPSON, T., PEPLINSKI, J. D., KOCH, P. N., AND ALLEN, J. K. Meta-models for Computer-based Engineering Design: A Survey and recommendations. *Engineering with Computers* 17 (2001), 129–150.
- [129] SIMPSON, T. W., MAUERY, T. M., KORTE, J. J., AND MISTREE, F. Comparison of Response Surface and Kriging Models for Multidisciplinary Design Optimization. *7th AIAA/USAF/NASA/ISSMO Symposium on Multidisciplinary Analysis and Optimization* (1998).

- [130] STARK, J. Product Lifecycle Management , 21st Century Paradigm for Product Realisation. *Springer London* (2005).
- [131] STEVENSON, A., AND SOANES, C. Oxford Dictionary of English. *Oxford University Press* (2010).
- [132] TAKAI, M. A New Architecture and Expert System for Aircraft Design Synthesis. *PhD, Stanford University* (1990).
- [133] TAM, W. F. Improvement Opportunities for Aerospace Design Process. *AIAA Space Conference & Exhibit* (2004).
- [134] TOREENBECK, E. Synthesis of Subsonic Aircraft Design. *Delft University Press* (1982).
- [135] TOREENBECK, E. Advanced Aircraft Design- Conceptual Design, Analysis and Optimization of Subsonic Civil Airplanes. *John Wiley & Sons* (2013).
- [136] WEBER, C., DEUBEL, T., KÖHLER, C., WANKE, S., AND CONRAD, J. Comparison of Knowledge Representation in PDM and by Semantic Networks. *Int. Conf. on Engineering Design* (2007).
- [137] WEBER, C., WERNER, H., AND DEUBEL, T. A different view on Product Data Management/Product Life-Cycle Management and its future potentials. *Journal of Engineering Design* 14 (2003), 447–464.
- [138] WEISS, M., GMELIN, T., SUN, X., DZIKUS, N., AND GRUNWALD, G. Enhanced Assessment of the Air Transportation System. *AIAA Aviation Technology, Integration and Operations Conference* (2011).
- [139] ZHANG, M., AND RIZZI, A. RDS-SUMO: from lofting to physics-based grids. *Aircraft Engineering and Aerospace Technology* 84 (2012).
- [140] ZHANG, M., TOMAC, M., WANG, C., AND RIZZI, A. Variable Fidelity Methods and Surrogate Modeling of Critical Loads on X-31 Aircraft. *51st AIAA Aerospace Sciences Meeting, Grapevine, USA, AIAA 2013-1081* (2013).
- [141] ZILL, T., BÖHNKE, D., NAGEL, B., AND GOLLNICK, V. Preliminary Aircraft Design in a Collaborative Multidisciplinary Design Environment. *AIAA Aviation Technology, Integration and Operations Conference* (2011).

Bibliography

- [142] ZILL, T., CIAMPA, P. D., AND NAGEL, B. Multidisciplinary Design Optimization in a Collaborative Distributed Aircraft Design System. *50th AIAA Aerospace Science Meeting* (2012).

A Complexity

Complexity is a measure for the transparency of a mathematical expression. Each mathematical operator and operand is assigned a cost value as given in Table A.1. Complexity is the sum of all cost in the expression. For example $1 + x$ has a cost of 3. Similar, $\cos(1 + x)$ has a cost of 6. Apart from the function error a low complexity is an objective in Symbolic Regression. The values applied in this study have their origin in the Eureka toolbox, published by Schmidt and Lipson [121].

Name	Complexity	Name	Complexity
Constant	1	Sine	3
Integer Constant	1	Cosine	3
Input Variable	1	Tangent	4
Addition	1	Exponential	4
Substraction	1	Natural Logarithm	4
Multiplication	1	Factorial	4
Division	2	Power	5
Negation	1	Square Root	4
Logistic	4	Minimum	4
Step	4	Maximum	4
Sign	4	Modulo	4
Gaussian	4	Floor	4
Hyperbolic	4	Ceiling	4
Error	4	Absolute	4

Table A.1: Complexity cost for various building blocks

B Validation Data

This appendix lists the validation data applied to check the derived models in the context of overall aircraft design. As a matter of fact, only conventional aircraft configurations can be listed. A validation out of the bounds of the conventional design space would require at least physical testing or prototyping.

The validation data base is limited to Boeing and Airbus aircraft. If one includes all engine options and gross weight variants the extend of this list will grow rapidly. Nevertheless, as the level of detail is comparably low it is hard to establish a significant separation effect. After all, as mentioned in chapter 1, the driving requirements for these aircraft may lie well outside of performance, e.g. family concepts.

Tables B.1 through B.5 list 25 aircraft. The data is constructed from publicly available documents like the *Aircraft Characteristics for Airport Planning* and must not reproduce the actual behavior of any of the products named.

B Validation Data

Manufacturer Model		Airbus 300-600	Airbus 310-300	Airbus 318-100	Airbus 319-100	Airbus 320-200
Fuselage						
Length	[m]	53.30	45.89	31.45	33.84	37.57
Height	[m]	5.64	5.64	4.14	4.14	4.14
Width	[m]	5.64	5.64	3.95	3.95	3.95
Wing						
Area	[m ²]	260	219	122.40	122.40	122.40
Span	[m]	44.84	43.90	34.10	34.10	34.10
Aspect Ratio	[]	7.73	8.80	9.50	9.50	9.50
Taper Ratio	[]	0.29	0.26	0.24	0.24	0.24
Sweep	[deg]	28	28	25	25	25
Vertical Tail						
Area	[m ²]	45.20	45.20	24.80	21.50	21.50
Height	[m]	8.30	8.30	7	6.26	6.26
Aspect Ratio	[]	1.52	1.52	1.97	1.82	1.82
Taper Ratio	[]	0.40	0.40	0.29	0.30	0.30
Sweep	[deg]	40	40	34	34	34
Horizontal Tail						
Area	[m ²]	69.45	64	31	31	31
Span	[m]	16.26	16.26	12.45	12.45	12.45
Aspect Ratio	[]	3.81	4.13	5	5	5
Taper Ratio	[]	0.40	0.44	0.26	0.26	0.26
Sweep	[deg]	33	34	29	29	29
Engine						
nEngine	[]	2	2	2	2	2
bypassRatio	[]	5.31	5.31	6	5.90	5.90
OPR	[]	32	32	27.30	27.30	27.10
Performance						
Cruise Mach	[]	0.78	0.80	0.78	0.78	0.78
Max. Seats	[]	345	265	120	156	180
Design Range	[km]	3620	5000	3600	3000	2780
Masses						
m_{TOM}	[kg]	165000	139500	68000	70000	73500
m_{OEM}	[kg]	86727	77000	35900	39700	42100

Table B.1: Validation data: A300, A310, A318, A319, A320

Manufacturer		Airbus	Airbus	Airbus	Airbus	Airbus
Model		321-100	330-200	330-300	340-200	340-500
Fuselage						
Length	[m]	44.50	57.77	62.68	58.42	66.03
Height	[m]	4.14	5.64	5.64	5.64	5.64
Width	[m]	3.95	5.64	5.64	5.64	5.64
Wing						
Area	[m^2]	122.40	363.10	363.10	361.60	439.40
Span	[m]	34.15	60.30	60.30	60.30	63.45
Aspect Ratio	[]	9.53	10.01	10.01	10.06	9.16
Taper Ratio	[]	0.24	0.25	0.25	0.25	0.22
Sweep	[deg]	25	30	30	30	31.10
Vertical Tail						
Area	[m^2]	21.50	47.65	45.20	45.20	47.65
Height	[m]	6.26	9.44	8.45	8.45	9.44
Aspect Ratio	[]	1.82	1.87	1.58	1.58	1.87
Taper Ratio	[]	0.30	0.35	0.35	0.35	0.35
Sweep	[deg]	34	45	45	45	45
Horizontal Tail						
Area	[m^2]	31	72.90	72.90	72.90	93
Span	[m]	12.45	19.40	19.40	19.40	22.59
Aspect Ratio	[]	5	5.16	5.16	5.16	5.49
Taper Ratio	[]	0.26	0.36	0.36	0.36	0.36
Sweep	[deg]	29	30	30	30	30
Engine						
nEngine	[]	2	2	2	4	4
bypassRatio	[]	5.90	4.70	5.10	6.60	7.50
OPR	[]	27.30	29.30	32	30.50	35.19
Performance						
Cruise Mach	[]	0.78	0.82	0.82	0.82	0.83
Max. Seats	[]	220	380	440	420	375
Design Range	[km]	3520	7780	6850	9260	12225
Masses						
m_{TOM}	[kg]	89000	233000	233000	275000	372000
m_{OEM}	[kg]	46800	120500	124500	129000	170900

Table B.2: Validation data: A321, A332, A333, A342, A345

B Validation Data

Manufacturer Model		Airbus 340-600	Airbus 380-800	Boeing 707-320	Boeing 717-200	Boeing 737-200
Fuselage						
Length	[m]	73.46	70.40	44.35	34.30	29.54
Height	[m]	5.64	8.41	4.33	3.35	4.01
Width	[m]	5.64	7.14	3.76	3.40	3.76
Wing						
Area	[m ²]	439.40	845	283.40	92.97	102
Span	[m]	63.45	79.75	43.40	28.40	28.35
Aspect Ratio	[]	9.16	7.53	6.65	8.68	7.88
Taper Ratio	[]	0.22	0.21	0.26	0.21	0.27
Sweep	[deg]	31.10	34	35.11	24.50	25
Vertical Tail						
Area	[m ²]	47.65	122.30	30.47	19.50	19.70
Height	[m]	9.44	13.66	7.20	4.35	5.85
Aspect Ratio	[]	1.87	1.53	1.70	0.97	1.74
Taper Ratio	[]	0.35	0.39	0.41	0.78	0.29
Sweep	[deg]	45	40	30	45	35
Horizontal Tail						
Area	[m ²]	93	222.57	58.06	24.20	31.31
Span	[m]	22.59	30.37	13.94	11.20	10.97
Aspect Ratio	[]	5.49	4.14	3.35	5.18	3.84
Taper Ratio	[]	0.36	0.41	0.40	0.38	0.26
Sweep	[deg]	30	35	36	30	30
Engine						
nEngine	[]	4	4	4	2	2
bypassRatio	[]	7.50	8.71	5.10	4.55	5.10
OPR	[]	35.19	36.62	27.30	27.30	27.30
Performance						
Cruise Mach	[]	0.83	0.84	0.73	0.77	0.74
Max. Seats	[]	475	853	189	117	130
Design Range	[km]	10560	12149	5200	2400	2225
Masses						
m_{TOM}	[kg]	368000	560000	141700	54800	54200
m_{OEM}	[kg]	177800	276300	64600	31000	28600

Table B.3: Validation data: A346, A380, B707, B717, A732

Manufacturer Model		Boeing 737-400	Boeing 737-500	Boeing 737-700	Boeing 737-800	Boeing 747-400
Fuselage						
Length	[m]	35.23	29.79	32.18	38.02	68.63
Height	[m]	4.01	4.01	4.01	4.01	8.10
Width	[m]	3.76	3.76	3.76	3.76	6.50
Wing						
Area	[m ²]	105.40	105.40	125	125	560
Span	[m]	28.88	28.88	34.32	34.32	64.40
Aspect Ratio	[]	7.91	7.91	9.42	9.42	7.41
Taper Ratio	[]	0.24	0.24	0.27	0.27	0.28
Sweep	[deg]	25	25	25	25	37.50
Vertical Tail						
Area	[m ²]	23.13	23.13	26.40	26.40	77.10
Height	[m]	6	6	6	6	10.16
Aspect Ratio	[]	1.56	1.56	1.36	1.36	1.34
Taper Ratio	[]	0.31	0.31	0.31	0.31	0.33
Sweep	[deg]	35	35	35	35	45
Horizontal Tail						
Area	[m ²]	31.31	31.31	32.80	32.80	136.57
Span	[m]	12.70	12.70	14.35	14.35	22.17
Aspect Ratio	[]	5.15	5.15	6.28	6.28	3.60
Taper Ratio	[]	0.26	0.26	0.19	0.19	0.27
Sweep	[deg]	30	30	30	30	32
Engine						
nEngine	[]	2	2	2	2	4
bypassRatio	[]	5.10	5.10	5.30	5.30	5.30
OPR	[]	27.30	27.30	24.41	27.30	32.40
Performance						
Cruise Mach	[]	0.74	0.74	0.79	0.79	0.84
Max. Seats	[]	168	132	149	189	600
Design Range	[km]	3241	3330	3890	3890	9273
Masses						
m_{TOM}	[kg]	68040	60500	70000	79000	396800
m_{OEM}	[kg]	33600	31300	37600	41400	178700

Table B.4: Validation data: B734, B735, B737, B738, B744

B Validation Data

Manufacturer Model		Boeing 757-200	Boeing 757-300	Boeing 767-200	Boeing 767-300	Boeing 777-200
Fuselage						
Length	[m]	46.97	54.08	47.24	53.67	62.94
Height	[m]	4.01	4.10	5.41	5.41	6.20
Width	[m]	3.76	3.76	5.03	5.03	6.20
Wing						
Area	[m ²]	185.25	185.25	283.30	283.30	427.80
Span	[m]	38.05	38.06	47.57	47.57	60.93
Aspect Ratio	[]	7.82	7.82	7.99	7.99	8.68
Taper Ratio	[]	0.24	0.24	0.27	0.27	0.15
Sweep	[deg]	25	25	31.50	31.50	31.64
Vertical Tail						
Area	[m ²]	34.37	34.37	46.14	46.14	53.23
Height	[m]	7.33	7.33	9.01	9.01	9.24
Aspect Ratio	[]	1.56	1.56	1.76	1.76	1.60
Taper Ratio	[]	0.35	0.35	0.31	0.31	0.29
Sweep	[deg]	39	39	39	39	46
Horizontal Tail						
Area	[m ²]	50.35	50.35	77.69	77.69	101.26
Span	[m]	15.21	15.22	18.62	18.62	21.53
Aspect Ratio	[]	4.59	4.60	4.46	4.46	4.58
Taper Ratio	[]	0.33	0.33	0.20	0.20	0.30
Sweep	[deg]	27.50	27.50	32	32	35
Engine						
nEngine	[]	2	2	2	2	2
bypassRatio	[]	4.10	4.10	4.80	4.80	6
OPR	[]	27.30	27.30	30	30	38.90
Performance						
Cruise Mach	[]	0.80	0.80	0.80	0.80	0.84
Max. Seats	[]	228	279	255	290	440
Design Range	[km]	5740	4450	3980	3980	8250
Masses						
m_{TOM}	[kg]	115650	122400	142800	158700	286900
m_{OEM}	[kg]	59350	64300	80100	86000	138100

Table B.5: Validation data: B752, B753, B762, B763, B772

C Design of Experiments

#	x_1	x_2	x_3	#	x_1	x_2	x_3
1	0.0000000	0.0000000	0.0000000	33	0.0000000	0.0000000	0.6666667
2	0.3333333	0.0000000	0.0000000	34	0.3333333	0.0000000	0.6666667
3	0.6666667	0.0000000	0.0000000	35	0.6666667	0.0000000	0.6666667
4	1.0000000	0.0000000	0.0000000	36	1.0000000	0.0000000	0.6666667
5	0.0000000	0.3333333	0.0000000	37	0.0000000	0.3333333	0.6666667
6	0.3333333	0.3333333	0.0000000	38	0.3333333	0.3333333	0.6666667
7	0.6666667	0.3333333	0.0000000	39	0.6666667	0.3333333	0.6666667
8	1.0000000	0.3333333	0.0000000	40	1.0000000	0.3333333	0.6666667
9	0.0000000	0.6666667	0.0000000	41	0.0000000	0.6666667	0.6666667
10	0.3333333	0.6666667	0.0000000	42	0.3333333	0.6666667	0.6666667
11	0.6666667	0.6666667	0.0000000	43	0.6666667	0.6666667	0.6666667
12	1.0000000	0.6666667	0.0000000	44	1.0000000	0.6666667	0.6666667
13	0.0000000	1.0000000	0.0000000	45	0.0000000	1.0000000	0.6666667
14	0.3333333	1.0000000	0.0000000	46	0.3333333	1.0000000	0.6666667
15	0.6666667	1.0000000	0.0000000	47	0.6666667	1.0000000	0.6666667
16	1.0000000	1.0000000	0.0000000	48	1.0000000	1.0000000	0.6666667
17	0.0000000	0.0000000	0.3333333	49	0.0000000	0.0000000	1.0000000
18	0.3333333	0.0000000	0.3333333	50	0.3333333	0.0000000	1.0000000
19	0.6666667	0.0000000	0.3333333	51	0.6666667	0.0000000	1.0000000
20	1.0000000	0.0000000	0.3333333	52	1.0000000	0.0000000	1.0000000
21	0.0000000	0.3333333	0.3333333	53	0.0000000	0.3333333	1.0000000
22	0.3333333	0.3333333	0.3333333	54	0.3333333	0.3333333	1.0000000
23	0.6666667	0.3333333	0.3333333	55	0.6666667	0.3333333	1.0000000
24	1.0000000	0.3333333	0.3333333	56	1.0000000	0.3333333	1.0000000
25	0.0000000	0.6666667	0.3333333	57	0.0000000	0.6666667	1.0000000
26	0.3333333	0.6666667	0.3333333	58	0.3333333	0.6666667	1.0000000
27	0.6666667	0.6666667	0.3333333	59	0.6666667	0.6666667	1.0000000
28	1.0000000	0.6666667	0.3333333	60	1.0000000	0.6666667	1.0000000
29	0.0000000	1.0000000	0.3333333	61	0.0000000	1.0000000	1.0000000
30	0.3333333	1.0000000	0.3333333	62	0.3333333	1.0000000	1.0000000
31	0.6666667	1.0000000	0.3333333	63	0.6666667	1.0000000	1.0000000
32	1.0000000	1.0000000	0.3333333	64	1.0000000	1.0000000	1.0000000

Table C.1: Full factorial sample plan

C Design of Experiments

#	x_1	x_2	x_3	#	x_1	x_2	x_3
1	0.52331659	0.45765820	0.01507784	33	0.63918007	0.02231173	0.13090356
2	0.71809038	0.89372781	0.85952820	34	0.83185877	0.42753005	0.82378877
3	0.69511576	0.85890331	0.97103776	35	0.85408129	0.62220017	0.38398620
4	0.58426099	0.84004166	0.58370791	36	0.86228206	0.41914107	0.46520390
5	0.74284686	0.71315798	0.29564375	37	0.59216821	0.73368085	0.64605606
6	0.81310049	0.84139029	0.47436997	38	0.86763896	0.26992637	0.27274147
7	0.11390271	0.12618325	0.09774527	39	0.73469115	0.35381744	0.84542967
8	0.56341826	0.75642848	0.82395697	40	0.40007721	0.94389484	0.51174435
9	0.91530287	0.42879988	0.47930155	41	0.49445554	0.61445659	0.66505015
10	0.67420375	0.63427120	0.52175372	42	0.51219017	0.84732147	0.97165884
11	0.51790356	0.37071847	0.44734474	43	0.14369980	0.94819837	0.64950757
12	0.71518788	0.07353518	0.28228377	44	0.64100494	0.00967303	0.88610897
13	0.74164764	0.30617696	0.58880503	45	0.57710951	0.45565062	0.14349256
14	0.16634986	0.76619005	0.01879928	46	0.90071925	0.24057979	0.06688968
15	0.94671337	0.04609987	0.49388867	47	0.86680254	0.23543555	0.19182521
16	0.40504128	0.00140480	0.78948953	48	0.45046498	0.09334541	0.48209940
17	0.41807317	0.51409126	0.42873985	49	0.57038754	0.87430360	0.57863079
18	0.19664306	0.16861785	0.17559114	50	0.41216012	0.82465468	0.42908250
19	0.89456693	0.59927050	0.49044858	51	0.38449930	0.99407591	0.16694501
20	0.59225885	0.78863836	0.61776694	52	0.76224420	0.80353644	0.80973757
21	0.39169583	0.67884819	0.16644614	53	0.99903590	0.14622386	0.19309968
22	0.43743011	0.70081238	0.79178761	54	0.69209516	0.54776919	0.68098166
23	0.46021940	0.85243878	0.98283524	55	0.12524882	0.64158823	0.62068282
24	0.19516284	0.16732447	0.61120669	56	0.44257123	0.07116753	0.43966730
25	0.14079472	0.75740699	0.43448020	57	0.35897089	0.68258132	0.68374916
26	0.59932567	0.15208340	0.39138571	58	0.05745481	0.15293680	0.89300671
27	0.97069937	0.10654628	0.59042444	59	0.58394015	0.81939178	0.83674567
28	0.25906796	0.98748716	0.89298724	60	0.30826290	0.79159012	0.23112717
29	0.08550308	0.92163676	0.85005209	61	0.75389985	0.48600321	0.25322016
30	0.17878178	0.84909104	0.83847600	62	0.21429770	0.02513174	0.06392401
31	0.48469373	0.87718459	0.94853716	63	0.51251830	0.33955413	0.32510014
32	0.53448369	0.13632465	0.02243996	64	0.81371631	0.37957814	0.94942816

Table C.2: Monte Carlo sample plan

#	x_1	x_2	x_3	#	x_1	x_2	x_3
1	0.75023428	0.30547817	0.61548616	33	0.28179929	0.60707575	0.92331832
2	0.84054856	0.03501466	0.64111988	34	0.98604379	0.31854682	0.48959589
3	0.80922993	0.29429211	0.80642170	35	0.49907227	0.42190504	0.63203698
4	0.63642583	0.39959424	0.01108287	36	0.39566663	0.35341001	0.47630142
5	0.15655831	0.78511818	0.11268622	37	0.78607707	0.98374034	0.09249502
6	0.84757113	0.05945731	0.26446924	38	0.04525572	0.71125143	0.82000194
7	0.38359696	0.36037531	0.90170080	39	0.19341872	0.06787173	0.17218341
8	0.14328868	0.95692466	0.45272057	40	0.46546586	0.02664238	0.16948915
9	0.41758944	0.56181724	0.45526068	41	0.59316481	0.51248809	0.36353594
10	0.56388464	0.61931478	0.79664557	42	0.93244807	0.52918567	0.21551834
11	0.11756340	0.16922309	0.74065144	43	0.74000594	0.13239943	0.35736276
12	0.72095201	0.75086553	0.72778558	44	0.24425719	0.45181866	0.59710122
13	0.26210181	0.00666649	0.96740498	45	0.47318967	0.86406817	0.30359388
14	0.35750164	0.21365004	0.05044462	46	0.90286624	0.19850651	0.67521174
15	0.66054030	0.57894966	0.88026254	47	0.09329712	0.93424134	0.26943649
16	0.44814002	0.47794830	0.69384630	48	0.96375397	0.39039517	0.41877480
17	0.10021217	0.66214007	0.03730065	49	0.20596451	0.17501106	0.09549284
18	0.50367567	0.74483454	0.13867087	50	0.13464427	0.14260040	0.94597300
19	0.53682350	0.24647548	0.50716447	51	0.36717565	0.81099268	0.22449003
20	0.55261329	0.23098256	0.77513808	52	0.93944742	0.72300088	0.39343900
21	0.27588152	0.26584888	0.91395181	53	0.82427989	0.45553603	0.75766722
22	0.59873339	0.89190623	0.14287225	54	0.76870473	0.49245477	0.43050221
23	0.34123485	0.88515809	0.56174860	55	0.97614168	0.69207948	0.56789589
24	0.30616294	0.25527994	0.24470250	56	0.02575238	0.83081661	0.37867192
25	0.00647093	0.99258160	0.99491662	57	0.43508038	0.84585077	0.07163352
26	0.32614260	0.91511493	0.98224009	58	0.06193029	0.82619387	0.86803750
27	0.52131757	0.10406168	0.85151084	59	0.68225372	0.56342206	0.33489386
28	0.88828407	0.53255313	0.19789198	60	0.86877452	0.11736868	0.70364824
29	0.61519267	0.08593308	0.65947590	61	0.71689793	0.62662867	0.58698156
30	0.17488877	0.42077021	0.83168988	62	0.21958672	0.94271237	0.31414667
31	0.91670671	0.64575999	0.52553335	63	0.65146161	0.67550314	0.29332143
32	0.69782396	0.33786051	0.03028395	64	0.07790748	0.77780910	0.53574424

Table C.3: Latin hypercube sample plan

D Oswald Factor

This appendix lists data from the design study for the Oswald factor in chapter 4. Table D.1 gives the locations of all points within the initial design of experiments. Furthermore, the table provides the results of the Oswald factor both from Tornado and the surrogate model. Subsequently, table D.2 shows the same data of the verification points.

#	φ_{25}	AR	λ	τ_t	η_k	$e_{act.}$	$e_{pred.}$
1	3.351	14.133	0.450	-5.297	0.327	1.005	0.997
2	-5.578	18.793	0.326	-0.162	0.258	0.990	0.997
3	-0.231	14.508	0.761	-2.874	0.343	0.976	0.990
4	11.688	18.340	0.112	-8.724	0.216	0.959	0.996
5	-21.137	9.085	0.810	-4.100	0.230	0.995	0.996
6	8.960	22.293	0.857	-4.412	0.285	0.870	0.904
7	37.302	11.683	0.275	-8.914	0.294	0.981	0.923
8	-32.751	22.448	0.135	-4.759	0.362	0.549	0.551
9	-12.079	5.833	0.951	-7.622	0.276	1.004	0.997
10	-2.158	17.550	0.281	-0.860	0.355	0.997	0.998
11	-14.627	24.773	0.242	-6.216	0.240	0.945	0.953
12	23.171	21.263	0.546	-6.852	0.318	0.799	0.769
13	-36.717	10.096	0.580	-9.601	0.276	0.959	0.928
14	-29.490	10.541	0.734	-6.050	0.261	0.983	0.974
15	-25.453	15.547	0.689	-4.209	0.299	0.965	0.952
16	31.765	16.399	0.756	-8.469	0.356	0.662	0.635
17	-37.071	14.643	0.780	-1.399	0.320	0.886	0.891
18	17.207	11.414	0.960	-3.705	0.228	0.923	0.941
19	19.117	13.115	0.911	-6.340	0.266	0.899	0.904
20	33.475	23.863	0.413	-2.522	0.203	0.842	0.798
21	0.668	13.312	0.720	-3.459	0.330	0.985	0.992
22	-7.071	21.921	0.258	-2.316	0.242	0.973	0.991
23	-33.400	21.729	0.824	-6.400	0.298	0.730	0.817
24	-22.678	13.534	0.907	-6.939	0.271	0.988	0.991
25	30.490	17.231	0.930	-9.562	0.291	0.678	0.661
26	-14.304	6.118	0.741	-1.921	0.397	1.004	0.982

Continued

D Oswald Factor

#	φ_{25}	AR	λ	τ_t	η_k	$e_{act.}$	$e_{pred.}$
27	-27.468	20.174	0.143	-8.542	0.217	0.876	0.887
28	-6.029	23.174	0.206	-5.021	0.322	0.969	0.985
29	39.175	12.899	0.698	-7.038	0.312	0.775	0.764
30	22.254	16.176	0.880	-1.063	0.383	0.760	0.769
31	-7.738	17.906	0.425	-0.094	0.283	0.995	0.996
32	-9.972	15.845	0.372	-6.666	0.319	0.994	0.985
33	15.726	5.202	0.790	-5.633	0.260	1.005	1.000
34	-37.863	6.278	0.188	-3.320	0.201	0.867	0.908
35	35.579	17.693	0.339	-3.972	0.346	0.728	0.701
36	21.308	23.206	0.817	-2.230	0.250	0.753	0.786
37	25.857	8.161	0.211	-1.613	0.233	1.017	1.000
38	-4.391	12.478	0.705	-7.818	0.370	0.996	1.000
39	7.216	24.947	0.469	-9.140	0.212	0.979	0.972
40	2.002	13.660	0.994	-5.863	0.286	0.946	0.969
41	-3.859	21.146	0.235	-7.923	0.379	0.989	0.992
42	27.759	7.104	0.344	-2.458	0.303	1.015	0.999
43	20.701	6.418	0.978	-1.766	0.389	0.976	0.974
44	30.272	17.107	0.514	-0.260	0.310	0.824	0.804
45	-26.919	19.611	0.437	-0.444	0.225	0.948	0.935
46	-17.141	21.555	0.596	-6.558	0.218	0.977	0.985
47	-23.669	7.353	0.394	-2.772	0.222	0.966	0.963
48	32.597	10.672	0.421	-3.538	0.212	0.997	0.974
49	-29.705	9.746	0.639	-7.313	0.338	0.979	0.941
50	-34.928	8.832	0.222	-7.175	0.264	0.894	0.902
51	-24.799	12.283	0.152	-7.713	0.229	0.900	0.935
52	-15.471	6.770	0.727	-0.747	0.334	1.001	0.987
53	-20.406	15.144	0.119	-7.477	0.342	0.916	0.892
54	-18.668	23.550	0.855	-9.826	0.339	0.877	0.933
55	-38.738	9.463	0.895	-7.571	0.350	0.968	0.925
56	24.525	19.893	0.179	-4.543	0.381	0.829	0.811
57	4.366	20.963	0.566	-5.780	0.265	0.976	0.979
58	-8.435	12.099	0.552	-7.250	0.296	1.004	0.997
59	19.829	7.796	0.478	-5.311	0.364	1.012	0.993
60	3.104	24.445	0.984	-9.459	0.208	0.883	0.940
61	17.716	11.190	0.670	-4.397	0.330	0.967	0.953
62	-22.270	24.018	0.289	-4.169	0.369	0.778	0.774
63	-19.399	15.759	0.587	-5.506	0.281	0.985	0.974
64	-2.491	9.828	0.517	-8.262	0.386	1.011	0.999
65	14.877	9.376	0.244	-2.056	0.333	1.016	0.999
66	-34.036	19.017	0.195	-2.995	0.395	0.588	0.586

Continued

#	φ_{25}	AR	λ	τ_t	η_k	$e_{act.}$	$e_{pred.}$
67	39.248	18.090	0.660	-8.035	0.345	0.468	0.476
68	-39.740	7.969	0.624	-3.685	0.350	0.952	0.908
69	16.020	11.304	0.607	-8.889	0.301	0.985	0.968
70	26.938	20.733	0.269	-5.955	0.391	0.738	0.704
71	-17.604	22.925	0.369	-0.998	0.252	0.956	0.952
72	29.079	19.596	0.476	-0.548	0.223	0.895	0.867
73	-0.982	8.551	0.379	-8.620	0.314	1.013	0.994
74	-35.919	22.184	0.969	-9.906	0.269	0.741	0.820
75	5.098	8.266	0.491	-3.122	0.392	1.014	1.000
76	33.755	10.345	0.644	-9.303	0.359	0.911	0.864
77	-9.364	19.313	0.846	-4.983	0.376	0.956	0.999
78	36.744	22.641	0.866	-4.679	0.256	0.474	0.512
79	-11.634	6.857	0.570	-4.872	0.274	1.009	0.986
80	14.002	16.805	0.166	-9.002	0.235	0.987	0.990
81	-31.834	8.792	0.922	-1.588	0.377	0.979	0.964
82	-13.116	13.961	0.323	-8.164	0.205	0.981	0.986
83	1.190	24.357	0.939	-1.240	0.308	0.898	0.956
84	10.954	20.385	0.108	-9.797	0.242	0.948	0.991
85	-10.401	15.233	0.525	-3.090	0.316	0.996	0.993
86	5.790	7.490	0.399	-3.860	0.244	1.017	0.996
87	23.651	18.851	0.888	-0.335	0.388	0.639	0.672
88	-16.094	5.738	0.356	-3.217	0.280	0.985	0.949
89	-26.144	20.471	0.770	-1.805	0.249	0.939	0.958
90	25.217	5.075	0.799	-1.461	0.236	1.001	1.000
91	12.401	14.905	0.306	-5.428	0.372	0.998	0.975
92	35.129	18.572	0.157	-6.749	0.399	0.631	0.639
93	10.360	10.970	0.676	-2.672	0.305	0.984	0.982
94	-30.458	5.531	0.540	-2.102	0.353	0.976	0.926
95	28.215	12.734	0.838	-1.144	0.290	0.859	0.866
96	38.383	23.708	0.453	-8.345	0.325	0.409	0.371
97	8.197	16.600	0.498	-0.615	0.210	0.990	0.987
98	-28.309	14.242	0.651	-5.158	0.246	0.977	0.963
99	7.031	11.849	0.313	-9.212	0.364	1.013	0.999
100	12.835	16.557	0.620	-6.137	0.367	0.939	0.921

Table D.1: Oswald factor: sample points

D Oswald Factor

#	φ_{25}	AR	λ	τ_t	η_k	$e_{act.}$	$e_{pred.}$
1	3.436	15.248	0.194	-5.728	0.399	0.994	1.000
2	-15.949	7.030	0.255	-2.904	0.327	0.977	0.946
3	-5.160	5.891	0.932	-7.094	0.358	1.003	0.999
4	30.012	5.670	0.915	-8.891	0.366	0.984	0.975
5	13.093	21.881	0.143	-7.157	0.299	0.948	0.965
6	14.212	23.074	0.390	-0.887	0.247	0.960	0.942
7	-19.379	11.387	0.270	-2.295	0.233	0.958	0.965
8	39.165	14.567	0.187	-5.673	0.348	0.832	0.804
9	-8.928	17.636	0.132	-5.638	0.354	0.951	0.965
10	-19.744	8.994	0.421	-0.568	0.284	0.986	0.969

Table D.2: Oswald factor: verification points

E Wing Mass

This appendix lists data from the design study for the wing mass estimation in chapter 4. Table E.1 gives the locations of all points within the initial design of experiments. Furthermore, the table provides the results of the wing mass both from ELWIS and the surrogate model. Subsequently, table E.2 shows the same data of the verification points.

#	AR	λ	φ_{25}	t/c	W/S	$m_{act.}$	$m_{pred.}$
1	10.669	0.205	0.204	0.108	715.73	8931.76	9108.06
2	7.430	0.515	-0.369	0.135	698.22	7395.66	7300.43
3	8.485	0.401	-0.147	0.116	617.96	7685.50	7938.92
4	12.274	0.320	-0.307	0.154	671.34	9782.36	9957.38
5	6.026	0.511	0.440	0.151	690.84	6814.46	5879.89
6	7.327	0.565	-0.556	0.150	518.07	7676.32	7200.42
7	12.174	0.540	0.641	0.132	667.12	10669.65	9434.53
8	7.039	0.433	-0.694	0.138	551.58	8006.63	8187.36
9	10.517	0.345	-0.135	0.159	633.05	7997.98	7838.28
10	6.736	0.309	0.484	0.145	609.29	6922.19	6468.76
11	9.235	0.445	-0.494	0.129	678.41	9268.70	9893.13
12	11.794	0.421	-0.299	0.121	712.66	11600.23	12231.11
13	10.827	0.300	-0.097	0.159	664.55	8067.44	8001.43
14	12.806	0.593	0.054	0.103	725.71	12395.20	11070.20
15	11.213	0.235	0.428	0.133	513.46	7562.48	8485.78
16	8.987	0.559	-0.396	0.118	647.75	9155.26	9437.36
17	8.617	0.469	-0.077	0.113	526.36	7727.65	7763.32
18	8.166	0.453	0.309	0.134	576.25	7313.16	7098.37
19	9.375	0.502	-0.647	0.152	588.11	9977.68	9746.38
20	10.750	0.225	0.613	0.120	491.81	7684.11	8764.23
21	9.551	0.209	-0.356	0.115	561.76	9058.63	9790.09
22	12.014	0.586	-0.627	0.101	650.36	23536.01	23023.29
23	12.107	0.216	-0.572	0.131	536.87	14613.28	14083.15
24	12.548	0.357	0.670	0.110	581.91	9552.15	8239.73
25	8.840	0.560	0.334	0.122	653.85	7620.93	7883.56
26	6.823	0.331	-0.413	0.143	708.70	7213.73	6757.38

Continued

E Wing Mass

#	AR	λ	φ_{25}	t/c	W/S	$m_{act.}$	$m_{pred.}$
27	9.691	0.462	-0.444	0.135	614.38	9203.56	9595.80
28	6.291	0.578	-0.211	0.114	641.89	6777.66	6207.58
29	7.243	0.324	-0.017	0.108	595.91	7265.55	6793.12
30	9.136	0.299	-0.229	0.111	729.36	8393.43	9265.34
31	12.921	0.263	-0.255	0.123	686.84	11785.28	12994.10
32	6.447	0.239	-0.661	0.140	733.53	7364.24	7660.14
33	7.532	0.264	0.260	0.148	572.35	7171.74	6368.43
34	7.939	0.482	-0.515	0.124	660.71	8320.26	8738.56
35	10.848	0.550	0.413	0.158	504.91	7369.18	7702.92
36	12.981	0.364	0.126	0.105	720.79	11225.05	10427.56
37	8.549	0.223	-0.433	0.114	699.73	8504.95	9467.66
38	6.979	0.368	0.346	0.128	534.78	6869.48	6394.36
39	8.765	0.466	0.684	0.118	598.29	8288.55	8895.60
40	11.009	0.532	-0.163	0.130	519.77	8909.39	9328.58
41	12.361	0.247	-0.105	0.130	585.64	9475.07	10311.12
42	10.582	0.449	0.685	0.112	557.09	8969.82	9015.67
43	12.656	0.284	-0.389	0.135	528.58	12211.52	12196.65
44	10.906	0.242	-0.594	0.142	495.92	11476.04	11277.80
45	10.132	0.229	0.244	0.106	691.89	8543.94	8747.41
46	6.071	0.507	0.274	0.126	661.82	6695.60	5851.56
47	12.775	0.573	0.021	0.153	603.11	9090.26	8834.65
48	9.196	0.356	0.058	0.128	580.25	7642.58	7748.58
49	7.784	0.413	-0.641	0.102	642.57	10102.14	10381.52
50	7.562	0.553	-0.676	0.115	550.88	9649.55	9502.36
51	6.391	0.485	-0.250	0.148	493.42	6853.23	5568.75
52	9.582	0.389	-0.182	0.141	593.37	7905.73	8035.34
53	10.443	0.306	0.621	0.136	555.81	7840.76	8922.09
54	7.985	0.342	0.569	0.139	720.56	7770.57	7927.40
55	11.311	0.219	-0.479	0.109	715.06	13464.70	15060.80
56	11.587	0.407	0.076	0.125	655.78	9121.53	9424.75
57	8.909	0.476	0.012	0.139	575.60	7562.17	7304.68
58	11.922	0.270	-0.123	0.146	683.64	8859.77	9401.46
59	8.339	0.278	0.651	0.107	620.31	7986.78	8536.57
60	7.143	0.374	0.089	0.141	499.85	6975.79	5972.41
61	7.690	0.385	-0.043	0.110	507.63	7438.68	6966.20
62	10.237	0.384	0.528	0.158	600.57	7653.65	8068.99
63	9.912	0.547	0.388	0.154	511.62	7223.76	7491.35
64	11.109	0.367	0.508	0.157	706.68	8791.23	8530.61
65	11.385	0.204	0.191	0.101	684.21	9349.07	9366.86
66	6.619	0.479	-0.270	0.156	570.82	6964.44	5778.18

Continued

#	AR	λ	φ_{25}	t/c	W/S	$m_{act.}$	$m_{pred.}$
67	11.855	0.522	-0.583	0.122	615.44	17089.57	15584.56
68	6.872	0.333	0.101	0.137	680.92	7015.49	6184.57
69	7.871	0.442	0.589	0.104	539.83	7304.38	7838.02
70	10.060	0.377	0.143	0.156	723.57	7959.24	7640.17
71	11.692	0.398	0.404	0.119	590.75	8355.55	8828.64
72	8.397	0.295	0.123	0.105	534.03	7446.41	7493.72
73	9.328	0.494	-0.004	0.143	560.41	7732.86	7438.90
74	6.258	0.314	-0.281	0.141	637.37	7006.11	5898.44
75	11.651	0.260	-0.067	0.112	515.34	9484.93	10218.41
76	12.372	0.519	0.372	0.147	673.52	9289.28	8780.95
77	10.392	0.281	-0.038	0.155	544.82	8103.29	7601.22
78	11.114	0.350	-0.470	0.157	704.12	9730.00	9904.28
79	6.496	0.590	0.361	0.149	503.07	6731.10	5734.00
80	7.341	0.254	-0.610	0.117	657.41	8091.28	8862.91
81	12.602	0.339	0.584	0.145	732.05	10559.70	9337.32
82	7.106	0.249	0.451	0.150	695.27	7203.23	6673.57
83	6.650	0.409	-0.203	0.131	644.92	6925.43	6252.04
84	7.661	0.440	-0.518	0.116	566.77	8375.72	8481.96
85	8.245	0.582	0.300	0.138	701.09	7573.75	7291.68
86	11.415	0.498	-0.456	0.149	674.68	10702.31	10608.47
87	9.766	0.416	-0.339	0.127	636.26	9035.15	9521.32
88	9.031	0.598	0.035	0.125	629.64	7937.40	7852.66
89	6.186	0.395	-0.532	0.147	548.34	7036.69	6275.88
90	9.796	0.321	-0.174	0.120	590.04	8396.73	8994.81
91	9.990	0.492	0.554	0.109	543.57	7848.31	8506.27
92	8.707	0.528	0.492	0.153	625.28	7453.14	7526.45
93	11.507	0.275	0.470	0.124	501.34	7630.05	8607.88
94	9.467	0.291	0.216	0.127	524.38	7466.88	7747.01
95	12.493	0.536	-0.326	0.101	564.66	16409.31	15911.76
96	8.090	0.456	0.181	0.144	606.71	7271.08	6759.41
97	10.045	0.431	0.224	0.123	530.28	7598.38	8145.06
98	12.053	0.536	0.156	0.134	630.62	8875.65	9120.17
99	8.206	0.425	0.280	0.107	612.09	7542.17	7519.96
100	10.281	0.569	0.532	0.103	624.23	9145.15	8518.40

Table E.1: Wing mass: sample points

E Wing Mass

#	<i>AR</i>	λ	φ_{25}	<i>t/c</i>	<i>W/S</i>	$m_{act.}$	$m_{pred.}$
1	9.587	0.242	0.060	0.126	491.35	7661.66	7839.92
2	9.348	0.238	0.684	0.126	554.18	9076.66	8990.90
3	6.710	0.269	-0.278	0.143	579.67	7014.57	6114.42
4	10.423	0.214	-0.156	0.126	546.72	8425.36	9086.17
5	6.312	0.570	-0.090	0.117	541.26	6670.83	5853.03
6	7.398	0.343	-0.345	0.157	632.62	7278.89	6555.81
7	6.234	0.562	0.524	0.107	532.47	6696.39	6485.70
8	11.908	0.219	0.229	0.117	613.53	8433.84	9207.08
9	12.326	0.329	0.248	0.155	677.81	8425.34	8454.69
10	8.236	0.276	-0.338	0.146	695.42	7631.31	7549.01

Table E.2: Wing mass: verification points

F Strut Braced Wing Mass

This appendix lists data from the design study for the strut-braced wing mass estimation in chapter 4. Table F.1 gives the locations of all points within the initial design of experiments. Furthermore, the table provides the results of the strut-braced wing mass both from ELWIS and the surrogate model. Subsequently, table F.2 shows the same data of the verification points.

#	m_{TOM}	AR	φ_{25}	τ_t	t/c	S	η_s	c_s	$m_{wing,act.}$	$m_{wing,pred.}$	$m_{strut,act.}$	$m_{strut,pred.}$
1	82.7	16.1	0.188	-0.134	0.095	153.9	0.591	0.136	7852.7	7828.0	1024.1	1055.3
2	88.0	16.0	0.232	-0.133	0.087	119.0	0.331	0.180	8531.1	8528.5	899.9	811.8
3	83.2	14.0	0.246	-0.163	0.106	145.2	0.665	0.189	7236.8	7005.5	1467.9	1360.9
4	86.9	16.7	0.426	-0.167	0.090	146.6	0.603	0.189	8664.2	8204.1	1614.4	1584.0
5	77.8	16.9	0.239	-0.076	0.125	135.3	0.404	0.187	7471.5	7491.4	894.5	925.5
6	81.5	15.8	0.200	-0.101	0.120	114.7	0.651	0.176	5669.5	5814.9	970.3	981.9
7	77.7	14.0	0.328	-0.129	0.096	136.7	0.627	0.101	6678.6	6751.7	770.2	718.4
8	71.3	13.2	0.344	-0.163	0.082	114.5	0.303	0.135	6522.2	6419.3	718.6	642.9
9	76.1	14.5	0.310	-0.081	0.103	144.2	0.667	0.144	7040.7	7042.8	999.7	1046.0
10	77.2	13.3	0.187	-0.155	0.127	116.3	0.274	0.174	5982.8	6267.5	510.8	538.0
11	77.7	14.0	0.328	-0.129	0.096	136.7	0.627	0.101	6678.6	6751.7	770.2	718.4
12	80.5	13.2	0.273	-0.112	0.128	156.7	0.468	0.169	8021.4	7674.2	1033.6	974.8
13	70.0	16.7	0.240	-0.156	0.083	114.0	0.540	0.151	5860.9	6124.0	710.4	828.2
14	84.8	13.3	0.338	-0.121	0.118	137.7	0.475	0.107	7178.9	7130.6	687.9	668.2
15	88.1	15.8	0.420	-0.140	0.128	138.6	0.450	0.133	7891.4	7959.4	1038.1	872.3
16	72.1	13.4	0.216	-0.089	0.122	124.2	0.471	0.126	6180.5	5946.8	542.2	563.0
17	71.4	17.0	0.284	-0.093	0.127	136.8	0.439	0.126	7178.8	7249.6	609.5	672.4
18	78.9	13.6	0.304	-0.153	0.116	112.1	0.293	0.152	6727.6	6491.0	550.6	617.0
19	80.2	12.2	0.176	-0.104	0.126	102.3	0.677	0.125	5065.0	4742.7	553.8	529.7
20	83.5	14.6	0.415	-0.114	0.084	125.2	0.360	0.168	8241.3	7948.3	1054.7	990.5
21	85.3	13.9	0.350	-0.125	0.119	149.6	0.612	0.151	7686.1	7525.8	1180.7	1059.3
22	82.5	13.7	0.349	-0.152	0.105	121.0	0.464	0.115	6387.8	6467.9	649.6	673.6
23	76.3	14.8	0.370	-0.122	0.108	117.4	0.527	0.100	6057.2	6207.4	620.5	575.2
24	89.2	15.0	0.295	-0.099	0.097	119.9	0.549	0.194	6289.3	6710.6	972.4	1137.3
25	86.3	13.6	0.401	-0.149	0.123	113.5	0.461	0.120	6209.0	6256.4	541.7	655.4

Continued

#	m_{TOM}	AR	φ_{25}	τ_t	t/c	S	η_s	c_s	$m_{wing,act.}$	$m_{wing,pred.}$	$m_{strut,act.}$	$m_{strut,pred.}$
26	88.5	12.6	0.195	-0.077	0.126	158.3	0.306	0.157	7941.1	8278.5	695.6	721.2
27	89.1	15.6	0.336	-0.158	0.119	129.8	0.251	0.146	9294.5	9131.7	745.5	756.8
28	75.8	14.3	0.358	-0.168	0.086	106.7	0.662	0.147	5503.3	5448.6	774.5	852.0
29	83.3	13.1	0.421	-0.074	0.113	155.2	0.258	0.167	8944.7	9194.0	705.7	929.4
30	71.9	12.4	0.215	-0.075	0.123	100.9	0.363	0.186	4749.3	4949.0	568.5	557.6
31	75.7	13.1	0.192	-0.154	0.083	107.9	0.390	0.173	5977.3	5712.8	768.5	659.9
32	86.7	14.7	0.423	-0.170	0.082	128.4	0.552	0.150	6872.4	7196.5	909.1	1119.4
33	86.6	12.1	0.332	-0.137	0.091	142.4	0.359	0.156	7262.4	7655.4	966.5	889.8
34	87.8	12.3	0.373	-0.124	0.101	132.7	0.341	0.109	7093.4	7416.9	1057.7	724.4
35	85.1	16.1	0.380	-0.118	0.118	155.1	0.504	0.181	8277.8	8445.7	1290.5	1279.9
36	89.0	14.6	0.235	-0.136	0.098	131.4	0.459	0.137	7044.7	7297.5	764.6	802.8
37	75.4	14.9	0.313	-0.165	0.102	157.8	0.208	0.135	9561.5	10173.9	679.6	676.4
38	77.0	12.7	0.265	-0.152	0.103	127.6	0.536	0.159	6267.5	6126.6	835.8	840.7
39	70.4	12.0	0.218	-0.160	0.106	111.0	0.377	0.154	5049.9	5240.4	579.8	548.6
40	74.0	15.4	0.338	-0.093	0.099	108.6	0.534	0.122	5596.0	5859.9	634.3	652.1
41	80.7	15.3	0.287	-0.150	0.098	144.7	0.280	0.106	9398.5	9058.7	468.4	630.5
42	70.2	14.8	0.390	-0.135	0.127	125.0	0.418	0.169	6564.8	6575.2	763.3	758.1
43	87.3	12.1	0.315	-0.075	0.116	127.2	0.690	0.116	6423.8	6181.2	682.1	691.2
44	84.7	13.0	0.431	-0.110	0.112	150.9	0.371	0.178	7667.8	8220.1	1062.3	1063.3
45	78.5	15.2	0.269	-0.085	0.113	100.3	0.584	0.195	5053.6	5314.6	789.6	883.0
46	87.6	14.9	0.208	-0.096	0.111	140.3	0.649	0.113	6885.1	6995.5	828.2	810.8
47	88.3	12.5	0.181	-0.119	0.101	106.2	0.485	0.102	5542.7	5524.1	614.8	488.0
48	88.7	14.6	0.301	-0.097	0.109	111.4	0.510	0.166	6018.9	6263.6	786.5	867.3
49	87.1	15.1	0.368	-0.113	0.119	131.7	0.345	0.163	8109.4	7985.3	1054.9	880.7
50	85.5	15.9	0.330	-0.126	0.113	148.2	0.338	0.188	8976.9	8921.0	1049.1	1034.9

Continued

#	m_{TOM}	AR	φ_{25}	τ_t	t/c	S	η_s	c_s	$m_{wing,act.}$	$m_{wing,pred.}$	$m_{strut,act.}$	$m_{strut,pred.}$
51	80.8	15.2	0.199	-0.125	0.087	109.3	0.426	0.148	6396.5	6491.8	634.3	678.9
52	86.0	14.2	0.230	-0.105	0.112	104.1	0.216	0.144	7922.3	7909.7	484.5	516.2
53	74.1	13.7	0.260	-0.115	0.121	102.7	0.282	0.199	6073.4	5826.1	659.1	605.4
54	73.5	13.8	0.323	-0.085	0.081	115.1	0.555	0.170	5729.0	5879.8	834.4	938.6
55	82.0	13.8	0.397	-0.148	0.096	150.3	0.565	0.142	7553.1	7662.4	982.6	1069.9
56	84.5	15.5	0.376	-0.111	0.089	153.4	0.227	0.129	12113.7	11897.0	1157.7	835.5
57	86.9	15.0	0.183	-0.137	0.102	105.2	0.337	0.166	6871.8	6834.9	509.1	620.5
58	90.0	12.3	0.176	-0.167	0.096	128.0	0.248	0.120	7931.1	7876.4	356.1	489.5
59	76.9	16.6	0.348	-0.109	0.121	123.6	0.423	0.175	6885.4	7031.3	777.6	873.4
60	72.8	13.5	0.264	-0.106	0.124	124.6	0.623	0.196	6143.7	5912.3	1193.5	1010.8
61	85.1	14.1	0.272	-0.129	0.108	149.9	0.353	0.171	8408.3	8276.3	992.4	911.0
62	77.9	15.5	0.319	-0.121	0.088	132.0	0.318	0.111	8653.3	8364.7	589.1	667.2
63	86.4	13.7	0.405	-0.091	0.094	157.3	0.646	0.128	8035.6	7995.5	1024.7	1122.8
64	70.9	12.0	0.352	-0.167	0.114	142.7	0.696	0.146	7121.2	6620.4	1065.8	876.7
65	81.4	16.3	0.432	-0.082	0.099	122.9	0.298	0.179	9232.7	8762.9	1084.6	951.0
66	79.7	16.2	0.211	-0.119	0.081	144.5	0.501	0.132	7487.2	7957.3	861.4	903.0
67	89.7	15.6	0.436	-0.162	0.089	146.2	0.221	0.171	12634.4	12331.2	955.8	1042.2
68	72.4	16.5	0.414	-0.122	0.120	147.5	0.576	0.177	7616.7	7672.6	1179.5	1176.3
69	76.5	12.8	0.285	-0.102	0.084	122.2	0.557	0.163	5976.0	6002.1	804.1	913.1
70	76.1	14.4	0.356	-0.109	0.084	112.9	0.636	0.182	5654.4	5838.2	950.2	1081.5
71	76.6	14.5	0.357	-0.151	0.100	107.3	0.630	0.121	5329.4	5530.7	626.1	662.2
72	78.3	16.1	0.341	-0.165	0.093	141.5	0.380	0.150	8119.5	8283.2	722.3	910.2
73	71.1	15.2	0.236	-0.099	0.124	149.1	0.392	0.192	7705.5	7512.4	935.6	943.8
74	72.1	15.8	0.290	-0.070	0.093	110.1	0.682	0.198	5563.9	5627.7	998.7	1145.0
75	72.3	14.3	0.297	-0.171	0.099	138.0	0.315	0.146	7760.3	7483.2	641.8	702.6

Continued

#	m_{TOM}	AR	φ_{25}	τ_f	t/c	S	η_s	c_s	$m_{wing,act.}$	$m_{wing,pred.}$	$m_{strut,act.}$	$m_{strut,pred.}$
76	74.8	16.5	0.293	-0.143	0.105	101.4	0.205	0.159	8436.2	8518.2	432.8	567.6
77	70.8	13.6	0.435	-0.174	0.080	121.8	0.240	0.158	8000.3	7608.0	758.0	775.4
78	83.0	13.9	0.224	-0.098	0.087	135.7	0.402	0.118	7632.3	7522.1	850.7	672.1
79	78.4	12.8	0.324	-0.100	0.117	110.8	0.566	0.148	5574.7	5507.4	673.6	682.1
80	72.6	12.4	0.252	-0.135	0.121	146.1	0.399	0.137	6619.8	6905.7	635.9	658.3
81	78.8	12.9	0.360	-0.102	0.082	126.4	0.319	0.181	7264.7	7324.9	876.4	879.2
82	75.9	15.0	0.244	-0.126	0.104	109.6	0.489	0.115	5672.1	5806.5	541.9	561.4
83	77.3	14.5	0.231	-0.152	0.094	116.8	0.603	0.173	5686.0	5852.1	918.0	962.1
84	85.0	16.3	0.334	-0.089	0.086	139.0	0.327	0.102	9881.7	9672.8	1188.1	739.9
85	77.6	16.8	0.281	-0.098	0.109	143.6	0.264	0.128	9611.2	9424.2	887.1	658.5
86	80.4	16.4	0.325	-0.082	0.112	134.9	0.287	0.191	9001.4	8794.8	906.5	884.9
87	70.5	16.9	0.363	-0.148	0.088	123.2	0.213	0.197	9681.9	9919.8	813.0	781.7
88	73.9	16.8	0.213	-0.134	0.104	140.8	0.687	0.138	7270.1	6896.3	1057.6	1047.5
89	79.6	16.2	0.354	-0.144	0.104	147.7	0.255	0.164	9993.5	9884.5	679.8	858.6
90	87.2	14.1	0.247	-0.155	0.094	159.6	0.474	0.105	8219.1	8270.9	854.0	784.7
91	75.3	14.8	0.270	-0.092	0.101	156.4	0.382	0.121	8380.2	8248.9	755.2	735.2
92	77.4	16.8	0.403	-0.174	0.126	130.8	0.268	0.166	8516.7	8509.1	877.7	802.0
93	88.1	12.7	0.197	-0.095	0.124	104.6	0.262	0.108	6185.1	6339.2	274.1	416.0
94	79.2	16.4	0.243	-0.073	0.110	129.3	0.613	0.141	6426.7	6685.7	879.2	905.6
95	85.8	12.9	0.248	-0.139	0.107	158.6	0.618	0.127	7807.4	7555.5	1000.2	959.2
96	79.9	15.6	0.298	-0.149	0.093	159.8	0.681	0.103	8473.9	7919.7	955.7	946.0
97	70.3	12.5	0.266	-0.072	0.081	151.2	0.295	0.193	7790.4	7673.8	996.5	836.5
98	81.6	15.1	0.411	-0.108	0.091	159.0	0.515	0.190	8195.9	8537.2	1449.2	1458.1
99	79.8	13.4	0.275	-0.142	0.092	103.2	0.691	0.196	5013.0	5121.3	955.1	1032.8
100	84.3	16.6	0.219	-0.116	0.085	101.9	0.411	0.140	6856.1	7020.4	705.5	662.4

Continued

#	m_{TOM}	AR	φ_{25}	τ_t	t/c	S	η_s	c_s	$m_{wing,act.}$	$m_{wing,pred.}$	$m_{strut,act.}$	$m_{strut,pred.}$
101	78.7	16.0	0.383	-0.162	0.112	151.4	0.230	0.116	10294.2	10095.6	481.6	720.2
102	82.8	17.0	0.262	-0.158	0.130	128.9	0.430	0.112	7099.7	7249.3	729.1	617.7
103	83.9	14.2	0.238	-0.093	0.114	141.7	0.233	0.153	8623.8	8954.1	567.1	640.5
104	78.2	14.1	0.251	-0.170	0.098	118.6	0.671	0.197	5854.8	5789.2	1170.1	1159.1
105	83.5	12.2	0.329	-0.105	0.090	115.9	0.331	0.139	6497.7	6589.8	715.5	704.7
106	74.3	16.4	0.382	-0.081	0.107	105.8	0.658	0.184	5729.5	5678.1	936.2	974.4
107	89.3	16.9	0.408	-0.127	0.092	153.2	0.599	0.169	8888.2	8616.3	1417.4	1503.1
108	78.1	12.2	0.279	-0.146	0.111	134.1	0.246	0.133	7173.8	7243.1	552.6	576.6
109	74.6	14.5	0.287	-0.090	0.128	140.9	0.349	0.129	7632.6	7413.9	587.6	627.7
110	75.0	15.7	0.255	-0.141	0.100	104.4	0.443	0.134	5766.8	5886.3	564.0	612.0
111	84.2	13.0	0.428	-0.108	0.085	155.9	0.561	0.140	7867.7	7948.4	1012.6	1158.2
112	83.7	14.8	0.257	-0.083	0.104	146.9	0.484	0.103	7600.6	7726.9	798.2	705.3
113	74.5	14.4	0.221	-0.139	0.125	110.4	0.519	0.178	5519.7	5476.7	762.7	757.1
114	71.2	15.3	0.410	-0.131	0.092	106.8	0.498	0.183	5654.8	5863.6	841.3	911.5
115	81.2	12.7	0.395	-0.145	0.110	111.8	0.322	0.172	6016.0	6334.9	604.4	771.4
116	72.9	15.1	0.314	-0.166	0.125	143.0	0.356	0.155	7655.3	7561.5	666.7	757.4
117	86.1	16.5	0.322	-0.088	0.097	143.5	0.373	0.165	9051.8	9042.3	1246.2	1009.7
118	71.7	16.0	0.182	-0.084	0.090	117.2	0.496	0.125	6054.0	6230.2	566.0	641.7
119	82.4	16.3	0.254	-0.077	0.089	102.2	0.288	0.124	8430.5	8284.3	877.7	567.0
120	86.0	12.6	0.307	-0.078	0.095	129.2	0.698	0.160	6361.5	6323.6	1001.0	1078.6
121	81.8	14.4	0.391	-0.091	0.083	120.8	0.202	0.142	10406.5	10974.8	777.2	767.4
122	71.6	12.9	0.365	-0.073	0.113	132.4	0.237	0.174	8632.7	7317.9	434.8	700.7
123	89.8	12.1	0.371	-0.115	0.085	117.8	0.673	0.177	5895.4	5969.9	993.6	1144.8
124	82.2	12.5	0.388	-0.145	0.094	133.4	0.621	0.107	6598.1	6584.0	749.7	760.1
125	79.4	13.1	0.346	-0.172	0.116	157.6	0.210	0.149	8792.5	9198.7	653.0	731.0

Continued

#	m_{TOM}	AR	φ_{25}	τ_f	t/c	S	η_s	c_s	$m_{wing,act.}$	$m_{wing,pred.}$	$m_{strut,act.}$	$m_{strut,pred.}$
126	73.8	12.3	0.204	-0.129	0.117	154.1	0.445	0.110	6840.9	7088.0	575.4	591.3
127	85.6	14.2	0.367	-0.072	0.129	125.9	0.590	0.143	6634.1	6597.7	819.7	804.1
128	79.4	13.2	0.311	-0.123	0.105	145.4	0.394	0.161	6905.7	7492.6	959.7	877.9
129	81.0	14.7	0.258	-0.107	0.088	134.5	0.408	0.132	7588.1	7598.2	628.6	762.9
130	80.9	13.0	0.178	-0.141	0.085	130.1	0.479	0.192	6573.6	6511.3	966.3	964.8
131	82.4	13.9	0.317	-0.086	0.123	118.3	0.654	0.190	6019.3	5959.4	1002.6	1021.6
132	83.8	13.5	0.427	-0.080	0.091	100.4	0.277	0.105	7973.4	7218.3	770.2	705.0
133	89.5	13.4	0.277	-0.173	0.119	113.3	0.573	0.180	5776.9	5831.7	945.9	907.7
134	73.7	14.2	0.406	-0.159	0.090	125.9	0.570	0.164	6243.6	6416.4	926.9	1005.2
135	70.7	15.5	0.210	-0.130	0.100	137.3	0.366	0.158	7417.8	7280.3	705.0	738.6
136	80.3	15.9	0.223	-0.146	0.129	151.9	0.640	0.187	7730.7	7406.5	1611.2	1374.5
137	71.8	12.4	0.202	-0.161	0.115	120.5	0.454	0.157	5317.0	5604.4	739.2	641.7
138	88.8	16.4	0.378	-0.104	0.102	103.4	0.492	0.119	6184.6	6561.1	892.1	739.0
139	73.4	12.7	0.363	-0.087	0.117	105.4	0.385	0.185	5649.2	5462.1	627.6	695.0
140	74.9	16.7	0.398	-0.079	0.082	126.7	0.223	0.138	11178.5	11246.5	1015.9	760.0
141	74.7	14.3	0.413	-0.071	0.118	152.5	0.581	0.161	7834.1	7680.7	1042.6	1072.0
142	76.5	13.5	0.193	-0.117	0.086	130.7	0.303	0.193	7220.3	7375.9	917.3	730.7
143	73.4	14.9	0.206	-0.157	0.122	121.5	0.508	0.143	6061.2	5992.5	726.3	680.4
144	75.6	16.2	0.190	-0.143	0.110	156.2	0.516	0.184	7959.3	7747.9	1292.2	1226.1
145	75.1	15.4	0.227	-0.156	0.097	138.7	0.312	0.117	8209.4	8013.9	1025.2	585.9
146	73.1	15.9	0.227	-0.094	0.109	152.1	0.634	0.114	7363.4	7339.0	822.8	853.3
147	72.6	16.1	0.302	-0.103	0.115	134.4	0.414	0.130	7175.7	7238.4	601.4	697.0
148	76.9	12.5	0.306	-0.118	0.129	123.3	0.525	0.123	6233.2	5993.6	572.4	568.9
149	83.1	15.3	0.299	-0.138	0.115	115.7	0.643	0.156	5843.4	6025.5	895.9	890.0
150	81.9	14.7	0.400	-0.169	0.107	119.5	0.585	0.114	6152.2	6358.9	708.6	705.3

Continued

#	m_{TOM}	AR	φ_{25}	τ_t	t/c	S	η_s	c_s	$m_{wing,act.}$	$m_{wing,pred.}$	$m_{strut,act.}$	$m_{strut,pred.}$
151	80.1	13.9	0.203	-0.111	0.101	107.5	0.595	0.108	5244.1	5404.7	559.4	554.9
152	84.4	13.5	0.386	-0.112	0.124	139.9	0.269	0.110	8057.5	8291.9	405.5	684.7
153	89.4	13.8	0.342	-0.087	0.110	136.1	0.432	0.104	7560.1	7530.3	828.5	710.6
154	79.1	16.6	0.424	-0.120	0.121	112.7	0.544	0.131	6132.6	6374.8	836.4	701.8
155	88.4	15.6	0.279	-0.161	0.122	149.5	0.451	0.123	8049.3	8087.2	787.8	808.0
156	84.0	15.7	0.394	-0.131	0.130	108.3	0.528	0.112	5922.8	6124.6	731.4	572.9
157	81.3	15.3	0.292	-0.128	0.114	139.6	0.606	0.200	6995.8	7090.2	1348.5	1325.8
158	87.7	12.8	0.418	-0.096	0.106	133.4	0.436	0.118	6659.0	7254.0	768.9	805.5
159	73.0	15.7	0.186	-0.079	0.108	148.5	0.242	0.185	9315.1	8982.5	617.6	681.8
160	87.4	13.3	0.377	-0.132	0.095	154.6	0.420	0.153	7642.6	8342.3	1099.8	1055.1

Table F.1: SBW mass: sample points

#	m_{TOM}	AR	φ_{25}	τ_t	t/c	S	η_s	c_s	$m_{wing,act.}$	$m_{wing,pred.}$	$m_{strut,act.}$	$m_{strut,pred.}$
1	72.3	16.2	0.265	-0.148	0.087	158.7	0.684	0.182	8664.2	7706.9	1603.7	1610.0
2	82.9	15.6	0.426	-0.086	0.102	113.6	0.255	0.139	9126.6	8729.4	959.4	787.0
3	77.9	12.4	0.284	-0.076	0.115	137.6	0.280	0.163	7041.4	7268.5	616.7	680.8
4	76.2	17.0	0.274	-0.080	0.129	123.6	0.505	0.190	6438.3	6621.2	955.5	969.9
5	71.4	15.5	0.369	-0.131	0.104	132.3	0.390	0.124	7218.9	7235.8	547.8	697.0
6	88.2	16.3	0.296	-0.114	0.098	142.1	0.668	0.142	7665.5	7526.9	1117.4	1162.1
7	80.6	13.7	0.236	-0.108	0.095	155.5	0.636	0.109	7439.9	7429.5	838.9	856.8
8	83.7	13.2	0.244	-0.157	0.112	129.9	0.481	0.147	6577.4	6528.0	892.3	772.8
9	78.2	14.5	0.315	-0.095	0.107	104.9	0.370	0.160	6204.7	6128.7	718.8	679.4
10	89.5	15.1	0.198	-0.168	0.124	109.5	0.621	0.120	5531.8	5673.9	692.1	627.4
11	70.7	13.3	0.389	-0.139	0.109	116.3	0.544	0.178	5788.7	5756.1	847.4	840.2
12	75.5	15.9	0.334	-0.097	0.127	119.3	0.303	0.155	7307.5	7198.4	619.4	662.7
13	74.6	14.6	0.349	-0.159	0.094	106.7	0.445	0.200	5848.0	5876.7	766.2	899.5
14	87.2	15.0	0.205	-0.119	0.117	135.2	0.404	0.173	7452.3	7438.4	937.3	858.2
15	79.3	14.1	0.372	-0.102	0.082	153.6	0.579	0.169	7568.2	7813.4	1204.5	1323.1
16	73.5	12.7	0.406	-0.174	0.118	149.6	0.560	0.104	7626.3	7274.0	662.9	631.8

Table F.2: SBW mass: verification points

Lebenslauf

Name	Böhnke
Vorname	Daniel
Geburtsdatum	08.05.1984
Geburtsort, -land	Trier, Deutschland
08.1990 - 06.1994	Grundschule Höfchensweg in Aachen
08.1994 - 06.2003	Pius-Gymnasium in Aachen
10.2003 - 09.2009	Studium an der Universität Stuttgart Abschluss: Dipl.-Ing. Luft-und Raumfahrttechnik
10.2007 - 02.2008	Studium an der University of Southampton Erasmus Stipendiat
10.2009 - heute	Wissenschaftlicher Mitarbeiter an dem Institut für Luft- transportsysteme im DLR e.V. an der Technischen Uni- versität Hamburg-Harburg